Distribution Categories:
Energy Conservation--Buildings and
Community Systems (UC-95D)
Active Solar Heating and Cooling
(UC-231)

ANL--88-15

DE88 013622

ANL-88-15

ARGONNE NATIONAL LABORATORY
9700 South Cass Avenue
Argonne, Illinois 60439

MEASUREMENTS OF PRESSURE DROP AND HEAT TRANSFER IN TURBULENT PIPE FLOWS OF PARTICULATE SLURRIES

by

K. V. Liu, U. S. Choi, and K. E. Kasza

Materials and Components Technology Division

May 1988

*Work supported by the U.S. Department of Energy, Conservation and Renewable Energy, Office of Buildings and Community Systems, under Contract W-31-109-ENG-38.

LEGIBILITY NOTICE

A major purpose of the Technical Information Center is to provide the broadest dissemination possible of information contained in DOE's Research and Development Reports to business, industry, the academic community, and federal, state and local governments.

Although a small portion of this report is not reproducible, it is being made available to expedite the availability of information on the research discussed herein.

Table of Contents

Table of Contents (Contd.)

List of Figures

List of Figures (Contd.)

List of Figures (Contd.)

List of Tables

List of Symbols

C_D	drag coefficient for free-falling sphere, defined by Eq. (15)
Cp	specific heat [kJ/kg-K]
D	inside tube diameter [m]
D_p	diameter of solid particle [m]
f	friction factor defined by Eq. (2)
Fr	Froude number defined by Eq. (16)
g_c	dimensional conversion factor = 1 $kg/N\text{-}s^2$ = 32.2 $lbm\text{-}ft/lbf\text{-}s^2$
h	film coefficient [$W/m^2\text{-}°C$]
i	head loss for pipe flow [meters of water]
k	thermal conductivity of fluids [W/m-°C]
L	length of test section [m]
M	total mass [kg]
$\dot{m}$	mass flow rate of slurry [kg/s]
Nu	Nusselt number = hD/k [dimensionless]
p	pressure [psi], 1 psi = 1 lbf/in^2 = 6.895 kPa
Pr	Prandtl number = $Cp\mu/k$
Q	power input [W]
q	local heat flux [W/m^2]
Re	Reynolds number = $\rho uD/\mu$ [dimensionless]
r_i	inside tube radius [m]
r_o	outside tube radius [m]
s	relative density, ρ_s/ρ_c
St	Stanton number = $h/\rho Cpu$ [dimensionless]
T_b	bulk fluid temperature [°C]
T_{win}	inside tube wall temperature [°C]
T_{wout}	outside tube wall temperature [°C]

U	velocity [m/s]
U_∞	terminal velocity of sphere settling in an unbounded fluid [m/s]
x	length of test section segment [m] or coordinate along the downstream direction

Greek

δ	degree of thermal equilibration defined by Eq. (B.9).
ε	particle mass fraction [%]
μ	dynamic viscosity [N-s/m^2]
ν	kinematic viscosity [m^2/s]
ρ_{HDPE}	density of HDPE particles [kg/m^3]
ρ_{H2O}	density of water [kg/m^3]
ϕ	particle volumetric loading [%]

Subscripts:

av	average quantity
c	carrier fluid
i	segment number, from 1 to 5
s	slurry
w	wall condition or water

MEASUREMENTS OF PRESSURE DROP AND HEAT TRANSFER IN TURBULENT PIPE FLOWS OF PARTICULATE SLURRIES

by

K. V. Liu, U. S. Choi, and K. E. Kasza

ABSTRACT

Argonne National Laboratory (ANL), under sponsorship of the U.S. Department of Energy, Office of Buildings and Community Systems, has been conducting a comprehensive, long-range program to develop high-performance advanced energy transmission fluids for use in district heating and cooling (DHC) systems.

ANL has identified two concepts that hold considerable promise for improving the performance of DHC systems. These two concepts are (1) utilization of very low concentrations of non-Newtonian additives to the carrier liquid to reduce flow frictional losses, and (2) utilization of a pumpable phase-change slurry, comprising particles of material with a high heat of fusion conveyed by a liquid, to enhance both bulk convective energy transport and heat transfer coefficients at the heat exchanger surfaces. The two concepts can be used separately or combined to achieve maximum benefits. When the concepts are combined, the energy transmission fluid is composed of the phase-change particles, friction-reducing additive, and carrier liquid.

The current study focuses on the development of phase-change slurries as advanced energy transmission fluids. The objectives are (1) to establish proof-of-concept of enhanced heat transfer by a slurry, with and without phase change, relative to heat transfer in a pure carrier liquid; (2) to investigate the effect of particle volumetric loading, size, and flow rate on the slurry pressure drop and heat transfer behavior with and without friction-reducing additives; and (3) to generate pressure drop and heat transfer data needed for the development and design of improved DHC systems. Two types of phase-change materials were

used in the experiments: ice slush for cooling, and cross-linked, high-density polyethylene (X-HDPE) particles with diameters of 1/8 and 1/20 in. (3.2 and 1.3 mm) for heating. The friction-reducing additive used in the tests was Separan AP-273 at 65 wppm. This report describes the test facility, discusses the experimental procedures, and presents significant experimental results on flow and heat transfer characteristics of the non-melting slurry flows.

The frictional loss associated with phase-change-type slurry flows was found to be significantly less than that typically associated with heavy particle slurries. Under some conditions, X-HDPE slurries with 1/20-in.-diameter particles at loadings up to 30% and ice slush slurries exhibited significant friction reduction compared to pure water. A threshold particle loading was also found in slurries, above which the pressure drop reduction phenomenon disappears; this threshold was <5% and 30% for slurries with 1/8 and 1/20-in.-diameter particles, respectively.

No satisfactory correlations have been identified to accurately predict the slurry pressure drop and viscosity measured in the laboratory. The slurry tests also showed that the flow behavior is strongly influenced by the particle size, which is either neglected or considered to be a weak function in existing correlations.

The heat transfer measurements for X-HDPE slurries with 1/8-in.-diameter particles under non-melting conditions showed a modest enhancement of heat transfer over that of water, but the data with 1/20-in.-diameter particles showed a modest degradation. The results also show a significant effect of particle size on slurry heat transfer, which requires further study.

The results for combined-concept fluids have demonstrated that a friction-reducing additive can substantially reduce

pressure drop for a slurry of water and X-HDPE particles. This effect should also exist for other types of particulate slurries.

The data for slurry pressure drop and heat transfer with and without friction-reducing additives highlight the existence of a very important new phenomenon which has been called flow re-laminarization. At flow rates that are normally considered to be in the fully turbulent regime, the slurry flow can revert to laminar behavior if the particle loading is sufficiently high. The re-laminarization is found to be a strong function of particle size.

In future work, slurry pressure drop and heat transfer with different particle sizes will be examined and experiments will be performed with melting X-HDPE slurries. The phase-change effects, which represent a second heat transfer enhancement mechanism, are important for understanding slurry behavior in DHC systems. Ultimately, engineering design correlations will be developed.

1. INTRODUCTION

It has been estimated that 2.5 quadrillion Btus of the nation's energy consumption can be saved annually by the year 2010 if District Heating and Cooling (DHC) systems are fully utilized. Other potential benefits of DHC include the utilization of a variety of low-cost energy sources such as solid fuels, geothermal energy, and waste heat from industrial processes, and reduced environmental concern for urban communities. However, for DHC to be economically competitive with individual heating and cooling systems, the current DHC technology has to be improved to reduce operating and capital costs, and to enhance the thermal-hydraulic performance of DHC systems.

Argonne National Laboratory (ANL), under sponsorship of the U.S. Department of Energy, Office of Buildings and Community Systems, has embarked upon a comprehensive research program to develop high-performance energy transmission fluids for use in DHC systems. In comparison to pure water and steam, which serve as energy transmission fluids in existing DHC systems, advanced energy transmission fluids will transport thermal energy from the source to the end users with a dramatic reduction in the size of piping, heat

exchangers, pumps, and energy storage tanks. Hence, they will reduce the capital costs of DHC systems and will significantly improve thermal-hydraulic efficiency (through reductions in pumping power and improvements in energy transport). Figure 1 illustrates one of the potential benefits of using advanced energy transmission fluids in DHC systems.

Detailed scoping studies conducted by ANL [1-3] have highlighted two concepts for improving the performance of DHC systems by means of additives to DHC transmission fluids. The concepts can be used separately or combined to achieve maximum benefits. The individual concepts are (1) use of a low concentration (20-200 wppm) of non-Newtonian additives to the appropriate carrier liquid to reduce frictional flow losses by 30-80% (Toms phenomenon) and (2) use of a pumpable phase-change slurry comprising particulate material with a high heat of fusion, conveyed by a liquid, to enhance the bulk convection energy transport and possibly the heat transfer coefficients at heat exchanger surfaces. Two examples of candidate particulates are ice crystals for cooling and cross-linked form-stable high-density polyethylene (X-HDPE) for heating. When the concepts are combined, the energy transmission fluid comprises the appropriate phase-change particles, friction-reducing additive, and carrier liquid.

As part of overall project efforts, the activities to identify robust friction-reducing additives for use in DHC systems have focused on three different categories of substances. They are (a) high-molecular weight linear polymers (Polyox, Separan, etc.), (b) surfactants (cationic Tenside, etc.), and (c) large-aspect-ratio fibers or filaments (nylon, glass fibers, iron whiskers, etc.). All of these additives consist of highly elongated semi-elastic filaments or fibers which suppress small-scale turbulence in a pipe flow and thus reduce frictional losses and pumping power requirements. Other characteristics of the additives are also being examined relative to compatibility with the conditions encountered in DHC applications. The additives should

(1) produce significant reduction in frictional losses under the thermal-hydraulic conditions encountered in DHC systems,
(2) exhibit long life under continuous flow shear,
(3) have no significant negative influence on heat transfer equipment,

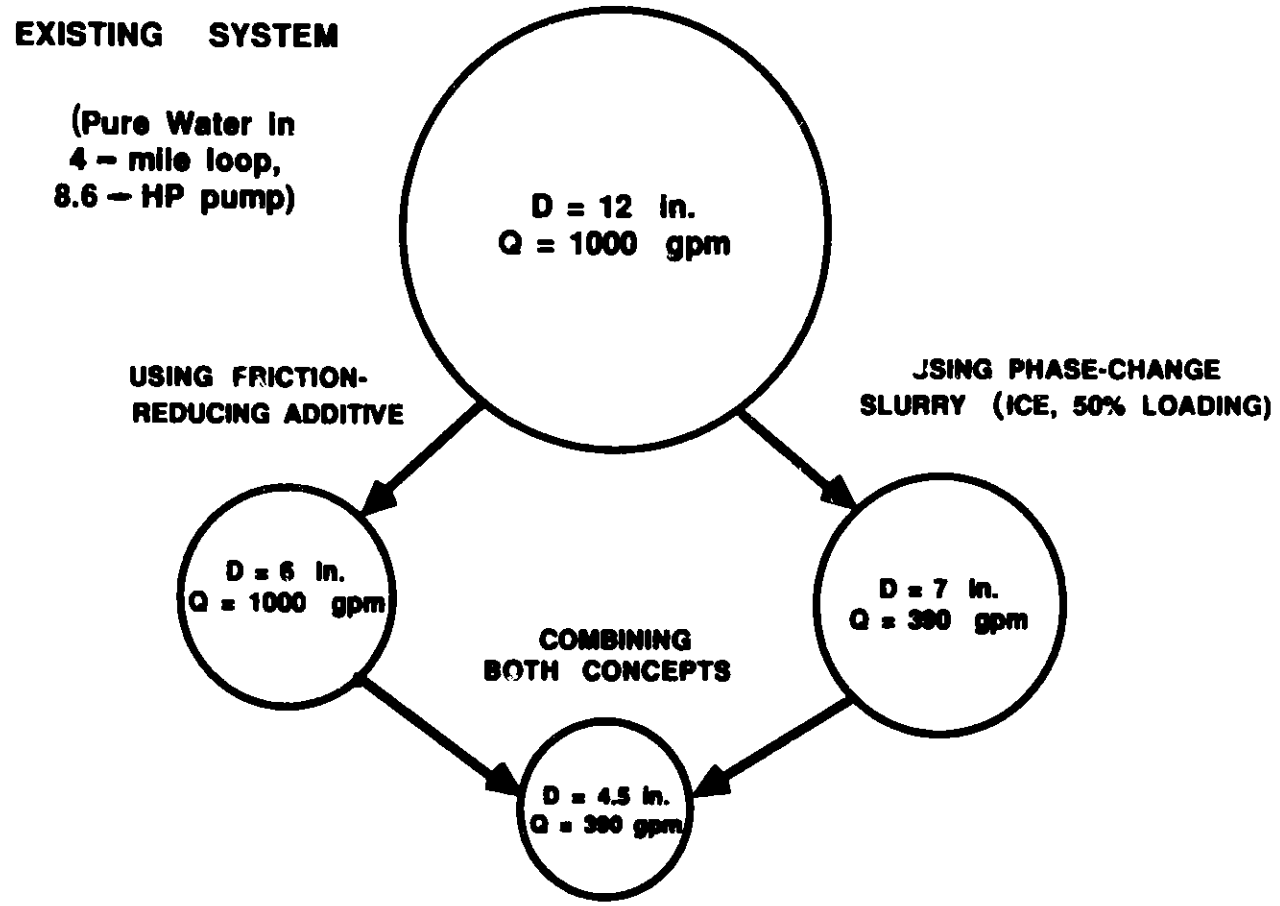

Fig. 1. Potential Pipe Size Reduction Achieved by Using Advanced Energy Transmission Fluids in Cooling Systems. Q = flow rate.

(4) be economical,

(5) undergo no detrimental chemical interactions with system hardware or water treatment chemicals (and, if possible, decrease corrosion), and

(6) exhibit no negative environmental or safety effects.

Significant progress has been made in identifying, screening, and testing additives in the ANL Friction Reduction Additive Degradation and Heat Transfer Test Loop. Detailed experimental results and analyses can be found in Refs. 4 and 5.

The second concept under development is to use a phase-change slurry as the system energy transmission fluid. This concept offers the following potential benefits:

(1) Increased thermal-energy transport density, due to the latent heat of the fusible materials in suspension, with a commensurate increase in load handling capacity.

(2) Possible increased fluid/solid-surface heat transfer coefficients resulting from several mechanisms, with concomitant reductions in the temperature difference required for a given amount of heat transfer and in heat-transfer surface area.

(3) Improved quality of usable thermal energy, with a smaller difference between the working-fluid end-use temperature and the heat-source temperature.

(4) Improved adaptability of energy storage concepts to thermal systems.

The mechanisms responsible for enhancement of heat transfer at a heat exchange surface by a slurry have been conjectured to be (a) microconvective enhancement of thermal conductivity adjacent to a surface resulting from the microscopic stirring motion of particles in the shear flow field; (b) the particle-particle and particle-wall interactions, which disrupt the laminar sublayer at the wall; and (c) the high heat of fusion of the particle, which increases the capacity of the fluid and thus increases the temperature gradient near a surface and the overall thermal conduction.

The reduction of frictional losses in slurry under some conditions is believed to be attributed to the damping effect of solid particles on turbulent velocity fluctuations. The concept of adding a small percentage

(20-200 wppm) of high-molecular-weight polymer to reduce the frictional loss associated with turbulent pipe flow in practical engineering applications has been under investigation for nearly 40 years [6]. This concept is also under study in the ANL Advanced Fluids Program. Polymeric friction-reducing additives are found to be very effective in reducing drag (by up to 70% relative to water [4,5]) in a turbulent flow but not at all effective in a laminar flow. It is believed that the long-chain polymer molecule causes a significant reduction of the fluctuating velocities and the eddy motions in turbulent flow. Similarly, filamentary substances with large aspect ratio such as nylon and polyester fibers have been found to suppress small-scale turbulence and reduce frictional losses [3,7]. The reduction of frictional loss in a turbulent gas flow by adding solid particles has also been reported [8-10]; the friction reduction increases as the particle size decreases [8]. For a solid-liquid system, a few studies have reported a decrease in frictional loss for flowing water as a result of the addition of low concentrations of suspended matter such as fine coal or ash [11,12].

An example of a phase-change material with potential for use in district heating applications is X-HDPE. This material is formed by electron beam irradiation of polyethylene, which alters its molecular structure and renders it form stable. At ~270°F (132°C), X-HDPE undergoes a phase transition that evolves 72 Btu/lbm (168 kJ/kg). In the "molten" phase, individual particles in the slurry retain the shape they had in the solid phase and tend not to agglomerate or stick to heat transfer surfaces (providing that they have been sufficiently cross-linked). Cross-linking can also be explored for other materials with different melting points to meet the needs of various applications. On the other hand, ice slush slurries are being explored for use with some district cooling applications.

The research on phase-change slurries at ANL is addressing the following issues: (a) the effect of particle volumetric loading, size, and flow rate on slurry pressure drop and heat transfer relative to the single-phase carrier fluid; (b) heat exchanger performance with phase-change slurries under both melting and non-melting conditions; (c) slurry pressure drop and heat transfer behavior when a friction-reducing additive is combined with the slurry; (d) the pumpability, valve controllability, and flow blockage potential with highly loaded slurries; and (e) the adequacy of existing engineering

correlations and information for designing DHC systems that incorporate slurries.

Specifically, this report presents experimental results on the pressure drop and heat transfer characteristics of non-melting slurry flows which confirm and support many of the conjectures about the viability of using phase-change slurries. The experiments were conducted with X-HDPE slurries with particle diameters of 1/8 and 1/20 in. (3.2 and 1.3 mm); particle volumetric loadings varying from 0 to 45%; and mass flow rates ranging from 5.6 to 35.5 gpm. In addition to the X-HDPE slurry experiments, scoping ice slurry experiments were conducted. In Section 2, the test section and the measuring instruments used in the ANL Slurry Heat Transfer Test Facility are described. Details of data acquisition and experimental procedures including particle handling and particle volumetric loading determinations are discussed in Section 3. Pressure drop, flow characteristics, and rheology of solid-liquid slurry flows based on current experimental results are presented in Section 4. The primary focus is on slurry pressure drop compared to that for pure water, especially as influenced by particle volumetric loading and slurry mass flow rate. In Section 5, slurry heat transfer data are presented. The results indicate a modest heat transfer enhancement with 1/8-in.-diameter slurry particles and a modest degradation of heat transfer with 1/20-in.-diameter slurry particles. In all cases, bulk energy transport is dramatically improved by using slurry flows with high loadings of phase-change particles. Section 6 presents preliminary test results for the combined-concept slurry under non-melting conditions. The influence of particle loading on friction reduction in slurries containing a friction-reducing additive is examined. Dramatic pressure drop reduction is observed with particle loadings below 30%. Finally, in Section 7 an overview of important findings and significant accomplishments is presented, and the need for further research is discussed.

2. DESCRIPTION OF ANL SLURRY HEAT TRANSFER TEST FACILITY

2.1 Major Components

A schematic diagram of the overall Slurry Heat Transfer Test Facility is shown in Fig. 2. The test facility consists of the following major components:

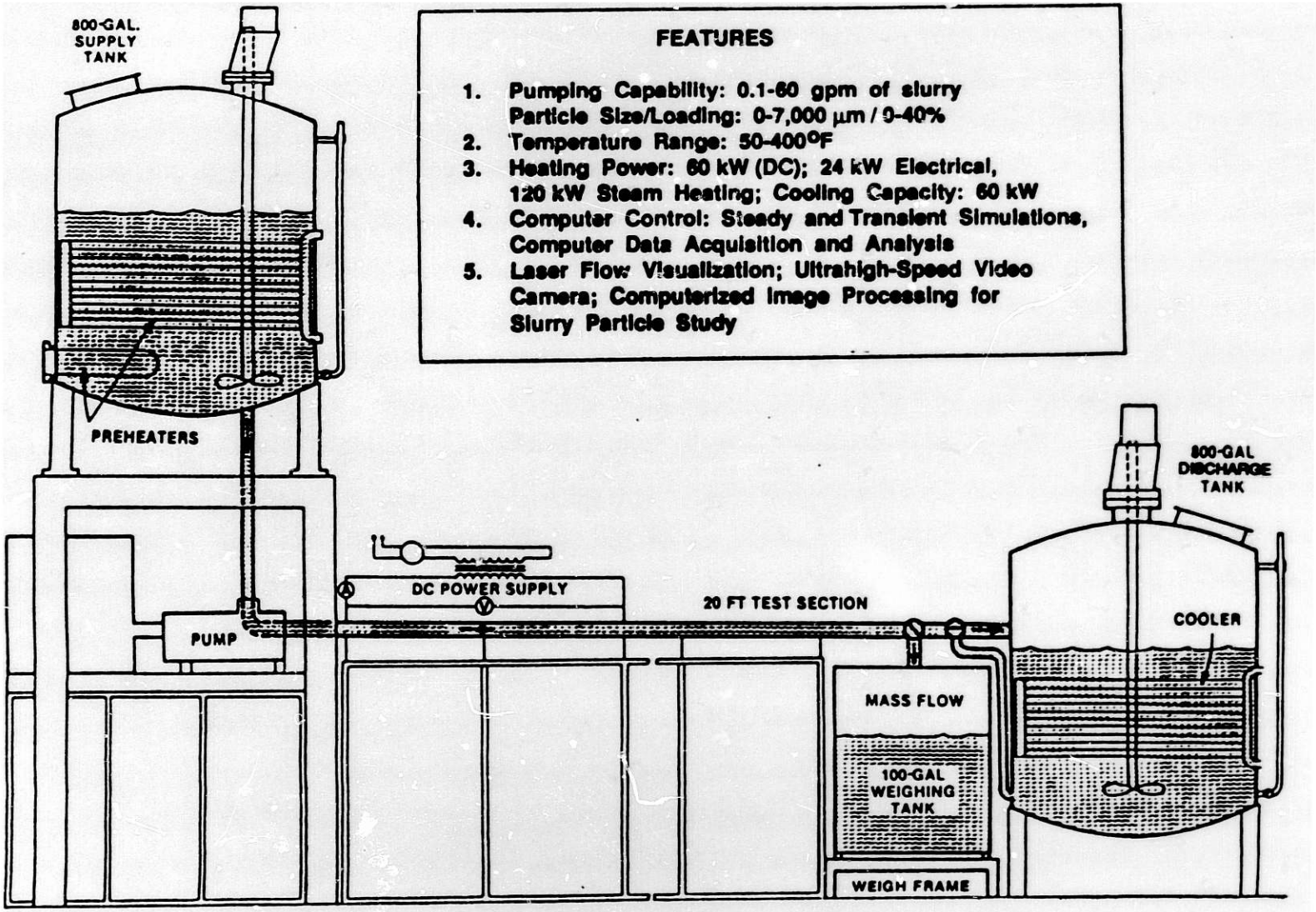

Fig. 2. ANL Slurry Heat Transfer Test Facility.

(1) An 800-gal supply tank.
This tank contains a pneumatic mixer for maintaining thermal equilibrium and homogeneity of the particle suspension in the test mixture. Two 12-kW electrical heaters preheat the slurry. Additional heating coils inside the tank can supply up to 120 kW of steam heat.

(2) An 800-gal discharge tank.
This tank also contains a pneumatic mixer and a cooling coil with 60 kW of cooling capacity.

(3) A 100-gal weighing tank.
This flow diversion tank is used for mass flow measurements and separation of particles from the carrier fluid for accurate determination of the volumetric loading fraction.

(4) Two progressive-cavity variable-speed slurry pumps.
The smaller pump has a capacity of 0.1-4.0 gpm, and the larger pump has a capacity of 3.0-60.0 gpm. The capacities vary with particle size and loading.

(5) Two DC electrical power supplies.
Two power supplies connected in series can supply in excess of 60 kW to the heat transfer test section, which is a thin-walled stainless steel tube approximately 20 ft (6.1 m) long.

2.2 Test Section

The electrically heated test section and its associated instrumentation are shown in Figs. 3-5. The test section is a straight tube of Type 304 stainless steel with an O.D. of 1.0 in. (25.4 mm). The tube wall thickness is 0.028 in. (0.71 mm), resulting in an I.D. of 0.944 in. (23.98 mm). The total length of the test section, 19.71 ft (6 m), is divided into five voltage-monitored subsections, each approximately 3.94 ft (1.2 m) long. A short, clear glass tube is connected immediately downstream of the stainless steel tube to allow visualization of slurry flow behavior.

An end view of the test section is shown in Fig. 4. The test section is insulated with Fiberfrax® Durablanket™ S insulation. This material is manufactured in blanket form and is composed primarily of Al_2O_3 and SiO_2. It has a density of 8 lb/ft^3 (128 kg/m^3) and its thermal conductivity is

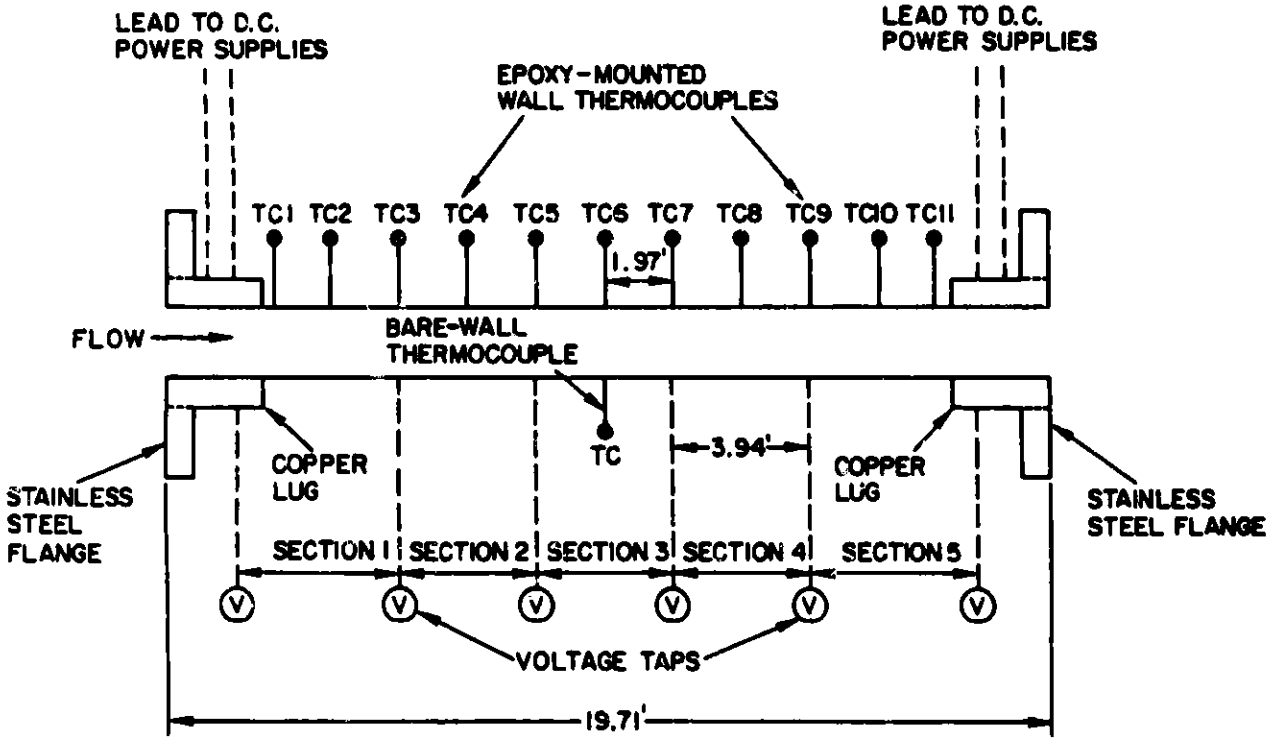

Fig. 3. Schematic Diagram of the Electrically Heated Test Section.

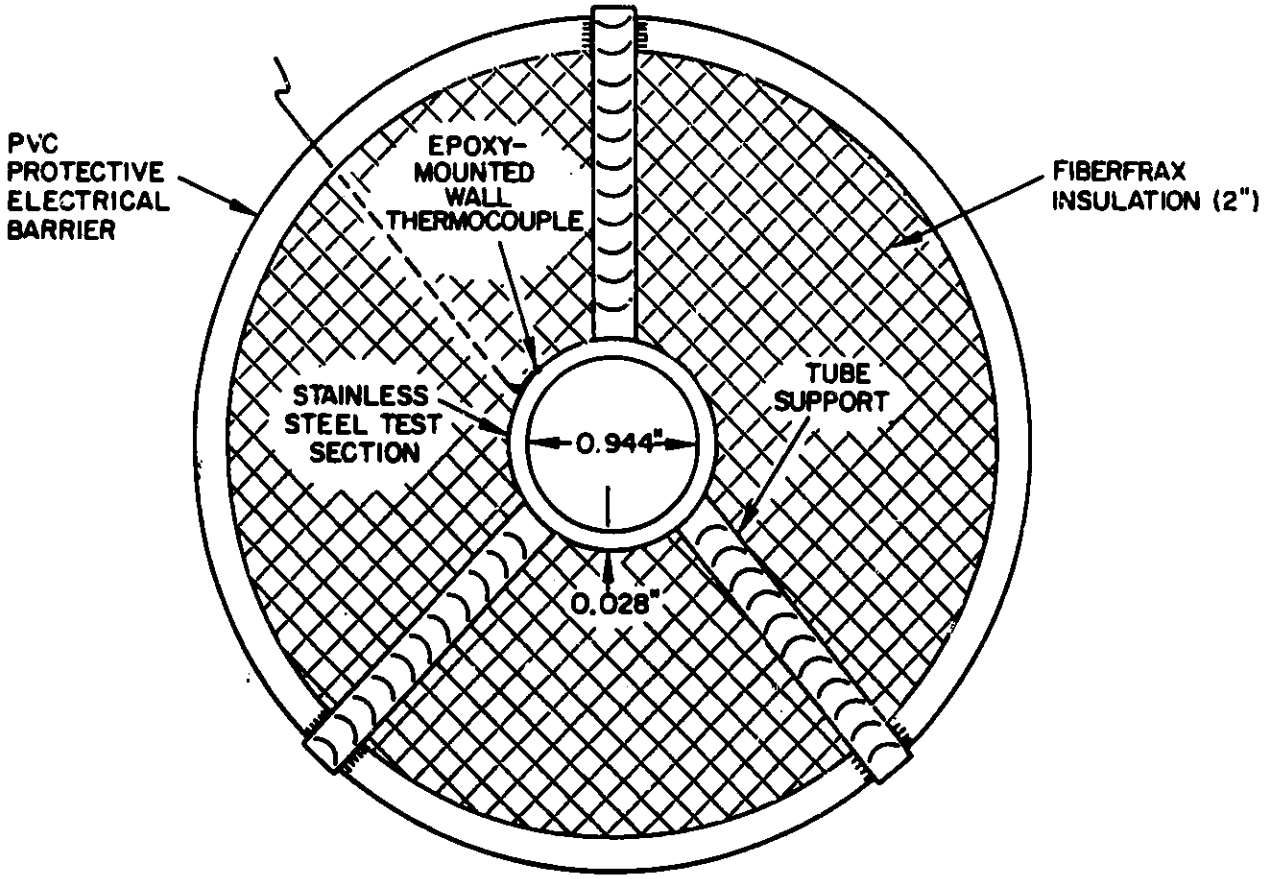

Fig. 4. End View of the Electrically Heated Test Section.

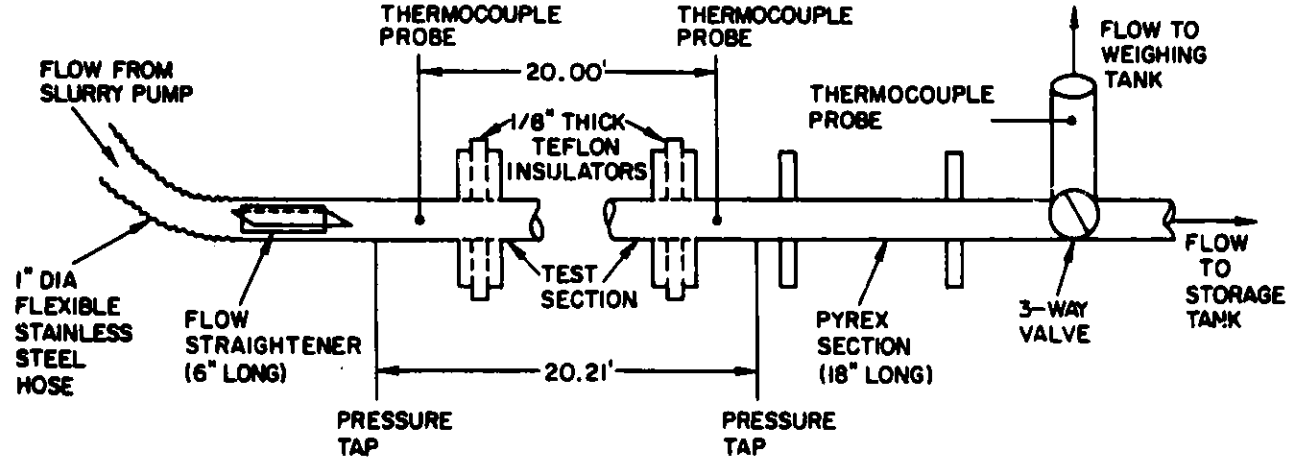

Fig. 5. Upstream and Downstream Connections to the Electrically Heated Test Section.

1.68×10^{-2} Btu/hr-ft-°F (2.9×10^{-2} W/m-°C) at 200°F (93°C). Two layers are used along the test section, for a total insulation thickness of 2.0 in. (50.8 mm). A protective PVC plastic tube surrounds the insulation and serves as an electrical safety barrier.

2.3 Measuring Instruments

The instrumentation for the electrically heated test section consists of 12 thermocouples and 6 voltage taps, all mounted on the tube's outer wall as shown in Fig. 3. Eleven of the thermocouples are attached to the top of the tube with a thermally conducting, electrically insulating epoxy. Among these 11 thermocouples, the 9 interior thermocouples are spaced 1.97 ft (0.6 m) apart along the length of the test section. The two outer thermocouples (TC1 and TC11) are positioned approximately 0.42 ft (0.13 m) from the ends of the tube. This arrangement is necessary because copper lugs are brazed to each end of the test section to allow connection of the electrical power supply cables to the test section.

The twelfth thermocouple is mounted directly on the bottom of the outer tube wall without epoxy (Fig. 3). This thermocouple is placed at the same axial location as the central thermocouple (TC6). This twelfth thermocouple provides information on both the temperature drops through the epoxy patches and the magnitude of circumferential temperature differentials on the tube. Also shown in Fig. 3 are six voltage taps. These are spot welded to the surface of the test section. The voltage taps are positioned evenly, 3.94 ft (1.2 m) apart, along the length of the test section. Their axial locations correspond to the axial locations of alternate surface thermocouples. The presence of six voltage taps allows measurement of local power input into each segment of the test section for calculation of local heat transfer and provides information on the uniformity of the electrical heating.

The overall pressure drop across the test section is measured by pressure taps. The pressure taps are placed before and after the test section (see Fig. 5) and are separated by a distance of approximately 20 ft (6.1 m). Two thermocouples are inserted into the flow stream entering and leaving the test section to monitor the inlet and outlet flow temperatures for calculation

of overall heat transfer. One additional thermocouple is placed in the flow stream at the exit of the test section to measure the mixture temperature as it enters the weighing tank. An additional thermocouple is placed ~10 ft (3 m) downstream of the test section and inside the weighing tank to check the overall average mixture temperature. The temperature of fluids inside the supply tank is monitored by six thermocouples positioned vertically on a support rod. A safety interlock is connected to the power supplies to prevent overheating of the test section in the event of flow stoppage. If the temperature, measured with a thermocouple mounted on the tube wall near the exit of the test section, exceeds a preset limit of ~220°F (104°C), the safety interlock will automatically shut down the power supplies.

All test data are recorded by a Fluke Model 2285B Data Logger. The data recorded include temperature, pressure drop, flow rate, and electrical power input to the test section. The data logger automatically scans a series of channels and records the test data at regular, preselected time intervals during a given test run.

2.4 Piping System

The plumbing upstream of the test section from the pump and downstream from the test section to the weighing or discharge tanks is illustrated in Fig. 5. A short section of straight pipe upstream of the test section contains a flow straightener that has two perpendicular stainless steel vanes. This section of pipe is connected to the pump by a 3-ft (0.91-m) section of flexible stainless steel hose with an I.D. of 1.0 in. (25.4 mm). A section of Pyrex glass tubing, 1.5 ft (0.46 m) long, is connected downstream of the test section for flow visualization. Downstream of the glass, a three-way valve enables the flow to be diverted from the discharge tank into the weighing tank for measuring slurry mass flow rates. The flow diversion is accomplished with a single-control handle that simultaneously opens and closes two valves to avoid stopping the flow in the test section.

3. EXPERIMENTAL PROCEDURES AND DATA ACQUISITION

Four types of experiments were conducted: (a) pressure drop and heat transfer reference tests with pure water, 0% particle loading; (b) pressure

drop and heat transfer tests with a slurry of water and X-HDPE particles without phase change; (c) pressure drop tests on ice slush slurries; and (d) pressure drop and heat transfer tests on combined-concept fluids comprising X-HDPE particles and Separan, a friction-reducing additive. X-HDPE slurries with two particle sizes, 1/8-in. and 1/20-in. diameter, were tested over a wide range of particle volumetric loadings (0-45%) and flow rates. For these non-melting tests, the fluid temperature in the supply tank was maintained slightly above the ambient temperature.

3.1 Test Procedures

The procedure for performing a pressure drop and heat transfer test is as follows:

(1) The supply tank is first filled, by direct weighing, with X-HDPE particles and water in the proportions required to achieve a desired particle volumetric loading, e.g., 5%, 15%, 25%, 30%, 35%, or 45%.

(2) The mixer and electric heater in the supply tank are turned on. The temperature of the mixture at three levels inside the supply tank is monitored continuously for uniformity.

(3) The electric heaters in the supply tank are turned off when the slurry is heated to the desired test section supply temperature, normally 92°F (33°C). The mixer is continually operated to ensure that a homogeneous slurry flows through the test section. The required speed of the mixer depends on the particle loading and supply tank water level. Stronger mixing is required with an increased loading and tank water level. The mixing can also be monitored by visually examining the flow condition from the top opening of the supply tank.

(4) When the desired slurry temperature and uniform mixing are achieved in the supply tank, the slurry pump is turned on to start the flow through the test section. At this stage, the three-way valve at the test section exit directs the flow into the large discharge tank (see Fig. 2). At this time, the DC power supplies are switched on, and the voltage is adjusted as needed to achieve a given tube wall heat flux.

(5) During the process described in (4), the data logger scans all data channels. When a steady-state condition has been attained, i.e., the slurry temperature and tube pressure drop have reached steady values, the three-way valve is switched to divert the slurry flow into the weighing tank. At this stage, the flow rate, accumulation of mass in the weighing tank, and all other data are recorded at regular intervals (e.g., every 15 sec).

(6) After enough data have been recorded from the data logger, i.e., after four continuous steady readings of mass flow rates, the flow is diverted back into the discharge tank.

(7) After the flow is diverted into the discharge tank, the power supplies are shut off.

(8) At this time, the particles are removed from the weighing tank with a sieve. After all the particles are taken out of the weighing tank, a single scan on the data logger is activated to record the water weight accumulated during the test.

(9) Because the just-removed particles are wet, a correction factor is used to account for the film of water left on the particles. The correction factor is defined as the ratio of the dry particle weight to the wet particle weight. A simple method for deriving this factor is to weigh a bucket of wet particles from the weighing tank. The dry particle weight is obtained when all particles in the bucket are dry. Normally, the correction factor is checked before and after a series of tests. The correction factor was found to have a nearly constant value of ~0.96 for the 1/8-in. particles and ~0.90 for the 1/20-in. particles. With this information, the dry particle weight can be computed and later used to calculate the actual particle volumetric loading, ϕ, as follows:

$$\phi = \frac{M_{HDPE)dry}}{M_{HDPE)dry} + \frac{\rho_{HDPE}}{\rho_{H2O}} M_{H2O}} . \qquad (1)$$

This particle loading can be checked against the value obtained from the initial supply tank filling process.

(10) All particles collected from the discharge and weighing tanks are returned to the supply tank. Fresh water is added to the supply tank to make up for the water used in a test.

3.2 Test Conditions

A sample matrix of test conditions for the experiments with pure water is presented in Table 1. The flow rates in Table 1 correspond to the various speed settings on the slurry pump. The flow velocities, pressure drops, Reynolds numbers, and power inputs in Table 1 are calculated for fluid temperature rises of 10°F (5.5°C) and 20°F (11.1°C) across the test sections. For slurry flows without phase change, the power requirement for a given pump setting would be nearly the same as that for pure water. The calculations of flow velocities and Reynolds number are based on the properties of water at 100°F (38°C). A sample data scan taken during a heat transfer test with pure water and pump setting number 3 is presented in Table 2. The recorded average mass flow rate (channel 96), pressure drop (channel 57), total current (channel 50), total voltage (channel 98), total power input (channel 95), and bulk fluid temperature rise between inlet and outlet of the test section, measured 0.145 ft (0.044 m) from both ends of the test section (channels 32-20), approximate the desired test conditions shown in Table 1. The power inputs required for a bulk fluid temperature rise of 10-20°F in the test section will also result in a nominal inner-wall-to-bulk temperature drop of 10-20°F within the desired range of flow rates. The bulk fluid temperature rise in every segment of the test section can be computed very accurately on the basis of an energy balance calculation. The results from these tests are presented and discussed in Sections 4-6.

4. PRESSURE DROP AND FLOW CHARACTERISTICS OF PARTICULATE SLURRIES

As was mentioned previously, the advantage of using phase-change slurries in a DHC system is an increase in the total thermal energy transport and possibly the heat transfer coefficient at heat exchanger surfaces. On the other hand, the use of phase-change slurries may incur significant pumping power penalties if the slurries are not properly designed. The knowledge needed to design effective slurry transmission fluids is not available in the literature. This section presents pressure drop measurement results for

Table 1. Test Conditions for Pure-Water Heat Transfer Experiments*

Pump Setting	Flow Rate (gpm)	Flow Rate (lb/min)	Velocity (ft/s)	Pressure Drop (psi)	Re	Power (kW) ΔT = 10-20°F	Current (A) ΔT = 10-20°F	Voltage Drop (V) ΔT = 10-20°F
1	5.6	46.8	2.59	0.27	2.75×10^4	8.22-16.44	315-446	26.1-36.9
2	7.9	65.4	3.62	0.50	3.85×10^4	11.50-23.01	373-527	30.8-43.6
3	10.2	84.8	4.69	0.79	4.99×10^4	14.90-29.80	424-600	35.1-49.7
4	13.3	110.2	6.09	1.26	6.48×10^4	19.36-38.71	484-684	40.0-56.6
5	16.9	140.2	7.75	1.95	8.25×10^4	24.64-49.28	545-771	45.2-63.9
6	21.2	175.7	9.72	2.94	1.03×10^5	30.76-61.52	609-862	50.5-71.4
7	25.9	214.4	11.86	4.20	1.26×10^5	37.63-75.27	674-953	55.8-78.9
8	34.8	288.2	15.94	7.15	1.70×10^5	50.77-101.54	783-1107	64.8-91.7

*Based on properties of water at 100°F.

Table 2. Sample Data Scan Taken During a Pure-Water Heat Transfer Test

Channel No.	Parameter	Recorded Value
36	Supply Tank Temp. (Bottom)	92.02°F
37	Supply Tank Temp. (Middle)	91.64°F
38	Supply Tank Temp. (Top)	87.45°F
20	Fluid Temp. at Test Section Inlet	91.62°F
21	Wall Temp. (TC1)	108.11°F
22	Wall Temp. (TC2)	111.58°F
23	Wall Temp. (TC3)	113.44°F
24	Wall Temp. (TC4)	115.51°F
25	Wall Temp. (TC5)	117.93°F
26	Wall Temp. (TC6)	119.26°F
27	Wall Temp. (TC7)	121.05°F
28	Wall Temp. (TC8)	122.99°F
29	Wall Temp. (TC9)	124.63°F
30	Wall Temp. (TC10)	126.46°F
31	Wall Temp. (TC11)	127.70°F
32	Fluid Temp. at Test Section Outlet	110.14°F
33	Fluid Temp. at Weighing Tank Inlet	110.69°F
35	Bare-Wall Temp.	124.28°F
50	Current	596.99 A
51	Voltage Drop Across Sec. 1	9.190 V
52	Voltage Drop Across Sec. 2	10.039 V
53	Voltage Drop Across Sec. 3	10.050 V
54	Voltage Drop Across Sec. 4	10.071 V
55	Voltage Drop Across Sec. 5	9.239 V
56	Updated Mass	197.33 lb
57	Pressure Drop	0.8012 psi
90	Power in Sec. 1	5486.3 W
91	Power in Sec. 2	5993.2 W
92	Power in Sec. 3	5999.8 W
93	Power in Sec. 4	6012.3 W
94	Power in Sec. 5	5515.8 W
95	Total Power In	29007 W
96	Mass Flow	92.212 lbm/min
98	Total Voltage	45.589 V

X-HDPE slurries with two particle sizes and a wide range of particle loadings (0-45%) and flow rates, and for ice slush slurries. Existing correlations for slurry pressure drop and viscosity are compared with the measured data. The effect of particle loading and size on pressure drop behavior is discussed, and several important new observations on slurry behavior are presented.

4.1 Pressure Gradient and Friction Factor for a Single-Phase Newtonian Pipe Flow

For a fully developed flow in a smooth pipe, the pressure gradient can be expressed as

$$-\frac{dp}{dx} = f\,\frac{\rho\, U_{av}^2}{2D} \tag{2}$$

where U_{av} is the mean velocity of the pipe flow and f is the friction factor. According to Hagen-Poiseville theory [13], the friction factor for laminar flow decreases monotonically with an increasing Reynolds number and can be expressed as

$$f = \frac{64}{Re} \qquad (Re < 2300) \tag{3}$$

with

$$Re = \frac{U_{av} D}{\nu}\ .$$

For fully developed turbulent flow in circular pipes, the friction factor, f, is normally determined by empirical relations based on experimental results. Commonly, it is expressed as inversely proportional to Reynolds number to a power of 1/n where n is an integer greater than 1. A number of empirical correlations have been developed that can be applied to different ranges of Reynolds numbers. The famous Blasius equation [13] has the simplest form and can approximate the friction factor with a smooth pipe surface condition:

$$f = 0.3164\ Re^{-1/4} \qquad (Re \le 2 \times 10^4). \tag{4}$$

The Knudsen and Katz equation [14] is considered to provide good agreement with experimental results over the higher range of Reynolds numbers:

$$f = 0.184\ Re^{-1/5} \qquad (Re > 2 \times 10^4). \tag{5}$$

Other correlations with more complex forms can be used to cover the full range of turbulent flow. Typical equations are given by Nikuradse [15],

$$\sqrt{f} = 2.0 \log\left(\frac{Re}{2}\sqrt{f}\right) - 0.2\ , \tag{6}$$

and Drew et al. [16],

$$f = 0.0056 + 0.50\ Re^{-0.32}. \tag{7}$$

As a check on the experimental apparatus and data handling, pressure drop data for pure water were compared with values calculated from Eq. (5). Figure 6 shows excellent agreement between the empirical correlation and measured results over the Reynolds number range of 3×10^4 to 2×10^5 for a temperature rise of about 20°F (11.1°C) across the test section.

4.2 Slurry Pressure Drop Measurements

4.2.1 Pressure Drop Data for X-HDPE Slurries

The measured pressure drop for slurry with 1/8-in. (3.2-mm)-diameter particles and with various flow rates and particle loadings is shown in Fig. 7. The maximum flow rates obtained for slurry tests at high particle loadings were less than that obtained for pure water, owing to a pump "choking effect" at higher flow rates. In general, the pressure drop for a given mass flow rate increases as the particle loading increases. Figure 8 shows the pressure drop penalty expressed as the percentage increase in pressure drop relative to that of pure water. The pressure drop associated with the presence of particles is obviously not greatly increased over that of water at the same mass flow rate if the particle loading is less than 30%. However, when particle loading is 30% or greater, the increase in the pressure drop jumps considerably.

Figure 8 also shows that (a) the percent pressure drop increase over that for pure water remains fairly constant for moderate to high flow rates and (b) the pressure drop increases considerably as the slurry flow

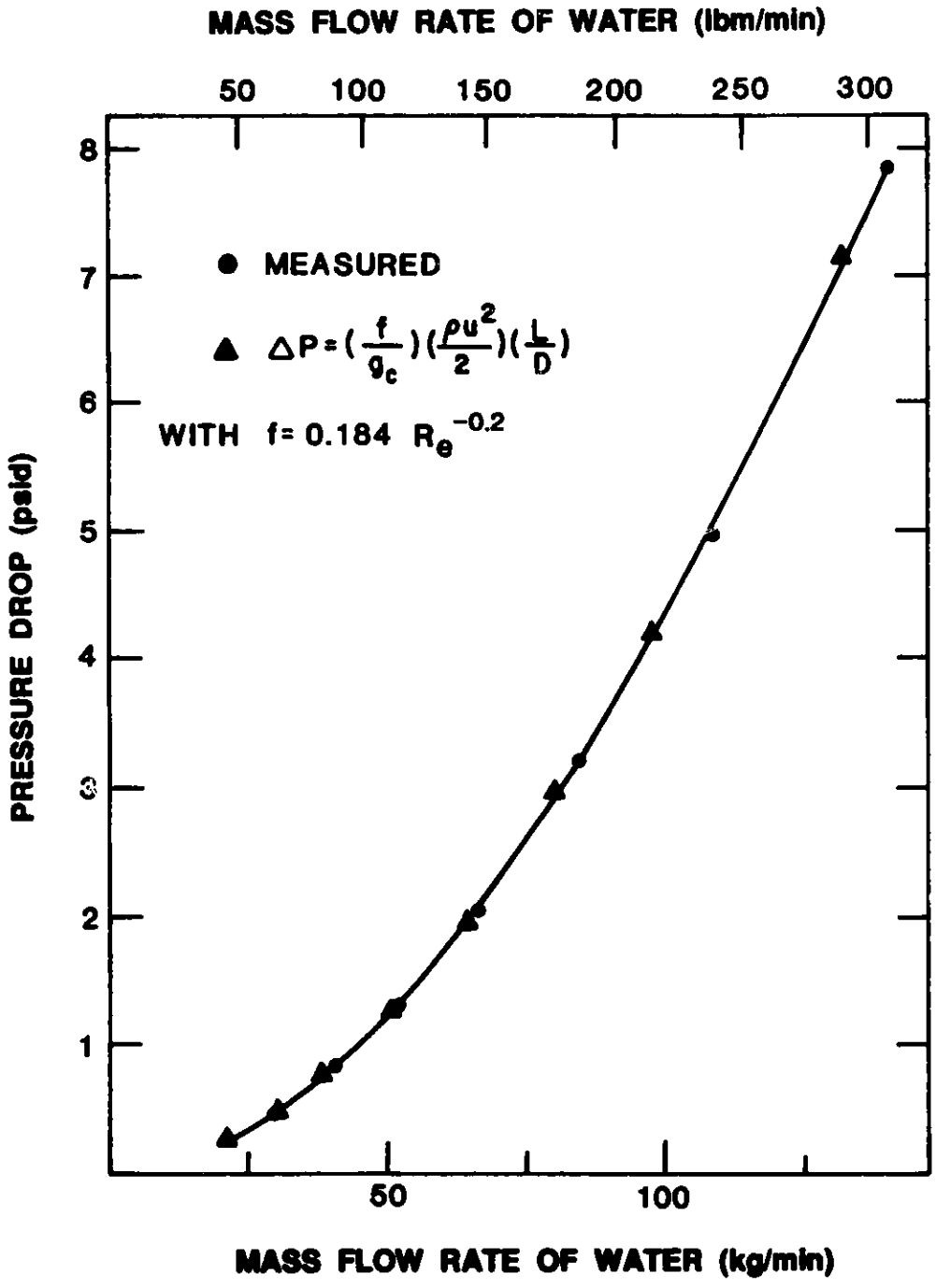

Fig. 6. Comparison of Correlated and Measured Pressure Drop Data for Pure Water.

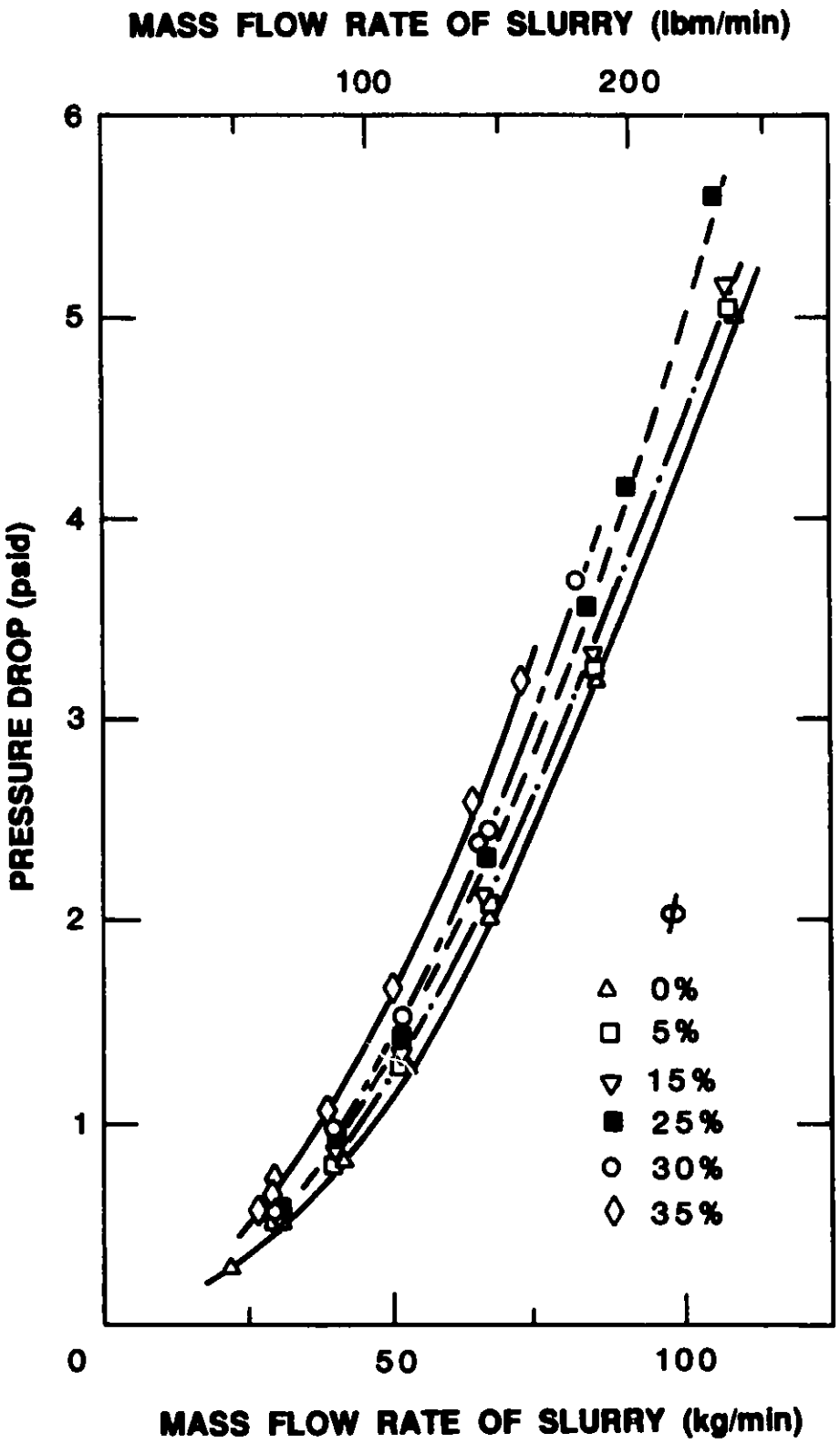

Fig. 7. Pressure Drop Measurements at Different Slurry Mass Flow Rates and Particle Volumetric Loadings for Slurry with 1/8-in.-Diameter Particles.

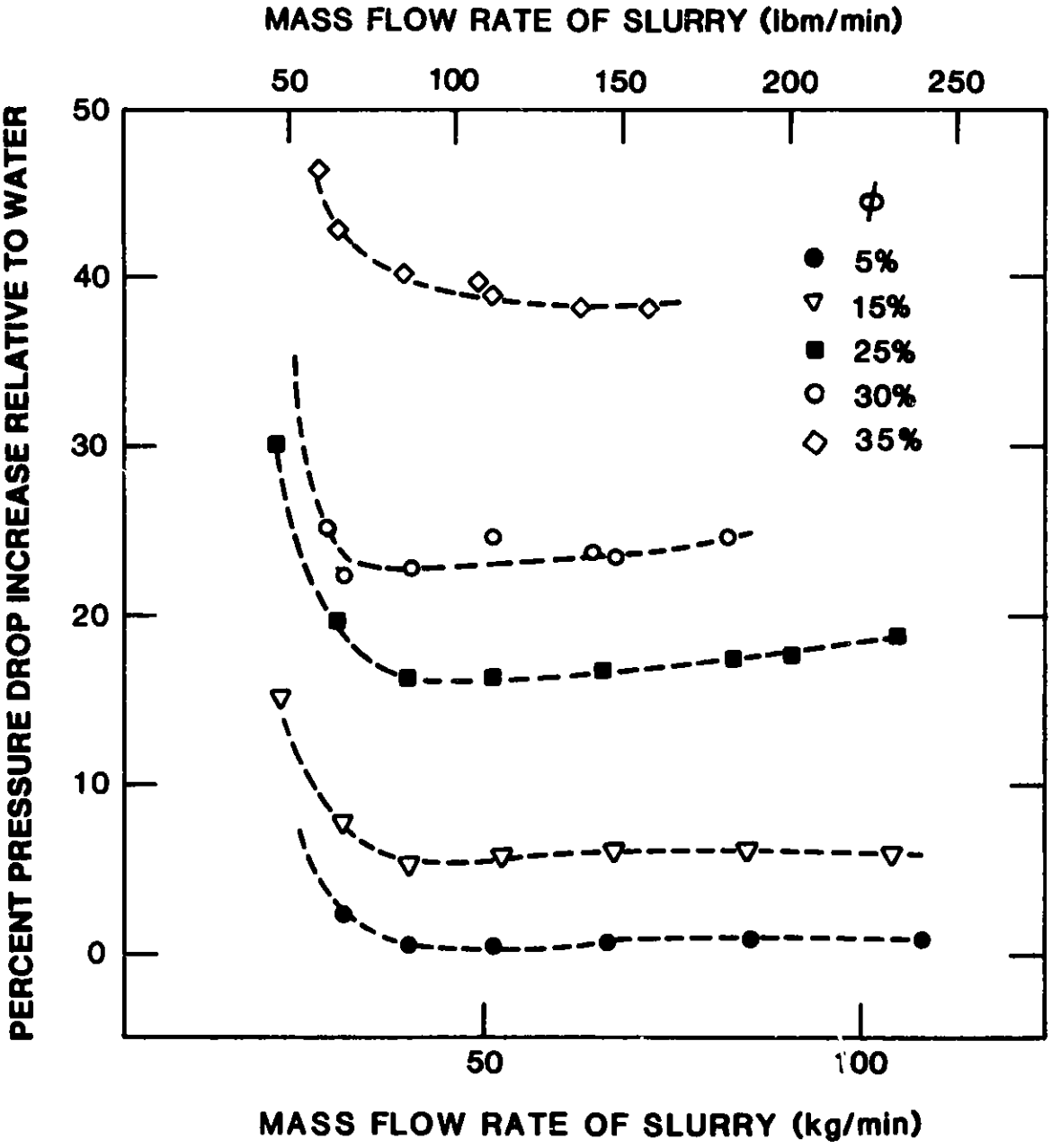

Fig. 8. Effect of Particle Loading on Percent Pressure Drop Increase for Slurries with 1/8-in.-Diameter Particles at Different Flow Rates.

rate becomes low, i.e., <70-80 lbm/min (32-36 kg/min). This observation confirms previously reported results [4]. The reason for this behavior is believed to be the particle stratification that occurs when less dense particles accumulate in the top of the pipe at a low flow rate.

A visual observation of the flow pattern at a low flow rate confirmed the particle stratification. In this stratified region, highly concentrated slurry that clusters near the upper portion of the pipe wall results in increased friction, as does the sedimentation occurring in the flow of dense suspensions. At high flow rates, strong turbulent mixing produces a homogeneous slurry. The prediction of pressure drop and onset of stratification will be discussed in detail later.

The percent pressure drop increase relative to water for X-HDPE slurry with 1/20-in. (1.3-mm)-diameter particles is shown in Fig. 9. As in the case of 1/8-in. particles, the percent pressure drop increase for the 1/20-in. particles reaches a plateau for moderate to high flow rate. But, surprisingly, the flow rate required to attain a constant pressure drop penalty with the smaller particles is found to be greater than that for the larger particles (Fig. 8). In contrast to the modest pressure drop increase relative to water for slurry with 1/8-in.-diameter particles for $\phi \leq 25\%$, a pressure drop decrease relative to water was found for slurry with 1/20-in.-diameter particles in the nonstratified homogeneous flow regime for $\phi \leq 25\%$ and at a mass flow rate greater than 120 lbm/min (55 kg/min). This pressure drop reduction relative to water for the 1/20-in. particles is significant and shows that particle size is an extremely important parameter in designing slurries for DHC.

In order to investigate the influence of particle loading and size on the slurry pressure drop behavior, a series of tests was conducted for slurries with both 1/8-in. and 1/20-in.-diameter particles and at a constant mass flow rate of ~140 lbm/min (64 kg/min). Figure 10 presents the data for percent pressure drop increase relative to water for both particle sizes over a wide range of particle loadings, 0-45%. Some similarities and considerable differences can be seen between the slurry test results for the two particle sizes. They are summarized as follows:

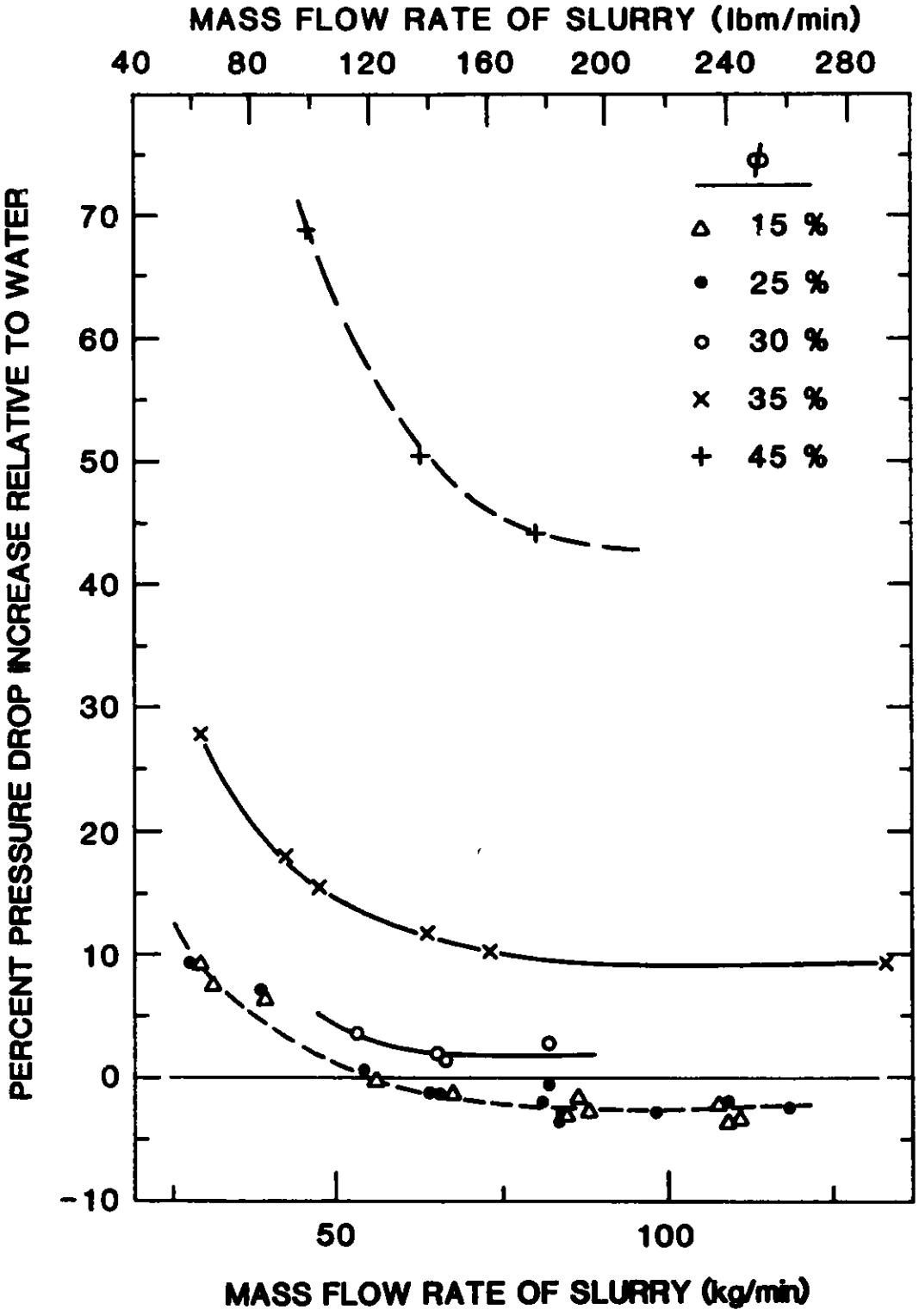

Fig. 9. Effect of Particle Loading on Percent Pressure Drop Increase for Slurries with 1/20-in.-Diameter Particles at Different Flow Rates.

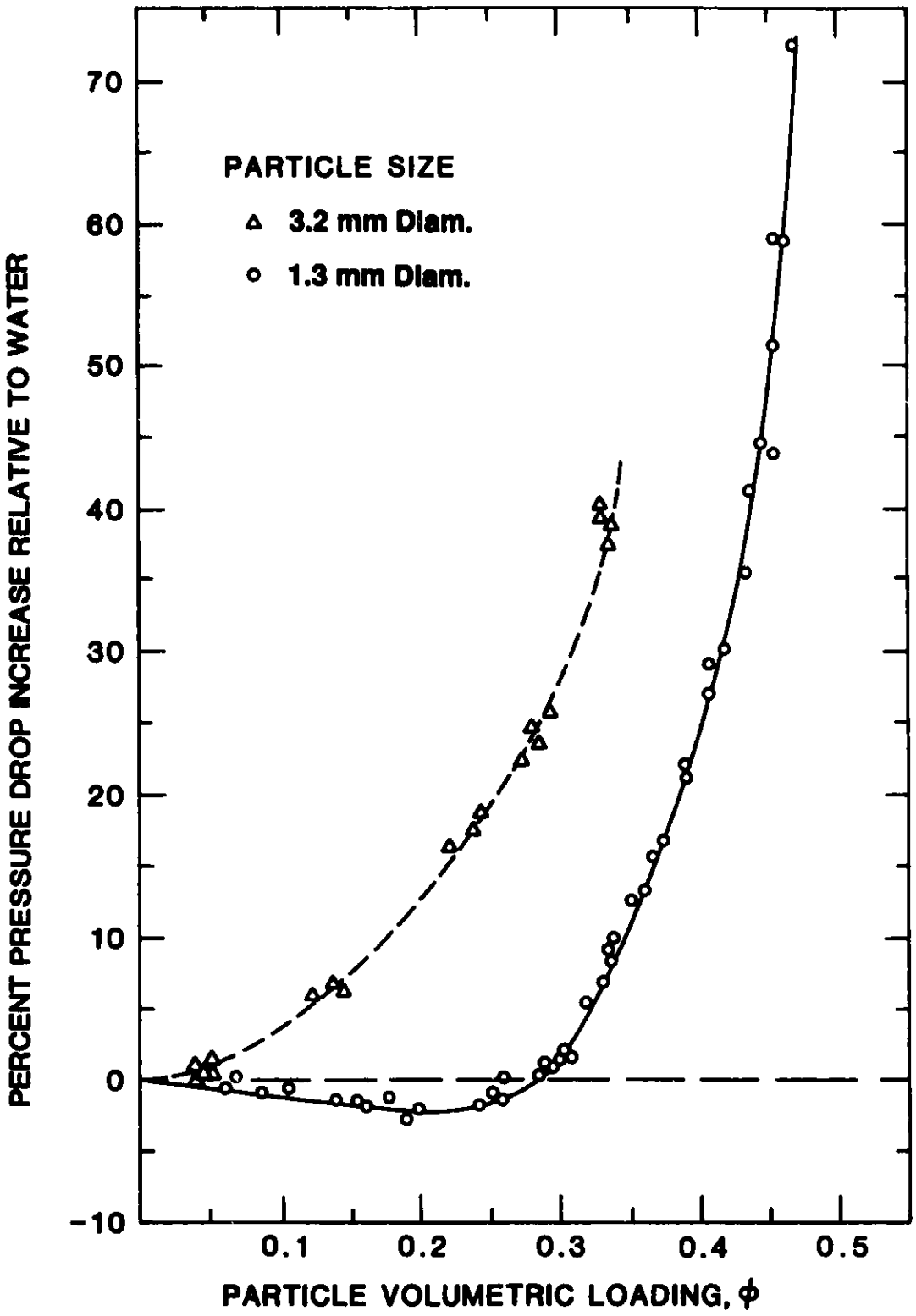

Fig. 10. Effect of Particle Size and Loading on Percent Pressure Drop Increase Relative to Water.

(1) A pressure drop reduction phenomenon is observed for the slurry with 1/20-in. particles. The pressure drop reduction exists for a wide range of particle loadings, 0-30%. For the slurry with 1/8-in. particles, only a very small pressure drop reduction was observed for very dilute suspensions, $\phi < 5\%$.

(2) Only a modest pressure drop increase relative to water was found for the slurry with 1/8-in. particles at particle loadings of less than 25%. At all loadings, the large-particle slurry exhibited a considerably greater pressure drop penalty than the small-particle slurry.

(3) The pressure drop penalty increases sharply when particle loading is greater than 30% for the slurry with large particles and 40% for the slurry with small particles. The behavior of pressure drop at high particle loadings is also illustrated in Fig. 11, which is a log-log plot of a portion of the data in Fig. 10.

4.2.2 Pressure Drop Data for Ice Slush Slurries

In the present investigation, limited tests were conducted in a preliminary study of pumpability and pressure drop behavior of an ice slurry. The ice slurry was produced by adding dry ice to the water in the supply tank to cool it to 32°F (0°C) and then adding crushed ice obtained from a commercial ice maker. The ice slush particle size ranged from 1/8 in. (3.2 mm) to 1/2 in. (12.7 mm). As the ice slush was pumped through the ANL Slurry Heat Transfer Test Facility, it appeared to flow in the form of ice flake clusters. The ice volume fraction was estimated to be less than 10%. The pressure drop reduction relative to pure water was found to be 3-5%.

An ice slurry generation and distribution system was used at the CBI Research Co. [17] to determine the effect of ice fraction and flow rate on pressure drop. The dimension of the ice crystals in the CBI tests was not well controlled or determined. Agglomeration of the ice slush, similar to that observed at ANL, was reported. The pressure drop reduction obtained at CBI for ice slurry compared to water was as high as 35% in a 2-in.-diameter

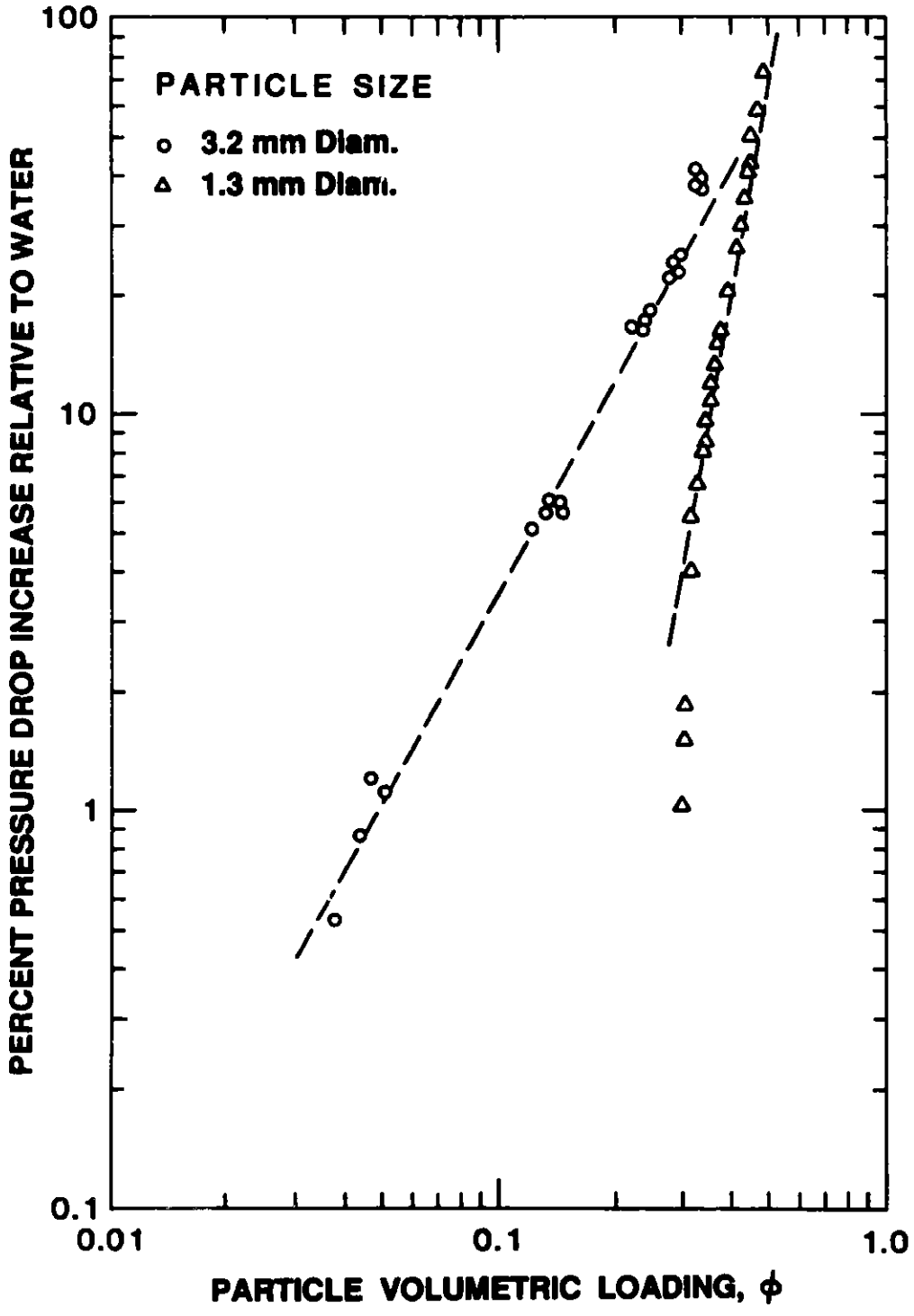

Fig. 11. Log-Log Plot of Effect of Particle Size and Loading on Percent Pressure Drop Increase Relative to Water.

pipe section at an ice fraction of 14-15%. A lower pressure drop reduction, 13-15%, was measured in a 6-in.-diameter pipe section at an ice fraction of 10-11%.

In summary, both ANL and CBI report a pressure drop reduction relative to water with ice slurry flows. The results obtained at ANL (with a smaller ice fraction than that used at CBI) show less pressure drop reduction relative to water compared to that obtained by CBI. The dependence of this pressure drop reduction on crystal size, loading, and pipe diameter is not known.

4.3 Slurry Relative Viscosity and Comparison with Rheological Literature

Over the past four decades, a number of correlations and semiempirical equations have been developed for predicting the viscosity of solid particles suspended in a Newtonian fluid. Predictions of slurry viscosity are used frequently by engineers to calculate slurry pressure drop from friction factor versus Reynolds number correlations. However, as shown below, this approach is not satisfactory for the type of slurries being developed for DHC. Most of the approaches to date attempt to extend Einstein's equation [18] for apparent viscosity of a two-phase mixture containing suspended spheres:

$$\mu = \mu_c(1 + 2.5\phi) \tag{8}$$

where μ_c is the viscosity of the carrier fluid and ϕ is the volume fraction of the solids. This equation only applies to very dilute suspensions because it assumes no mutual hydrodynamic interaction between particles. Subsequent studies of the rheology of suspensions have led to many theories and functional equations for the apparent viscosity of suspensions [19-27]. Several excellent reviews of this subject are available [26-29]. Some typical equations are listed in Table 3. In the review article by Rutgers [26], 97 effective-viscosity correlations were analyzed; some of the correlations were plotted by Rutgers and are reproduced in Fig. 12. Figure 12 clearly indicates a broad scatter among different correlations. Rutgers proposed an "average" curve, labeled 1 in Fig. 12, which was constructed on the assumption that the data scatter was due to experimental error. Later, Thomas [23] attempted to develop an improved correlation based on the experimental data shown in

Table 3. Functional Equations for Apparent Viscosity of Suspensions

Equation No.	Equation	Source and Remarks
8	$\mu = \mu_c(1 + 2.5\phi)$	Einstein [18]
9	$\mu = \mu_c \exp\left[\frac{k_1\phi + \theta(k_2 - k_1)\phi^2}{1 - B\phi}\right]$ $k_1 = 2.5,\ k_2 = 3.175,\ \theta = 4,\ B = 0.609$	Vand [24] (applicable to high concentration)
10	$\mu = \mu_c \exp\left[\frac{2.5\phi}{1 - S\phi}\right]$ S is crowding factor; $1.35 < S < 1.91$	Mooney [21]
11	$\mu = \mu_c \frac{1}{(1 - \phi)^{2.5}}$	Brinkman [25]
12	$\mu = \mu_c\left[1 + 2.5\beta\phi + 2.5(\beta\phi)^2 + B'\frac{\phi^2}{(\alpha K)^5}\right]$ B' is a function of α and β	Jeffery & Acrivos [22]
13	$\mu = \mu_c[1 + 2.5\phi + 10.05\phi^2 + 0.00273 \exp(16.6\phi)]$	Thomas [23]

Fig. 13a. He analyzed experimental data with particle size ranging from 0.1 to 435 μm. A broad scatter of the data (±75%) was found at a volume fraction of 50%. Thomas recognized that factors other than the volume fraction of solids influenced the slurry viscosity and obtained a reduced relative viscosity through various extrapolation procedures. He derived an empirical correlation for slurry relative viscosity, Eq. (13) in Table 3, and compared that with the reduced data in a plot reproduced in Fig. 13b. It is interesting to note that Thomas's equation does not agree well with Rutgers's equation.

In all the empirical correlations reported to date, the slurry viscosity has been expressed as a sole function of volume fraction of particles. Other variables such as particle shape, size, and size distribution were not taken into consideration. Because it is simple and easy to use, the empirical relation due to Thomas has been widely quoted [22,27-29]

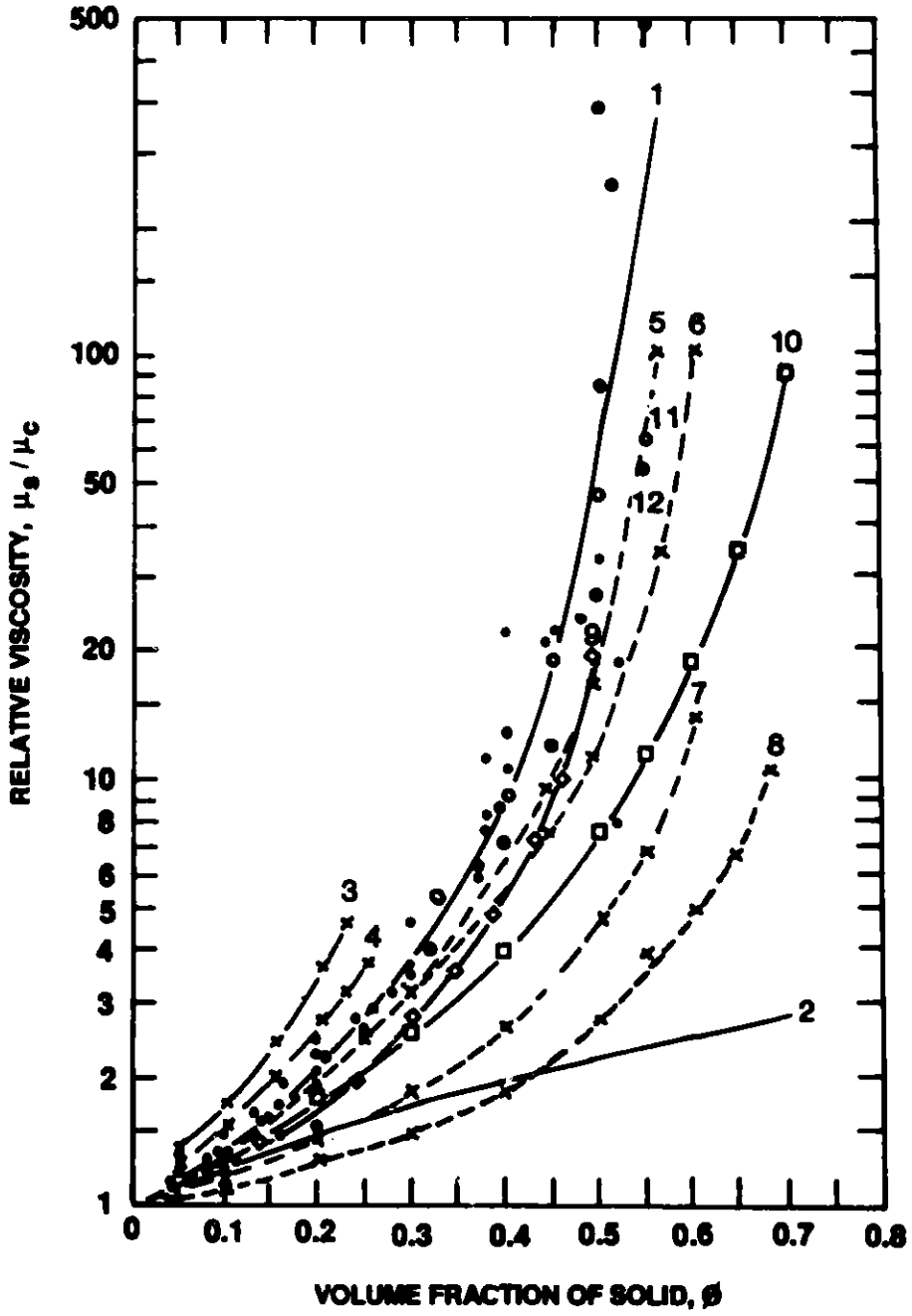

Fig. 12. Slurry Relative Viscosity Data Collected by Rutgers [26] and Plotted Against Volume Fraction. Curve 1 is Rutger's average curve. Explanations of the other curves can be found in the original paper.

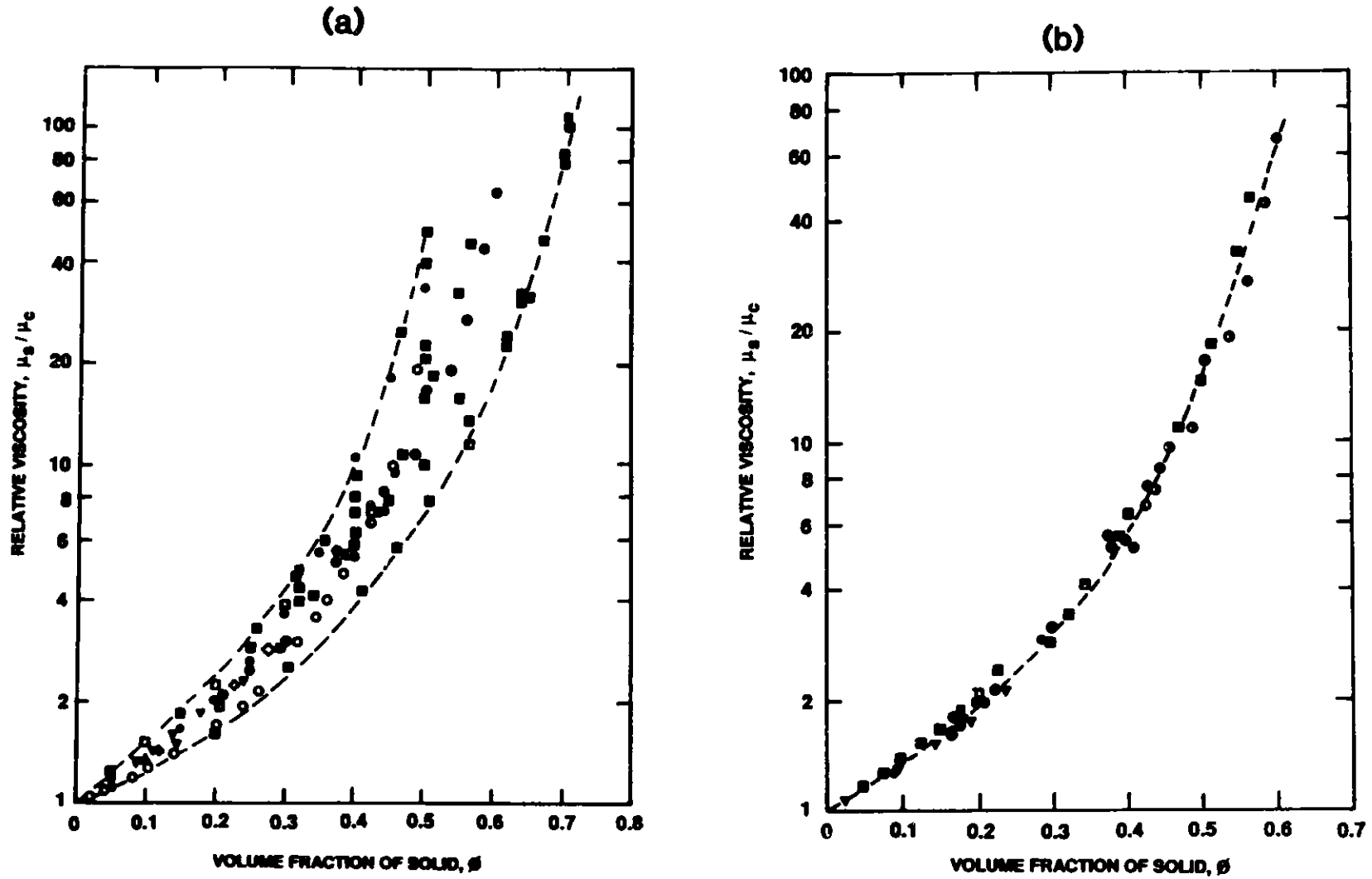

Fig. 13. Slurry Relative Viscosity Data Collected by Thomas [23] and Plotted Against Volume Fraction. (a) Raw data; (b) reduced data, compared with Eq. (13). Explanations of the symbols can be found in the original paper.

and recommended [30] for engineering applications. However, the following comparison of ANL X-HDPE data with Thomas's correlation indicates that the latter is of little value for DHC slurries.

If an analogy between turbulent single-phase and turbulent two-phase slurry pipe flow is assumed to exist, then the friction factor of the slurry flows can be expressed as the inverse 1/5th power of the slurry Reynolds number or the 1/5th power of slurry viscosity [see Eq. (5)]. Therefore, the viscosity of the slurry relative to that of pure water, μ_s/μ_w, can be expressed as the fifth power of the ratio of pressure drop measured for the slurry to that measured for pure water. This experimentally determined relative viscosity can then be compared with that estimated from the correlation by Thomas [23], as shown in Fig. 14. Surprisingly, the agreement for the slurry with 1/8-in.-diameter particles is fairly good except for the data at 35% particle volumetric loading. It is interesting to note that the simple relative-viscosity empirical relation due to Thomas was derived from a data base with a particle size ranging from 3.9×10^{-6} to 0.017 in. (0.1 to 435 μm); the present X-HDPE particle size of 1/8 in. (3175 μm) is considerably outside this range.

A similar approach was applied to obtain the slurry relative-viscosity relationship for X-HDPE slurry with 1/20-in.-diameter particles. The relative viscosities for both slurries are presented in Fig. 15. Obviously, a substantial discrepancy exists between Thomas's correlation and the data obtained for 1/20-in.-diameter particles. Significantly, the Thomas correlation as well as other empirical correlations did not account for particle size effects or the friction reduction phenomenon observed in the present slurry tests with the smaller particles. Furthermore, at high particle volumetric loading (35% for the 1/8-in.-diameter particles), the sudden sharp increase of the relative viscosity seems to suggest a mechanistic change of flow regime which was also not accounted for by the Thomas-type empirical correlations.

4.4 Pressure Drop Correlations and Transition Velocity for Slurry Transport

Most of the recent attempts at developing pressure drop correlations for slurry pipe flow can be traced to the form originally proposed by Durand

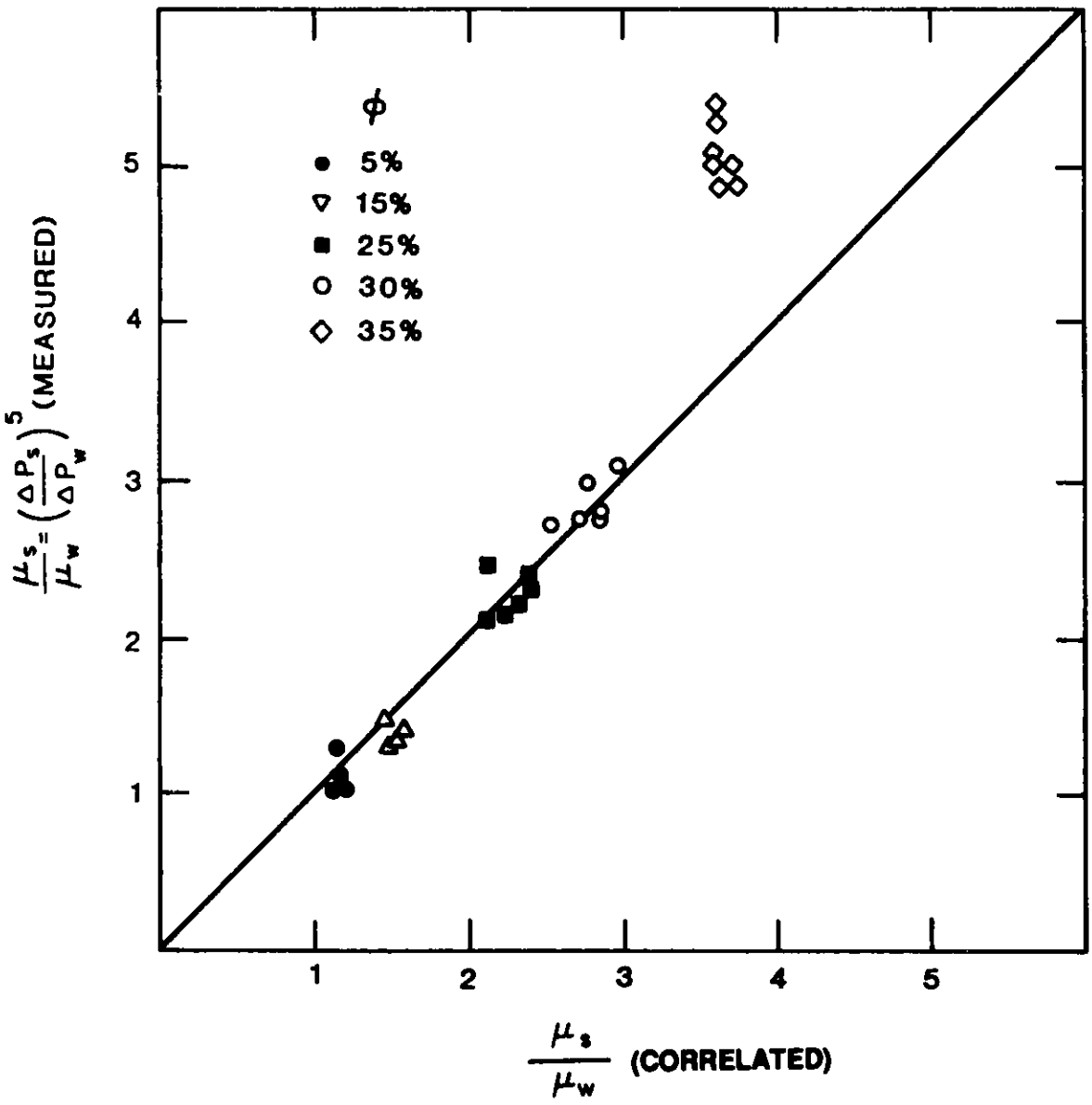

Fig. 14. Comparison of Relative Viscosity Predicted by Thomas's Correlation [23] and Measured Data for Slurries with 1/8-in.-Diameter Particles.

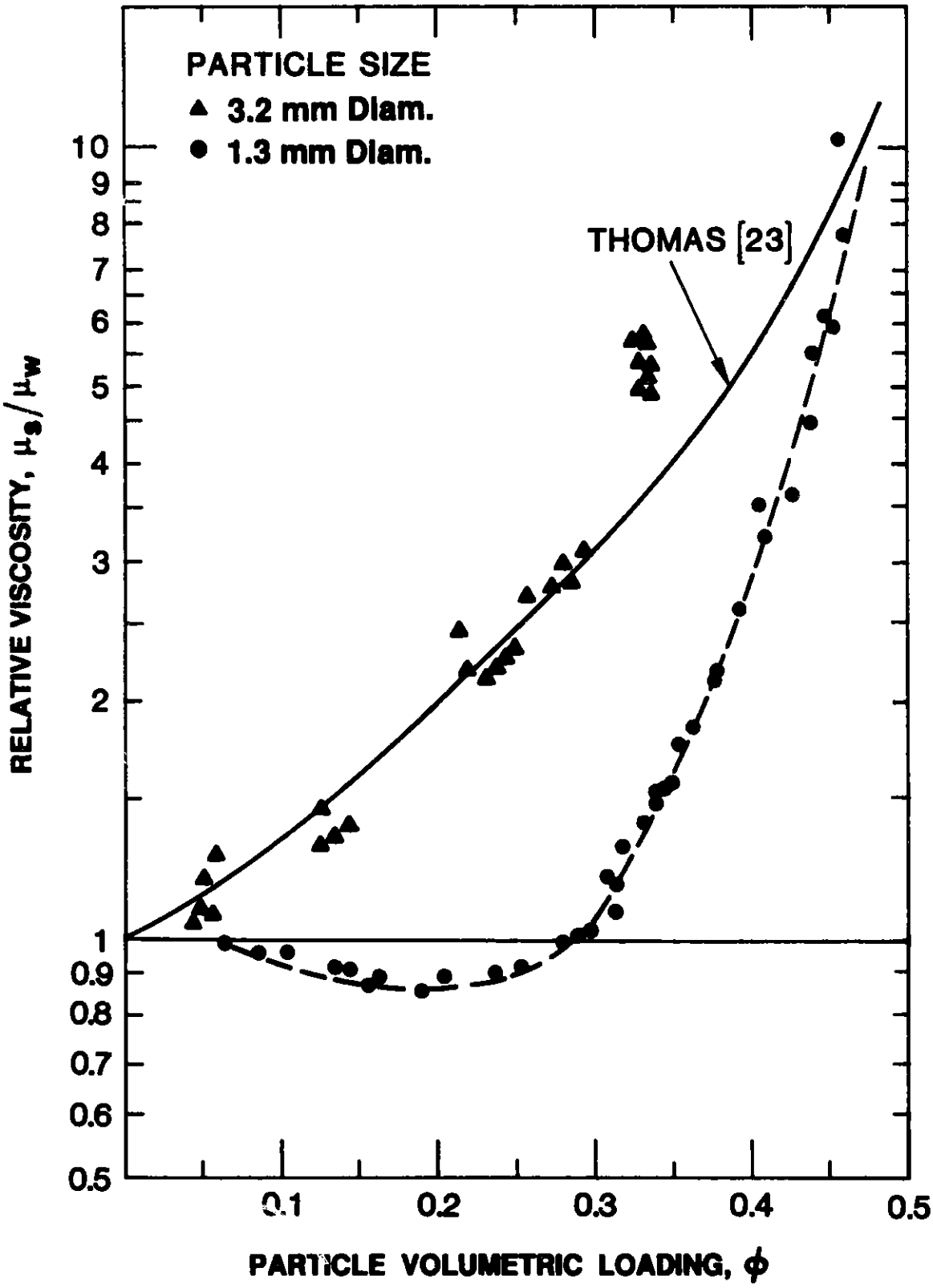

Fig. 15. Effect of Particle Size and Loading on Slurry Relative Viscosity.

and co-workers [31-33] in the early 1950s. They expressed the frictional loss in non-dimensional form by

$$\frac{i - i_c}{i_c} = K \phi [Fr \sqrt{C_D}]^m \tag{14}$$

where i and i_c are the head losses for slurry pipe flow and for pure carrier fluid, respectively; K and m are empirical constants (m is negative); ϕ is the solid volume fraction; C_D is the drag coefficient for a single particle in an infinite medium at the terminal velocity, defined by

$$C_D = \frac{4}{3} \frac{gD_p(s - 1)}{U_\infty} \tag{15}$$

where s is the specific gravity of the slurry particles; and Fr is a modified Froude number, which may be interpreted as the ratio of inertia forces to gravity forces based on the pipe diameter and the solid-liquid density difference:

$$Fr = \frac{U^2}{gD(s - 1)} . \tag{16}$$

The presence of the Froude number suggests that this type of friction loss correlation is focused on the pressure drop due to maintaining the particles in suspension as a result of the density difference between the particles and the carrier fluids. Subsequent improvements of this form of correlation include (a) establishing different regimes with different sets of empirical constants (Zandi and Govatos [34], Babcock [35], Turian and Yuan [36]) and (b) establishing the power-law forms for the ϕ and C_D dependence (Turian and Yuan [36]). The correlations proposed by Turian and Yuan in 1977 appear to be the latest development. They developed four pressure drop correlations for each of the following four flow regimes: flow with a stationary bed, saltation flow, heterogeneous flow, and homogeneous flow. The correlation for the homogeneous-flow regime, based on 645 data points involving mostly heavy particles ranging from sand to lead, but also including 20 data points with wood (s = 1.15), is given by

$$\frac{f - f_c}{f_c} = 0.844 \, \phi^{0.5024} \, f_c^{0.428} \, C_D^{0.1516} \, Fr^{-0.3531} . \tag{17}$$

This expression ceases to be valid at low Froude numbers, when the flow undergoes a gradual transition to the heterogeneous flow regime in which there is marked stratification due to gravity forces.

Turian and co-workers derived a transition Froude number [36] by comparing the above equation with a similar equation for the heterogeneous flow regime of the form

$$Fr_{23} = 0.2859 \frac{\phi^{1.075}}{f_c^{0.67} C_D^{0.9375}} \tag{18}$$

where the subscript 23 denotes the transition between regimes 2, heterogeneous flow, and 3, homogeneous flow. This transition Froude number is different from but clearly related to the critical Froude number, which pertains to the onset of fully suspended flow as distinguished from flow in the presence of a particulate bed. Turian, Hsu, and Ma [37] compared a large number of correlations with published and their own data, with relative density, s, up to 9 and volume fraction up to 56%. They concluded that the semi-theoretical critical Froude number expression of Oroskar and Turian [38] was the most reliable:

$$Fr_{crit} = [5\phi\ (1 - \phi)^3]^{16/15} \left[\frac{D\ \rho_c\ [gD\ (s - 1)]^{1/2}}{\mu_c}\right]^{2/15} . \tag{19}$$

In Fig. 16, the pressure drop and transition criterion predictions from Eqs. (17) and (18) for ϕ = 35% are compared with the present data for X-HDPE slurries of both particle sizes. The following observations can be made:

(a) The predicted pressure drop penalty is much smaller than the observed results with X-HDPE. Furthermore, Eq. (17) indicates a decreasing pressure drop penalty that approaches zero with increasing flow rate (Froude number), a trend not found in the experimental results. This suggests that at large solid volume fractions, there is an additional pressure drop penalty (most likely associated with particle-particle interactions) which is not related to the gravitational effect and, hence, is not

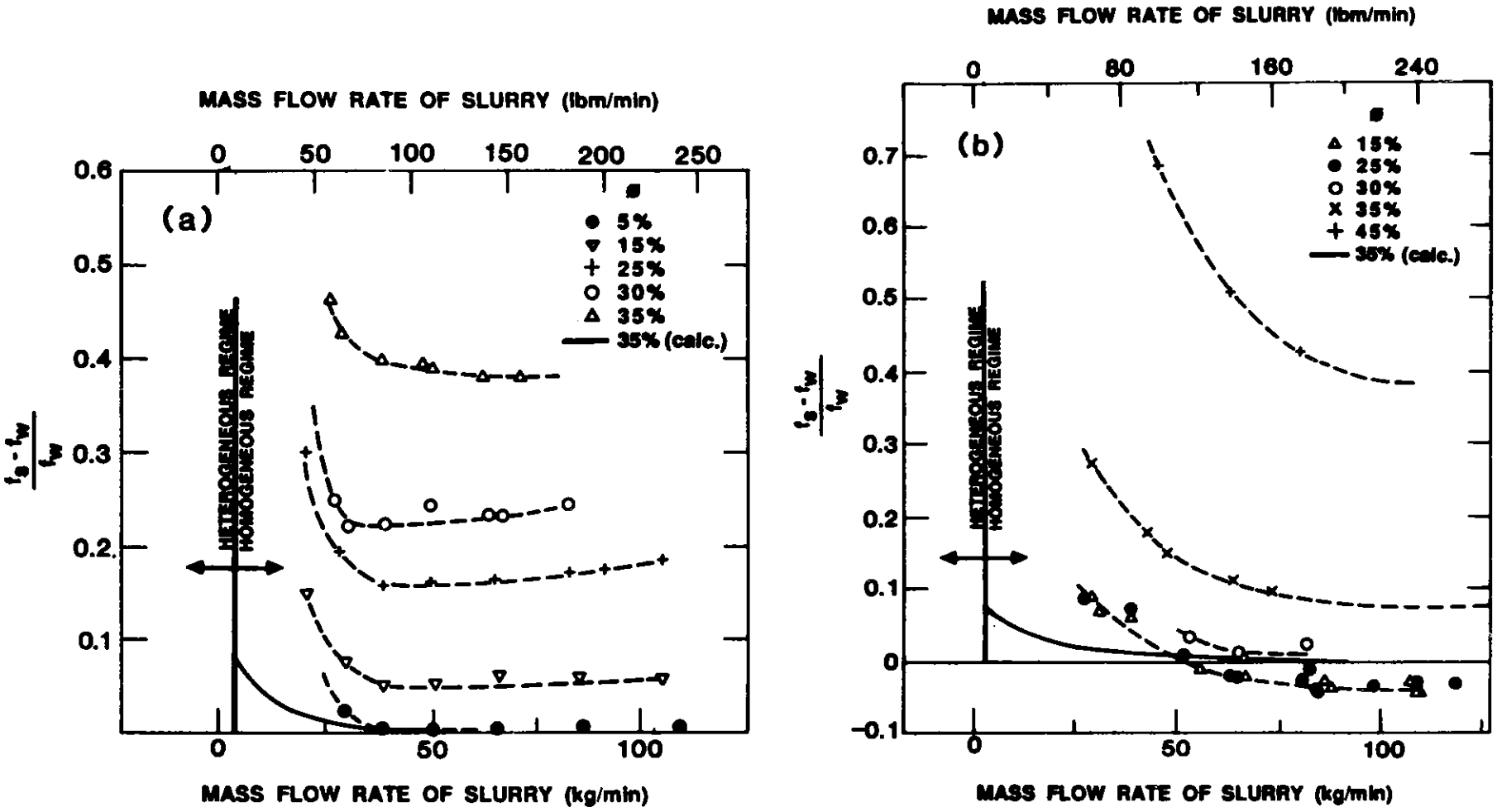

Fig. 16. Comparison of Friction Factor Change Relative to Water, as Calculated from Eqs. (17) and (18) of Turian and Yuan [36], and Measured Data for Slurry with (a) 1/8-in.- and (b) 1/20-in.-Diameter Particles.

accounted for by existing correlations that emphasize gravitational effects.

(b) The qualitative trend of the predicted stratification phenomenon at low Froude number (i.e., low flow rates) is in agreement with experimental observation, but the transition to stratified flow with X-HDPE seems to occur at a higher Froude number than the theoretical predictions. According to the transition Froude number criteria derived by Turian and Yuan, the transition velocity increases as the particle size increases. This means a higher flow rate is required to maintain a homogeneous suspension for a slurry with 1/8-in. particles than for 1/20-in. particles. However, the opposite trend is found in the present X-HDPE experiments. No explanation can be given to date for this behavior. Further investigation with different particle sizes is needed to clarify the discrepancy. This behavior may be related to the different tendencies for laminarization associated with the two different particle sizes.

4.5 Discussion

4.5.1 Slurry Pressure Drop Reduction: Inadequacy of Existing Correlations

The current experimental results with X-HDPE show a pressure drop reduction for the slurry of 1/20-in.-diameter particles. The reduction increased from zero at zero loading to roughly 3% near 20% loading and then decreased to zero at or near 30% loading. For the slurry of large (1/8-in.-diameter) particles, the reduction in pressure drop was minimal and occurred only at very dilute suspensions, <5% loading. Apparently, the particle size affects the level of pressure drop (i.e., friction) reduction relative to water.

It is important for a designer of a DHC system to be able to predict the slurry frictional loss and hence pumping power requirements under various operating conditions. The present study has demonstrated that the commonly used engineering formulas fail to give reasonable predictions of slurry pressure drop and viscosity. No method is available, to our knowledge,

that can predict the existence or magnitude of the pressure drop reduction phenomenon. Furthermore, the flow rates, predicted from existing correlations, at which particle stratification occurs were far less than those measured. The current studies highlight the fact that both the particle loading and size significantly influence the level of particle-particle interaction and the interactive forces that govern slurry flow behavior. Existing correlations either neglect the size effect or show a very weak dependence on particle size. Further experimental studies with slurries of different particle sizes are required to establish a large enough data base for the development of satisfactory correlations.

4.5.2 Re-laminarization of Turbulent Slurry Flows

Slurry re-laminarization has been proposed as a possible explanation of the sharp increase in pressure drop observed in slurry flows of high particle loadings, i.e., $\phi > 30\%$ with 1/8-in.-diameter particles and $\phi > 40\%$ with 1/20-in.-diameter particles. A drastic change in slurry radial temperature profiles observed at high loadings (of the same order at which the pressure drop increases rapidly), to be discussed in Sections 5.2 and 5.3, also supports the postulation of a transition from a fully developed turbulent flow to a laminarized flow at high particle loadings. This section examines some of the implications of the postulated re-laminarization phenomena.

Assuming the slurry flow at a high particle loading behaves hydrodynamically like a fully developed single-phase laminar fluid flow, Eq. (3) can be used to express the slurry friction factor as a function of an effective "laminar" Reynolds number. Then an effective Reynolds number can be calculated for the laminarized slurry flow from the relationship

$$Re_L = \frac{64}{f_w\left(1 + \frac{f_s - f_w}{f_w}\right)} ; \qquad (20)$$

the terms on the R.H.S. of Eq. (20) can be obtained from experimental data (see Fig. 16).

Figure 17 shows the map of the effective "laminar" slurry Reynolds number superimposed on the pressure drop penalty plot of Fig. 16b.

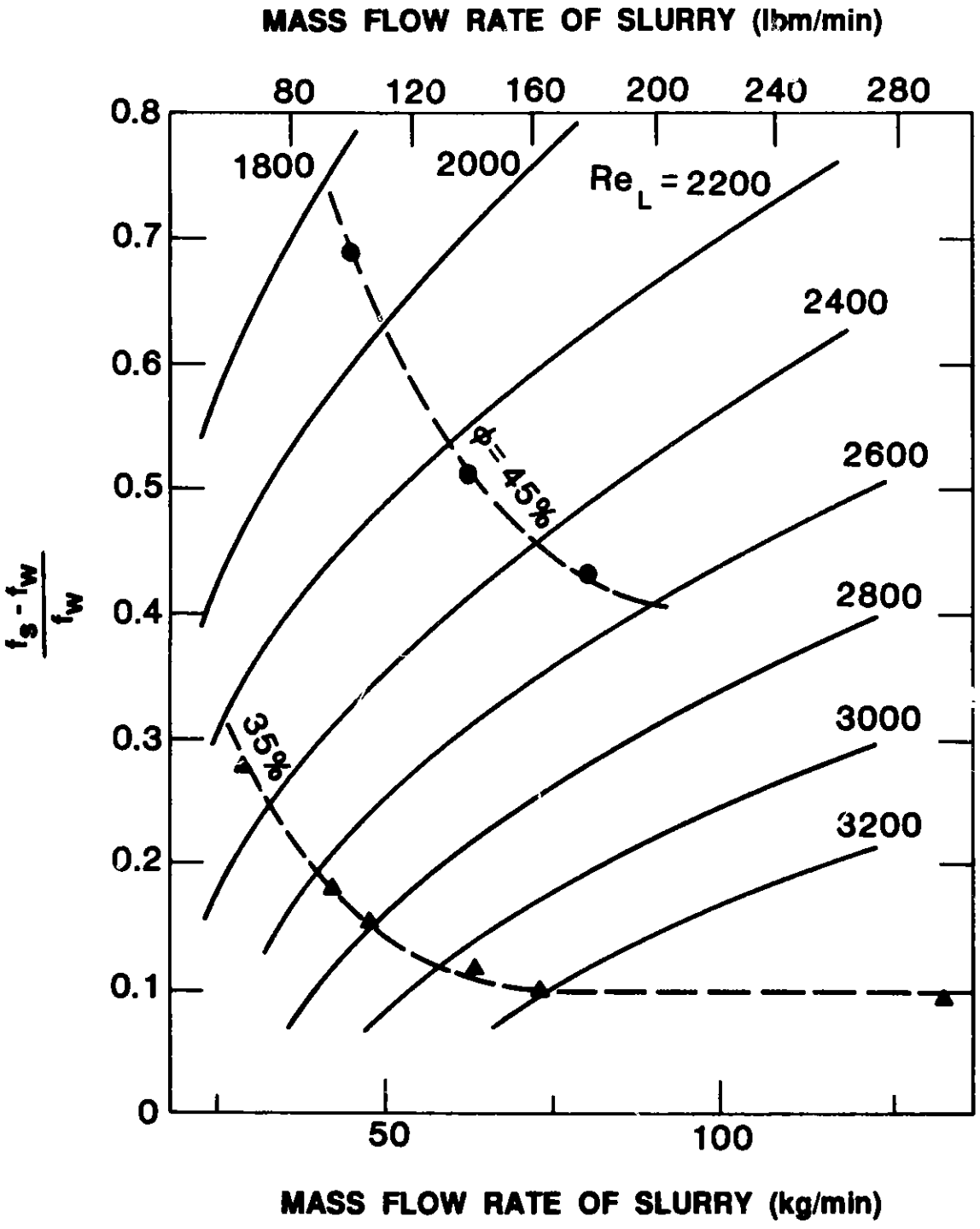

Fig. 17. Relationship Between the Friction Factor Increase Relative to Water and the Effective "Laminar" Reynolds Number for Slurries with 1/20-in.-Diameter Particles.

The low effective Reynolds number associated with the highly loaded slurry conditions clearly indicates that the slurry could be laminarized and hence, the re-laminarization phenomenon is a plausible mechanism for the large increase in pressure drop under these conditions.

It is also very interesting to compare the effective "laminar" viscosity of the slurry, ν_{eff} (derived from Re_L), with that of turbulent pure-water carrier fluid, ν_w, for the same mass flow rate. For a slurry flow rate of order 200 lbm/min (91 kg/min) and loadings of 35-45%, the relative viscosity, ν_{eff}/ν_w, has a value varying from 30 to 53. This high effective slurry viscosity can cause a turbulent flow at a moderate Reynolds number to become a laminar flow.

5. HEAT TRANSFER CHARACTERISTICS OF PARTICULATE SLURRIES

In attempting to establish proof-of-concept of enhanced heat transfer relative to heat transfer in a pure single-phase liquid, and to further develop engineering correlations that can be used for the design of high-performance DHC systems, an understanding of the influence of the controlling parameters on the slurry heat transfer process is very important. Among the controlling parameters are particle loading, particle size, thermophysical properties of the particle and carrier fluid, flow rate, and the particle latent heat of fusion.

This section examines experimental results obtained for slurry flow with X-HDPE particles under non-melting conditions. Again, slurries of two particle sizes, 1/8 and 1/20 in. (3.2 and 1.3 mm) diameter, were tested for a wide range of particle loadings, 0-45%. The effect of particle loading and size on slurry heat transfer characteristics will be discussed. The next phase of the program will examine the influence of particle melting or freezing on heat transfer.

5.1 Slurry Heat Transfer Coefficients

For slurry pipe flows, there is a lack of experimental data and readily usable correlations for predicting the heat transfer rates. In the present study, the difference in thermophysical properties between phases (Appendix A), the degree of thermal equilibration, the particle volumetric

loading, and the particle size have been found to strongly influence the heat transfer and the radial temperature profiles in the slurry. Details of the data reduction process used to calculate slurry heat transfer coefficients are given in Appendix B. The first comparison of heat transfer in slurries with that in pure water was made in terms of the nondimensional Stanton number, St, as defined in Eq. (B.1). All parameters used in determining the Stanton number can be either measured or calculated accurately. The Stanton number for slurries with 1/8-in.-diameter particles at different loadings is plotted in Fig. 18. The Stanton number becomes larger as the loading increases at a fixed mass flow rate. More significantly, the Stanton number of the slurry consistently has a greater value than that of pure water over the entire range of flow conditions. This is a clear indication of heat transfer enhancement with non-melting, phase-change slurry flows. Figure 19 shows that at both low and high flow rate, the percent Stanton number increase relative to water becomes larger as the particle loading increases.

In contrast to the slurry heat transfer enhancement obtained with the 1/8-in.-diameter particles, the slurry heat transfer, expressed in terms of the Stanton number, for the 1/20-in.-diameter particles exhibited a modest reduction relative to water. Figure 20 shows the data for smaller particles at a flow rate of 140 lbm/min (64 kg/min). A small heat transfer enhancement occurs at low loadings (<10%). However, with increasing loading, a heat transfer reduction occurs; heat transfer reaches a minimum at a loading of ~28% and then rises as the particle loading increases further. The region of increasing heat transfer reduction (loadings of 10 to 28%) corresponds to the region of increasing pressure drop reduction (see Fig. 10). The data suggest that a reduction in slurry heat transfer coefficient occurs whenever the pressure drop reduction phenomenon occurs. This observation underscores the need for a better understanding of the influence of particle loading on pressure drop reduction.

The previous data for 1/8-in.-diameter particles are now presented in terms of the heat transfer Nusselt number versus Reynolds number. This relationship, like the Stanton number, has been widely used to analyze heat transfer data for single-phase pipe flows. The Nusselt number, Nu, is defined by Eq. (B.1). The thermal conductivity k has been taken to be the fluid thermal conductivity because no data on effective thermal conductivity for the

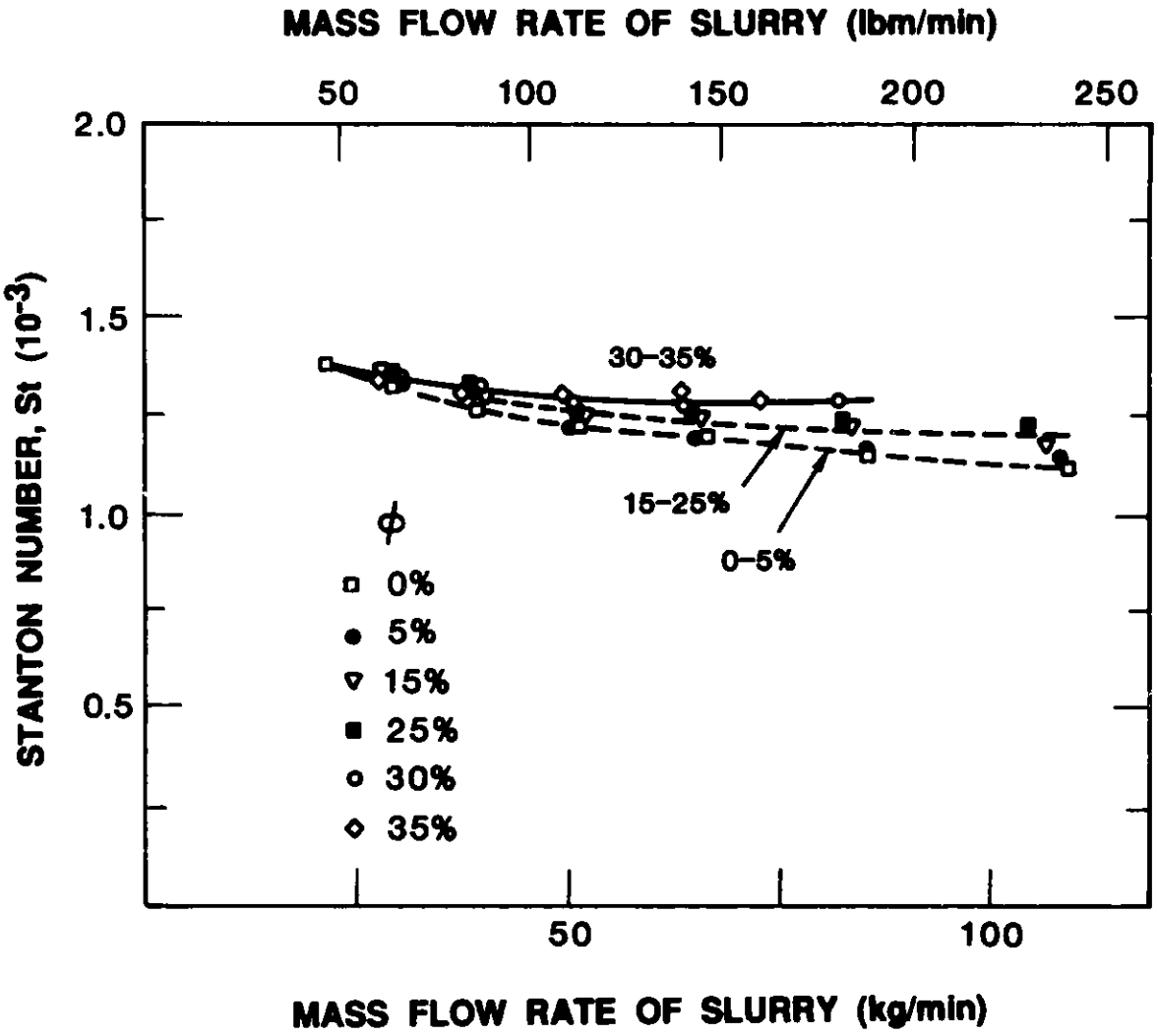

Fig. 18. Slurry Heat Transfer Enhancement in Terms of Stanton Number at Different Particle Loadings for Slurries with 1/8-in.-Diameter Particles.

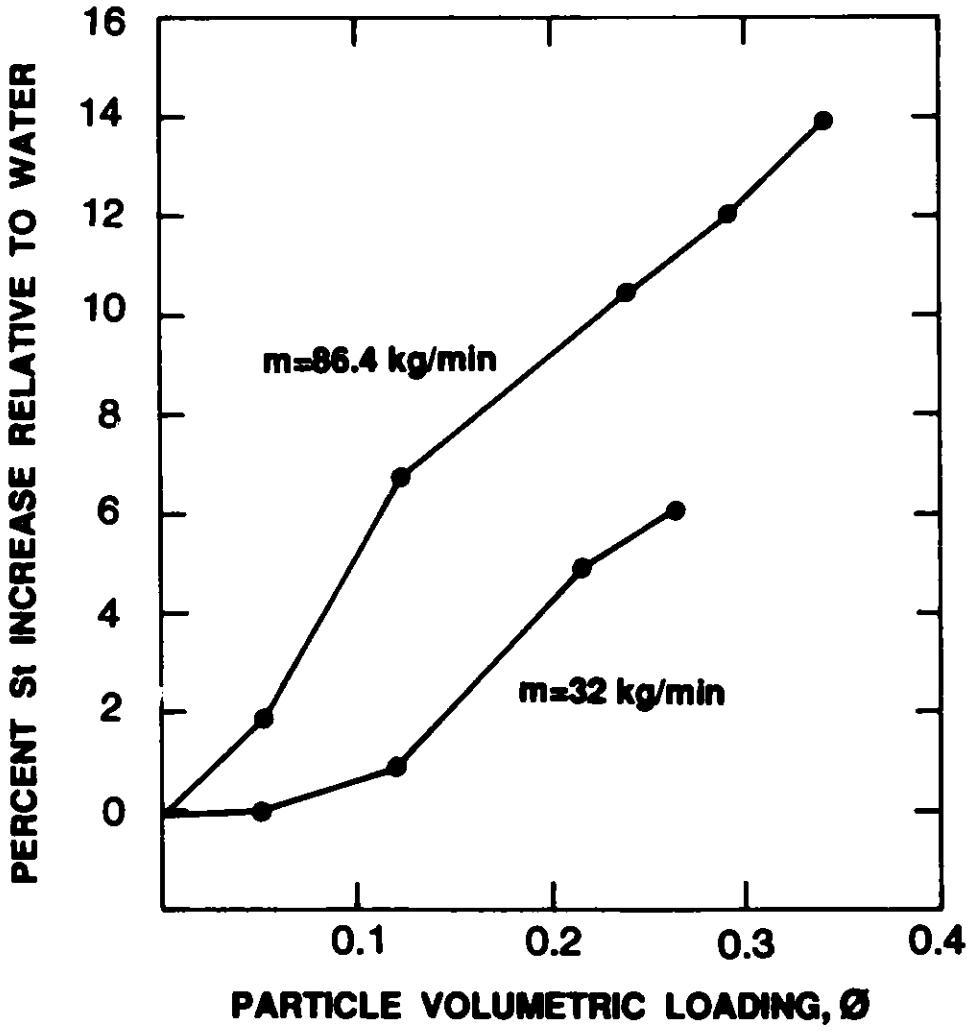

Fig. 19. Effect of Particle Loading on Slurry Heat Transfer Relative to Water for Slurries with 1/8-in.-Diameter Particles at Low and High Flow Rates.

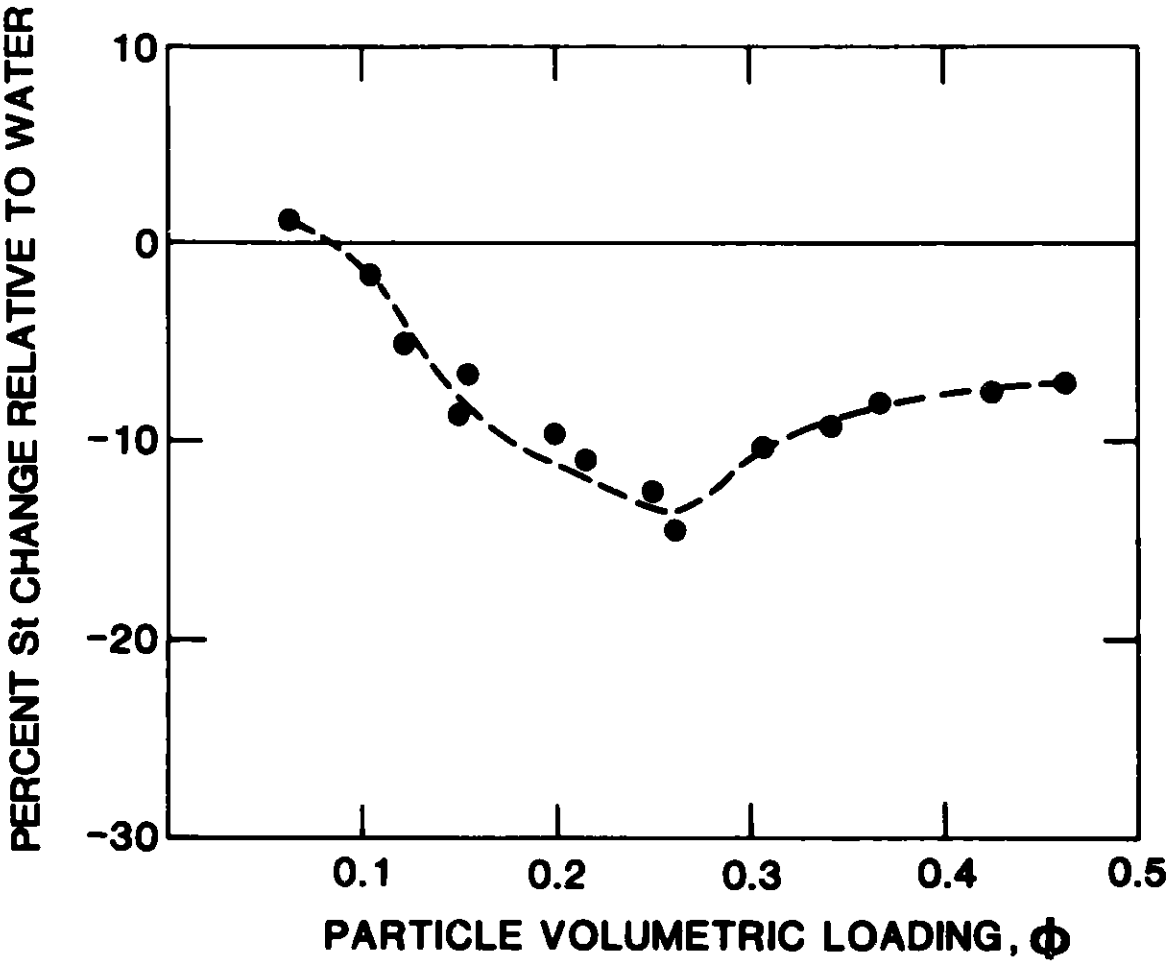

Fig. 20. Effect of Particle Loading on Slurry Heat Transfer Relative to Water for Slurries with 1/20-in.-Diameter Particles at a Mass Flow Rate of 140 lbm/min.

mixture were available. A modified Reynolds number was defined on the basis of an effective slurry viscosity, as shown in Fig. 15. As shown in Fig. 21, the slurry Nusselt number is larger than that for pure water for all conditions and increases with increasing particle loading. This Nu-Re relationship may be very useful in development of engineering correlations for slurry heat transfer similar to the one described in Appendix B (Sec. B.7) for single-phase flow.

The Nusselt number for the 1/20-in.-diameter particle slurries was not calculated because of the difficulty in defining an effective slurry viscosity when the pressure drop reduction phenomenon is present (see Section 4.3). Hence, with the current level of understanding of slurry heat transfer, no systematic, generally accepted method is available for presenting heat transfer data.

5.2 Centerline Fluid Temperature Versus Fluid Mixing Temperature

In the next two sections, results for temperature variation within the slurry are presented. These data are important because they furnish insight into the behavior of the slurry.

As described in Section 2.2, electrical-resistance wall heating was applied evenly over most of the test section (a 20-ft-long thin-walled stainless steel tube). Figures 22a-c show radial fluid temperature distributions measured at the exit of the test section for pure water at $Re = 0.73 \times 10^5$ and $Re = 1.49 \times 10^5$, and for slurry with 1/20-in.-diameter particles at $\phi = 33.4\%$, respectively. All three profiles show a highly symmetrical temperature distribution about the pipe centerline, indicating the absence of stratification effects and uniformity of pipe circumferential heat flux.

The slurry bulk temperature and heat transfer coefficients can be calculated from the data on radial temperature profiles. The bulk temperature estimated from the local radial temperature profile [see Appendix B, Eqs. (B.5) and (B.6)] can be compared with the value based on a global energy balance method [see Eq. (B.4)] and the fluid mixing temperature measured inside the weighing tank (see Fig. 2). The tank fluid mixing temperature has been found to be very close to the bulk temperature calculated either from the

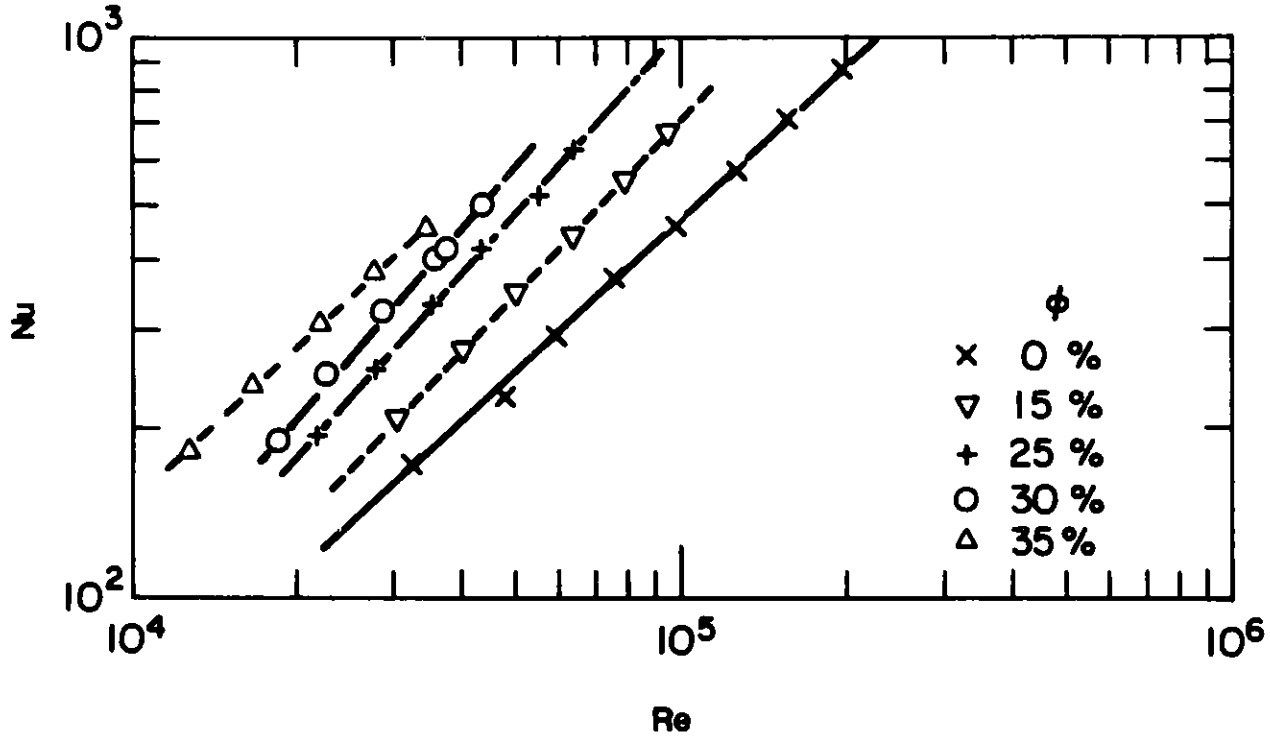

Fig. 21. Nusselt Number Versus Modified Reynolds Number at Different Particle Loadings for Slurries with 1/8-in.-Diameter Particles.

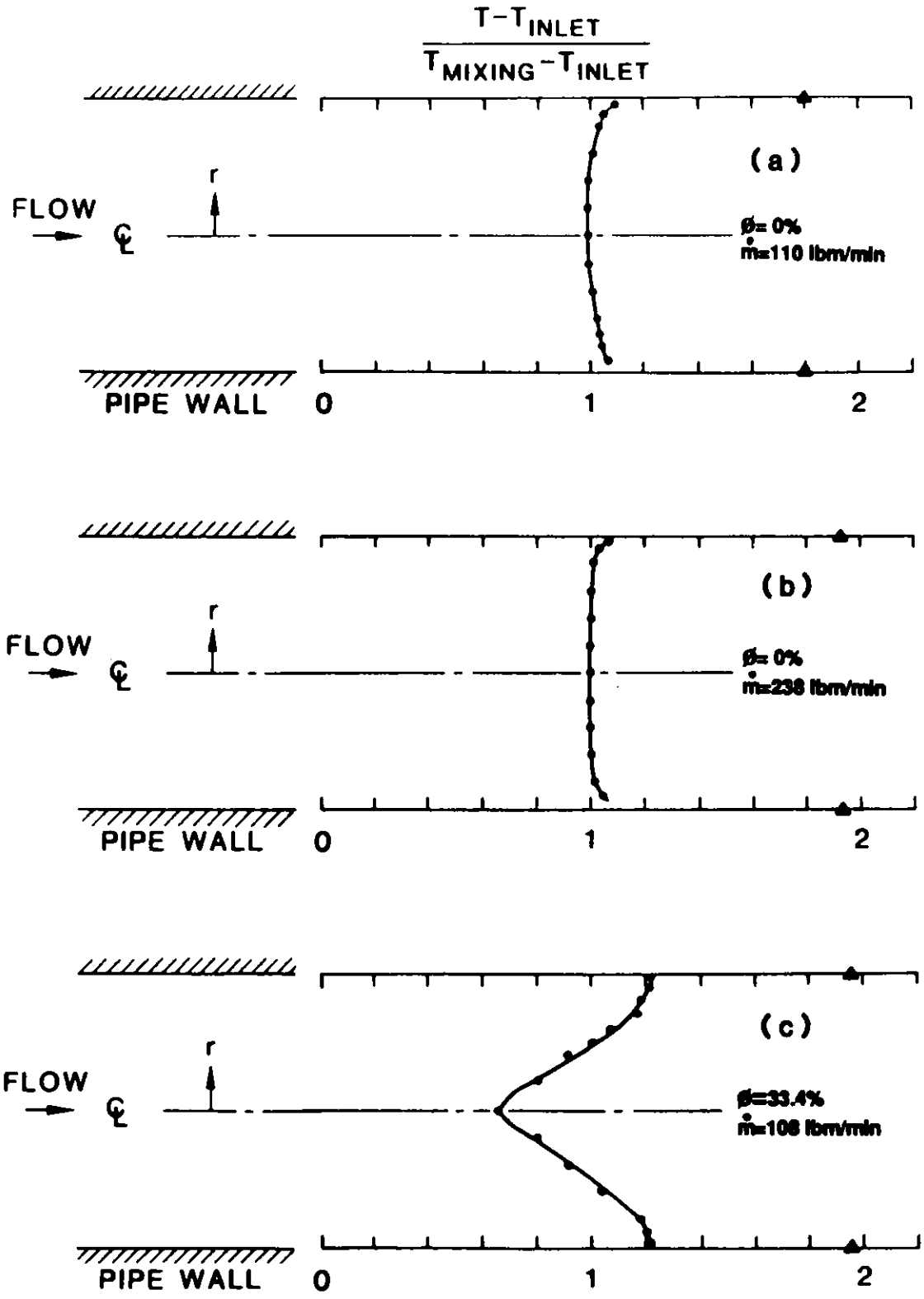

Fig. 22. Radial Fluid Temperature Distributions Measured at the Exit of the Test Section for (a) Pure Water (Re = 0.73×10^5), (b) Pure Water (Re = 1.49×10^5), and (c) Slurry with 1/20-in.-Diameter Particles.

total energy balance method or from the radial temperature profile measured at the exit of the test section. Since it is easy to continuously monitor the mixing temperature in the weighing tank, the bulk temperature rise, (T_{mixing} - T_{inlet}), has been used to normalize all local fluid temperatures.

The normalized pipe centerline fluid temperature, defined as (T_{mixing} - $T_{center\ at\ exit}$)/(T_{mixing} - T_{inlet}), was found to change as a function of the Reynolds number and the particle loading. For a fully developed turbulent single-phase pipe flow, only a small difference between the centerline temperature and the fluid mixing temperature will exist (Figs. 22a,b). However, the centerline fluid temperature becomes much lower than the fluid mixing temperature for some slurry conditions, as shown in Fig. 22c. The variation of the normalized difference between mixing temperature and centerline fluid temperature as a function of the particle loading at a flow rate of 140 lbm/min (64 kg/min) for slurries with 1/8 and 1/20-in.-diameter particles is presented in Fig. 23. The normalized difference between centerline fluid temperature and mixing temperature for slurry with 1/8-in.-diameter particles at a particle loading of $\phi < 30\%$ is very small, indicating good thermal mixing across the pipe and almost isothermal conditions across the bulk of the flow. Mixing across the pipe begins to deteriorate when ϕ exceeds 30% and the centerline temperature falls below the mixing temperature.

The temperature fields for slurry with 1/20-in.-diameter particles exhibit drastic changes with increasing particle loading, as shown in Figs. 22c and 23. The mixing temperature and centerline fluid temperature are almost equal when the particle loading is less than 15%. However, mixing across the pipe deteriorates and temperature variation increases dramatically for particle loadings in the range from 15 to 30%. This is the exact range of loadings for which the slurry pressure drop is reduced relative to pure water (see Fig. 10). At a particle loading of 30%, the normalized centerline fluid temperature variation exhibits a sudden change of slope, which indicates a change in the flow behavior at this particle loading. This is the exact point at which a transition from a pressure drop reduction to a pressure drop increase relative to water was observed. It is also observed in Fig. 23 that the normalized centerline fluid temperature begins to level off at particle loadings of >40%. At this high loading, the centerline fluid temperature

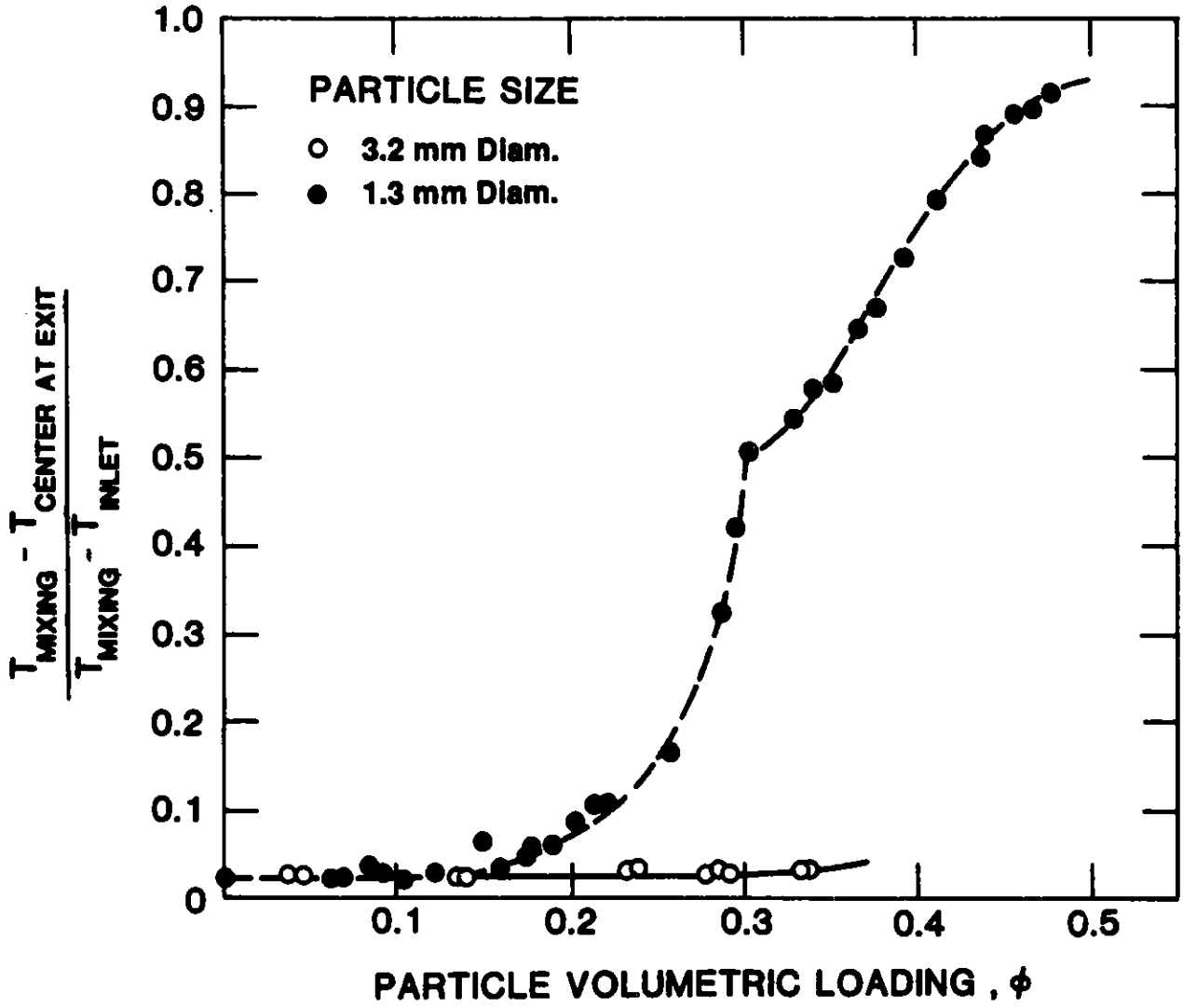

Fig. 23. Effect of Particle Size and Loading on Centerline Fluid Temperature Measured at the Exit of the Test Section.

becomes very close to the inlet fluid temperature (i.e., no heating occurs for the fluid moving along the center of the pipe because of the lack of transverse mixing). Further studies of both slurry pressure drop and thermal fields are needed to understand the mechanisms underlying their interrelated behavior.

5.3 Variation of the Radial Fluid Temperature Profile as a Function of Particle Loading

To further study the interesting behavior of slurry temperature fields, fluid temperature distributions were measured for a large number of conditions with 1/20-in.-diameter particles. Owing to the radial symmetry of the fluid temperature in the pipe, local fluid temperatures covering only half of the pipe diameter were measured. The particle loading varied from 20% to 45% and the mass flow rate ranged from 98 to 180 lbm/min (45 to 82 kg/min). The results are presented in Fig. 24.

The radial fluid temperature profiles for ϕ = 20% (Figs. 24a,b) show a slight decrease in centerline temperature compared to that of water (see Figs. 22a,b). An increase in mass flow rate from 117 lbm/min (53 kg/min, Fig. 24a) to 167 lbm/min (76 kg/min, Fig. 24b) at this loading does not cause a significant change in the temperature profile. As the loading is increased to 25% (Figs. 24c,d), the temperature non-uniformity across the pipe starts to increase: the temperature near the pipe center decreases and the temperature near the wall region increases. The shape of the temperature profile gradually skews from parabolic to linear as the particle loading reaches ~31% (Figs. 24e-g). When the particle loading reaches 33.7% (Fig. 24h), the temperature profile changes significantly and no longer exhibits turbulent temperature field characteristics. It looks more like the temperature profile of a laminar pipe flow. This trend becomes even more pronounced as the particle loading increases from 33.7% to 45% (Figs. 24i-l).

The above observations support the conjecture that the turbulent flow behavior of the slurry changes at high particle loadings and this behavior is also a strong function of particle size. The strong particle-particle interaction at high particle loadings produces a flow with very high effective viscosity, which causes laminarization. The observations from the pressure drop measurements also support this conclusion.

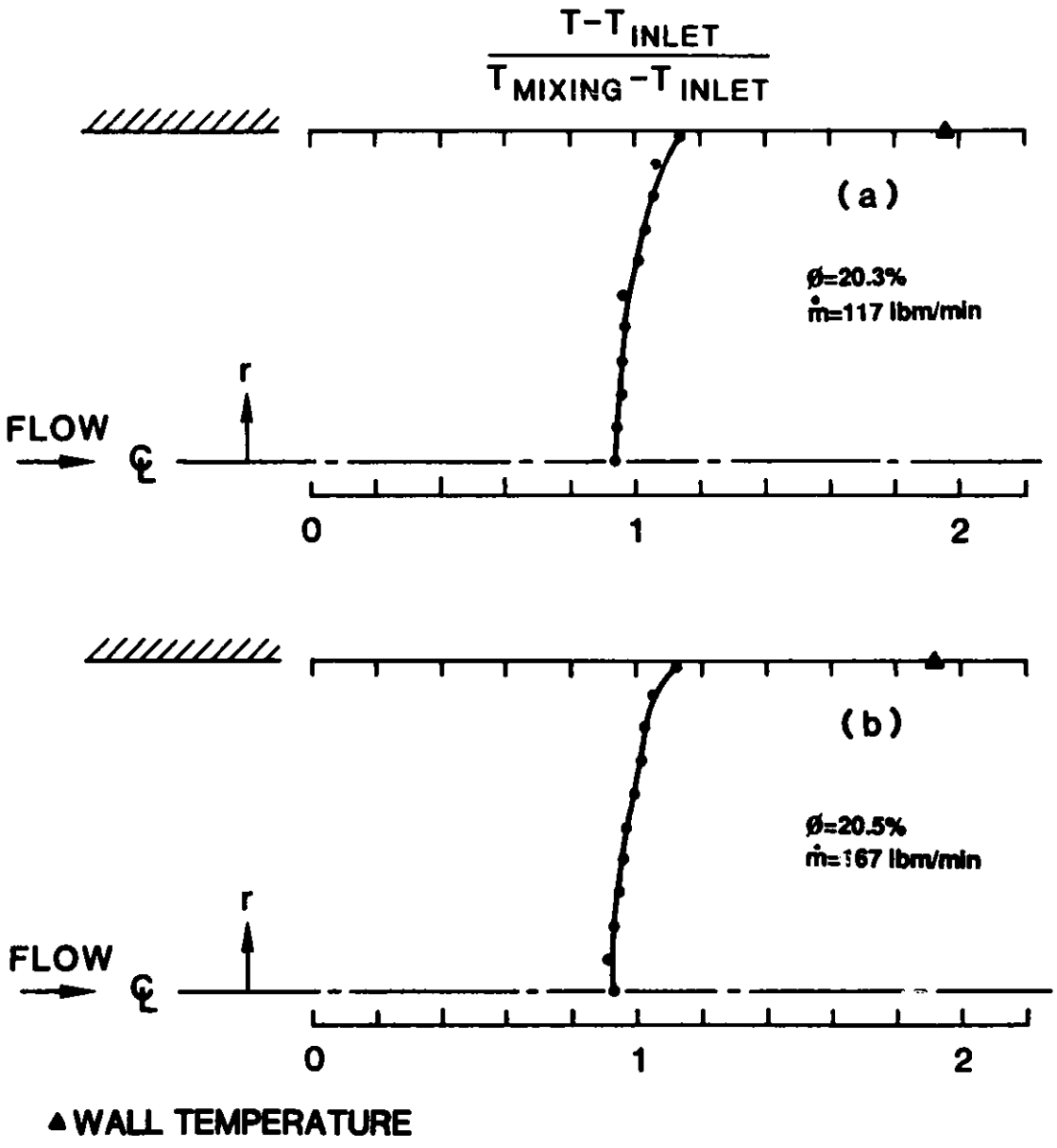

Fig. 24. Radial Fluid Temperature Distributions Measured at the Exit of the Test Section for Slurries with 1/20-in.-Diameter Particles at Loadings Ranging from ~20 to 45% and Mass Flow Rates Ranging from ~98 to 180 lbm/min.

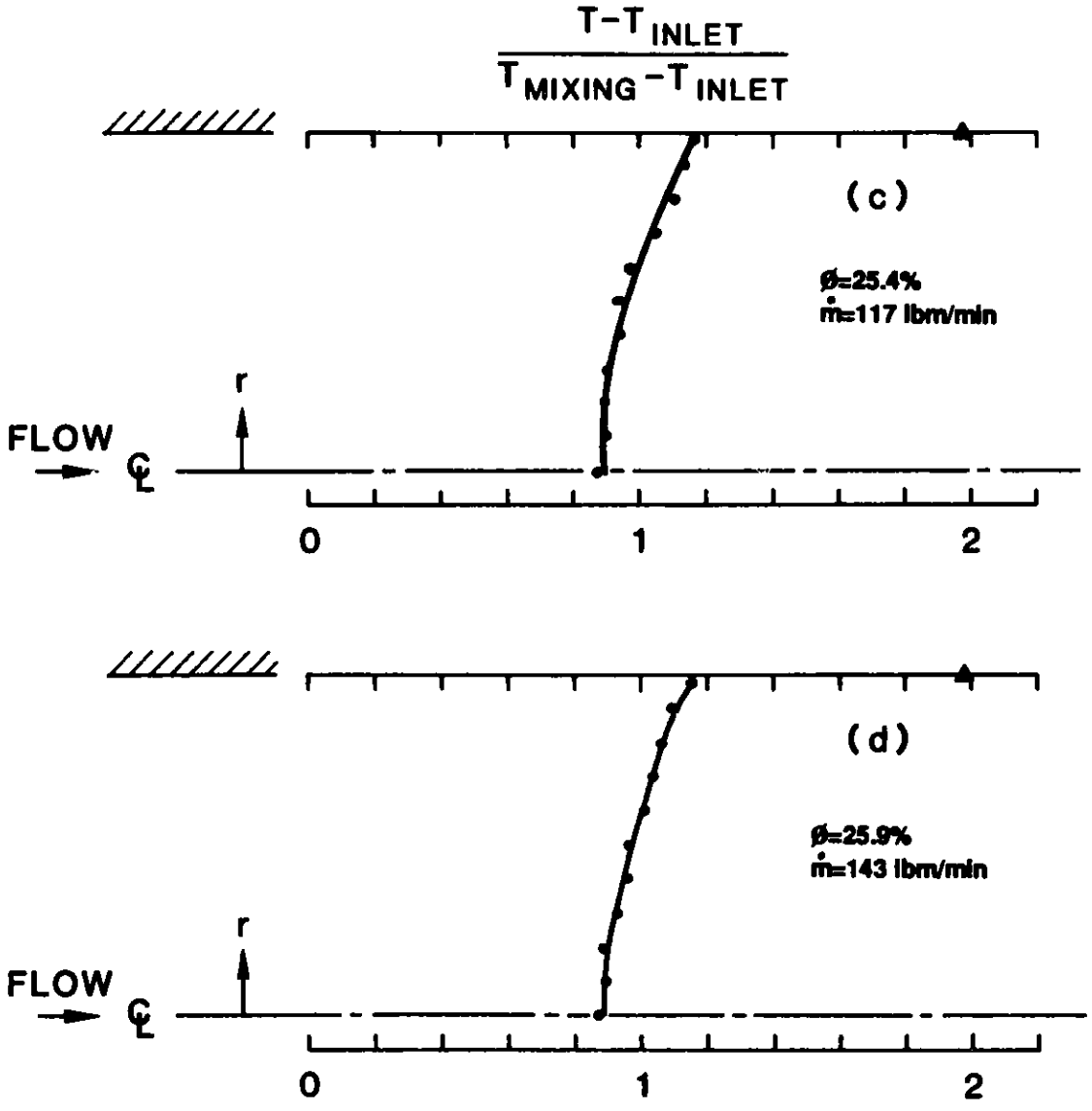
T-T INLET
T MIXING -T INLET
(c)
ø=25.4%
ṁ=117 lbm/min
r
FLOW
℄
0
1
2
(d)
ø=25.9%
ṁ=143 lbm/min
r
FLOW
℄
0
1
2

Fig. 24. (Contd.)

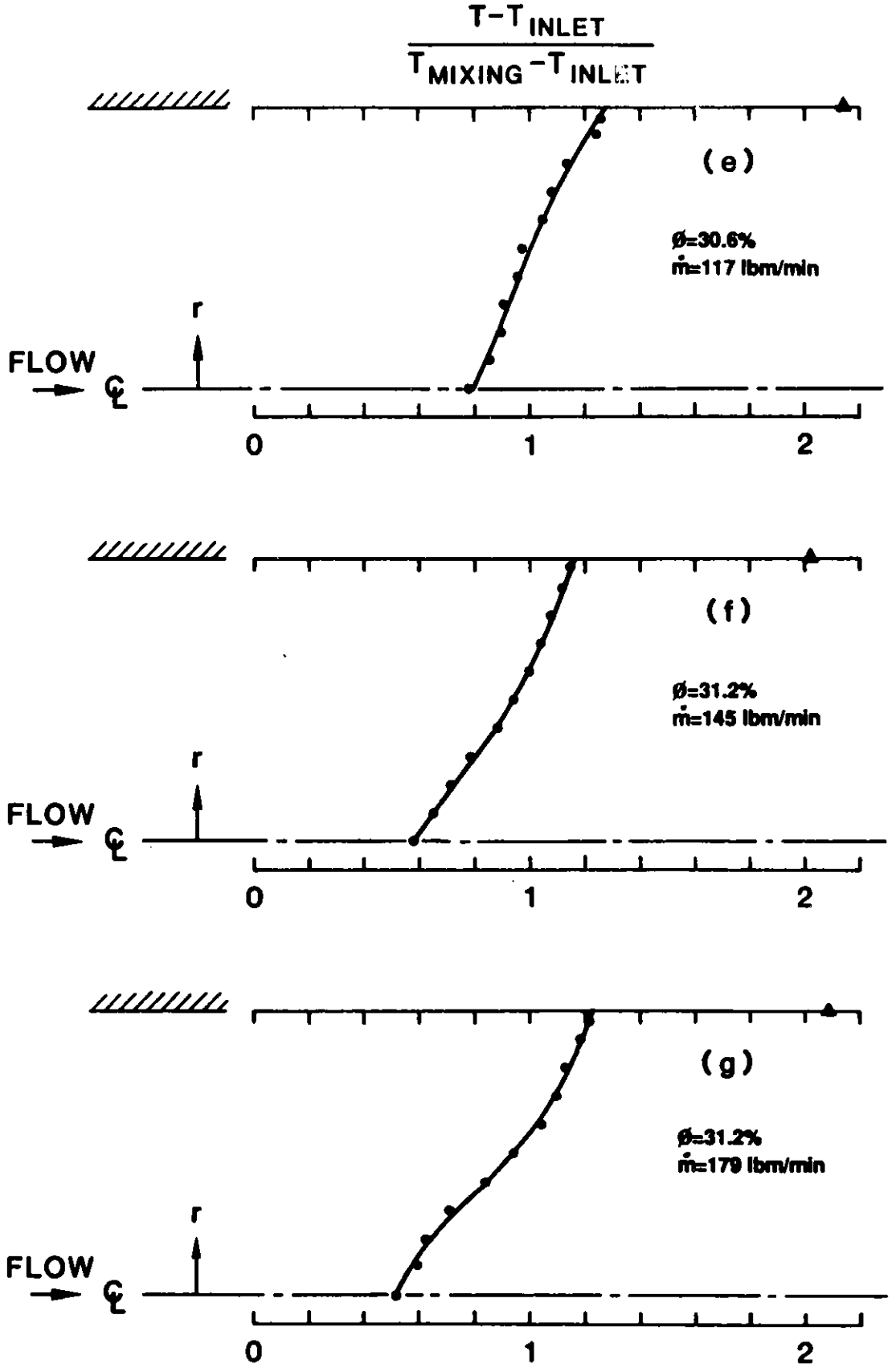
T-T INLET
T MIXING -T INLET
(e)
ø=30.6%
ṁ=117 lbm/min
r
FLOW
℄
0
1
2
(f)
ø=31.2%
ṁ=145 lbm/min
r
FLOW
℄
0
1
2
(g)
ø=31.2%
ṁ=179 lbm/min
r
FLOW
℄
0
1
2

Fig. 24. (Contd.)

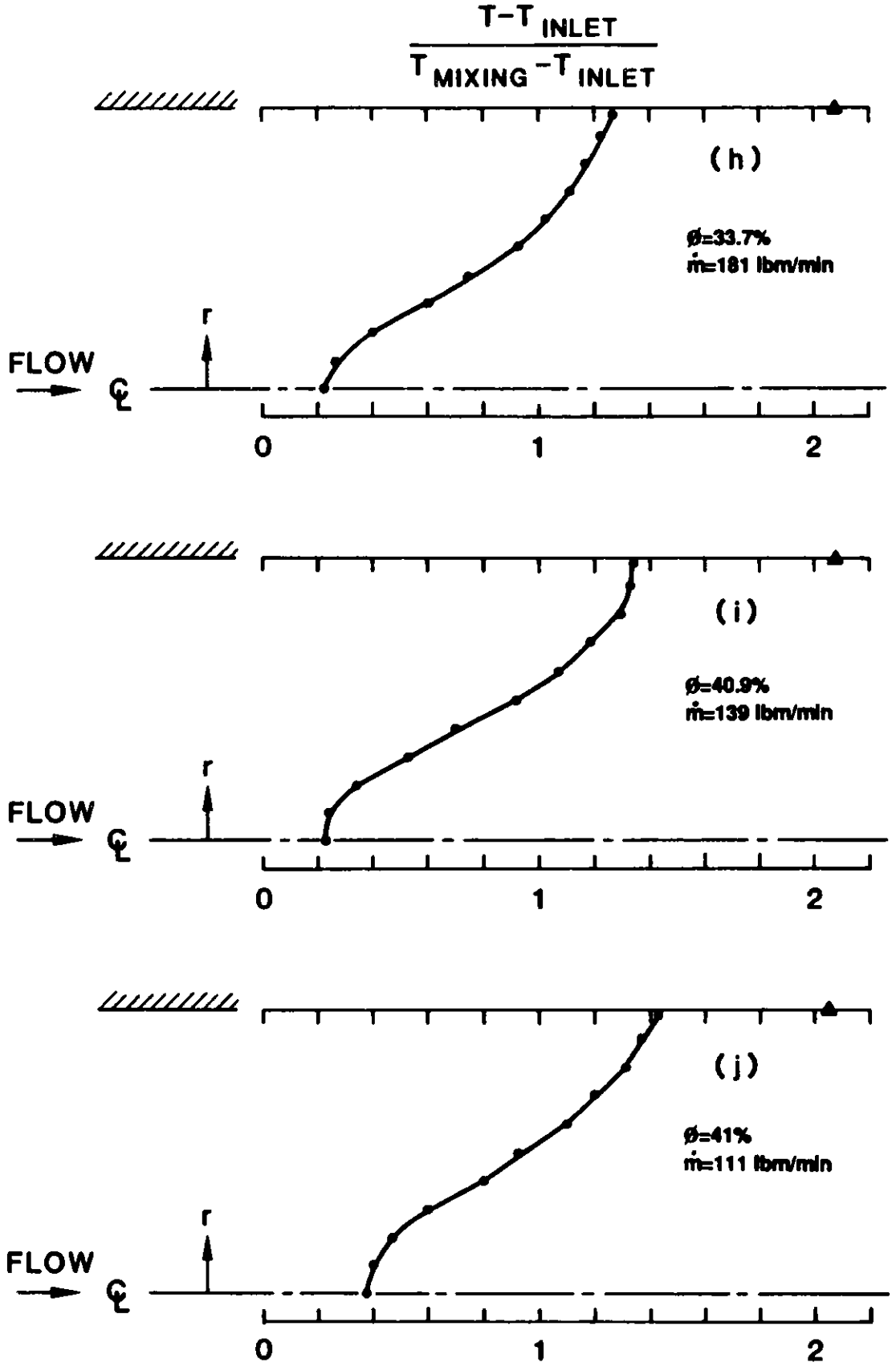
T-T INLET
T MIXING -T INLET
(h)
ø=33.7%
ṁ=181 lbm/min
r
FLOW
℄
0
1
2
(i)
ø=40.9%
ṁ=139 lbm/min
r
FLOW
℄
0
1
2
(j)
ø=41%
ṁ=111 lbm/min
r
FLOW
℄
0
1
2

Fig. 24. (Contd.)

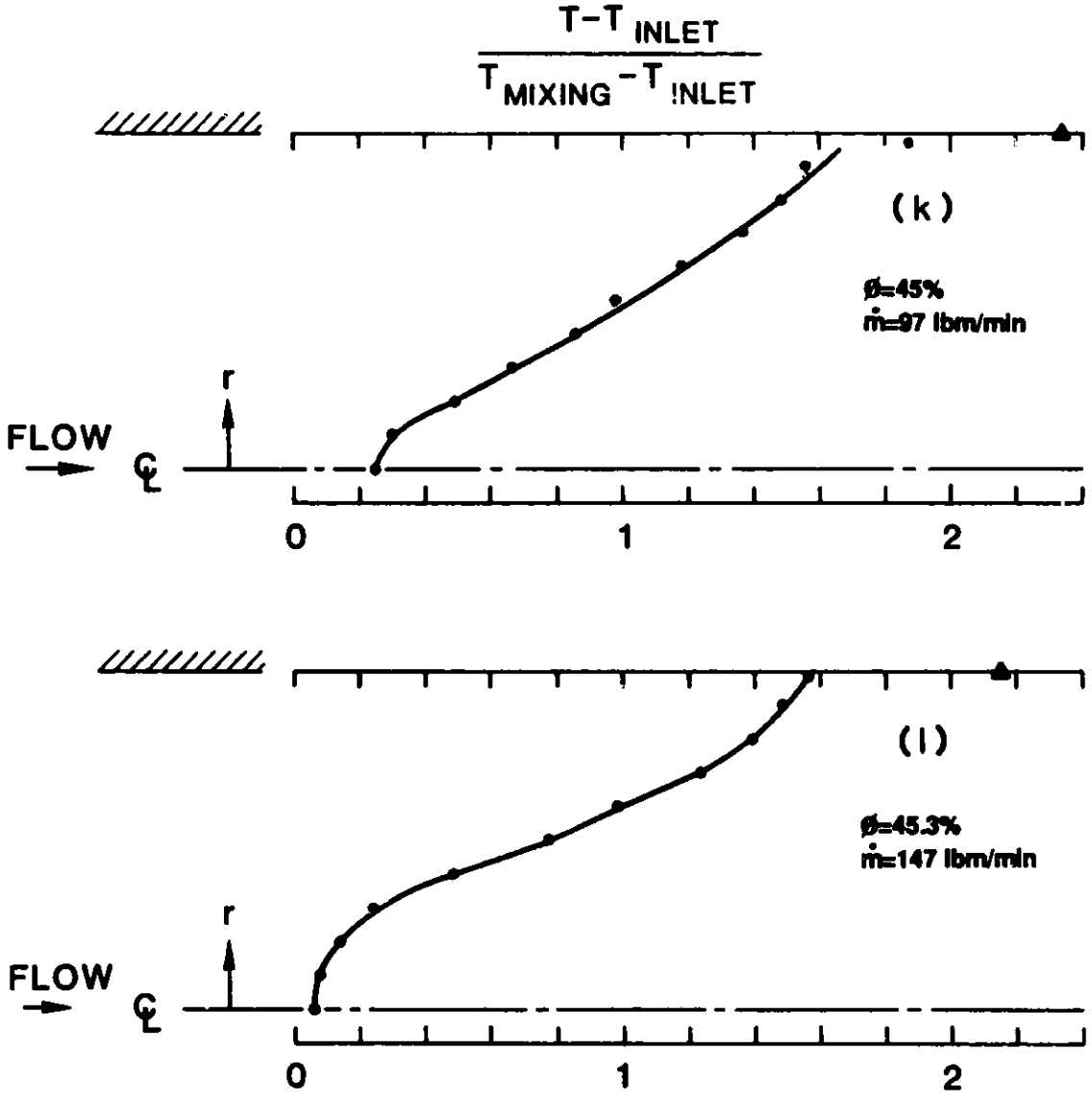
T-T INLET
T MIXING - T INLET
(k)
ø=45%
ṁ=97 lbm/min
r
FLOW
℄
0
1
2
(l)
ø=45.3%
ṁ=147 lbm/min
r
FLOW
℄
0
1
2

Fig. 24. (Contd.)

6. PRELIMINARY RESULTS FOR SLURRIES WITH FRICTION-REDUCING ADDITIVE

One of the objectives of the current program on advanced energy transmission fluids is to study the concept of combining friction-reducing additives with phase-change slurries. Experiments performed at ANL [3,5] have shown that the friction-reducing additive Polyox, a high-molecular-weight linear polymer, at a concentration of 30-200 wppm, can substantially reduce frictional loss for a slurry of pure water and 1/8-in.-diameter X-HDPE particles at 15% loading under isothermal room temperature test conditions. The value of the slurry pressure drop reduction relative to water reached 70% when the mass flow rate of the slurry was greater than 140 lbm/min (64 kg/min). As a part of a continuing testing effort on combined-concept fluids, the influence of friction-reducing additives on slurry pressure drop and heat transfer has been examined in more detail.

Separan, the friction-reducing additive used in the current investigations, is a different kind of high-molecular-weight linear polymer. In laboratory tests [5], Separan has been demonstrated to be effective for DHC applications over a wider temperature range than Polyox, and to be more "robust" with respect to long-term flow shear.

6.1 Friction-Reducing Additive Injection Tests

Separan was injected into the slurry flow at the inlet to the test section at a constant rate, yielding a mixture concentration of ~65 wppm. The transient pressure drop data taken from tests with three different particle loadings, ϕ = 0, 20, and 37%, are presented in Fig. 25 and summarized in Table 4. The pure water data, ϕ = 0%, served as a performance reference for the slurry tests. Pure water exhibited a substantial pressure drop reduction, ~70%, after the friction-reducing additive had mixed with the flow over the entire test section length. For both slurry loadings, the friction-reducing additive reduced pressure drop significantly, but less than for pure water. The data in Fig. 25 show that the ability of a friction-reducing additive to reduce frictional losses in a slurry is hindered by an increased solid volume fraction. Results presented in Table 4, and in Fig. 26 for additional data points, clearly demonstrate that the 70% pressure drop reduction observed in water tests is reduced to ~50% at 20% loading and to only 10% at 37%

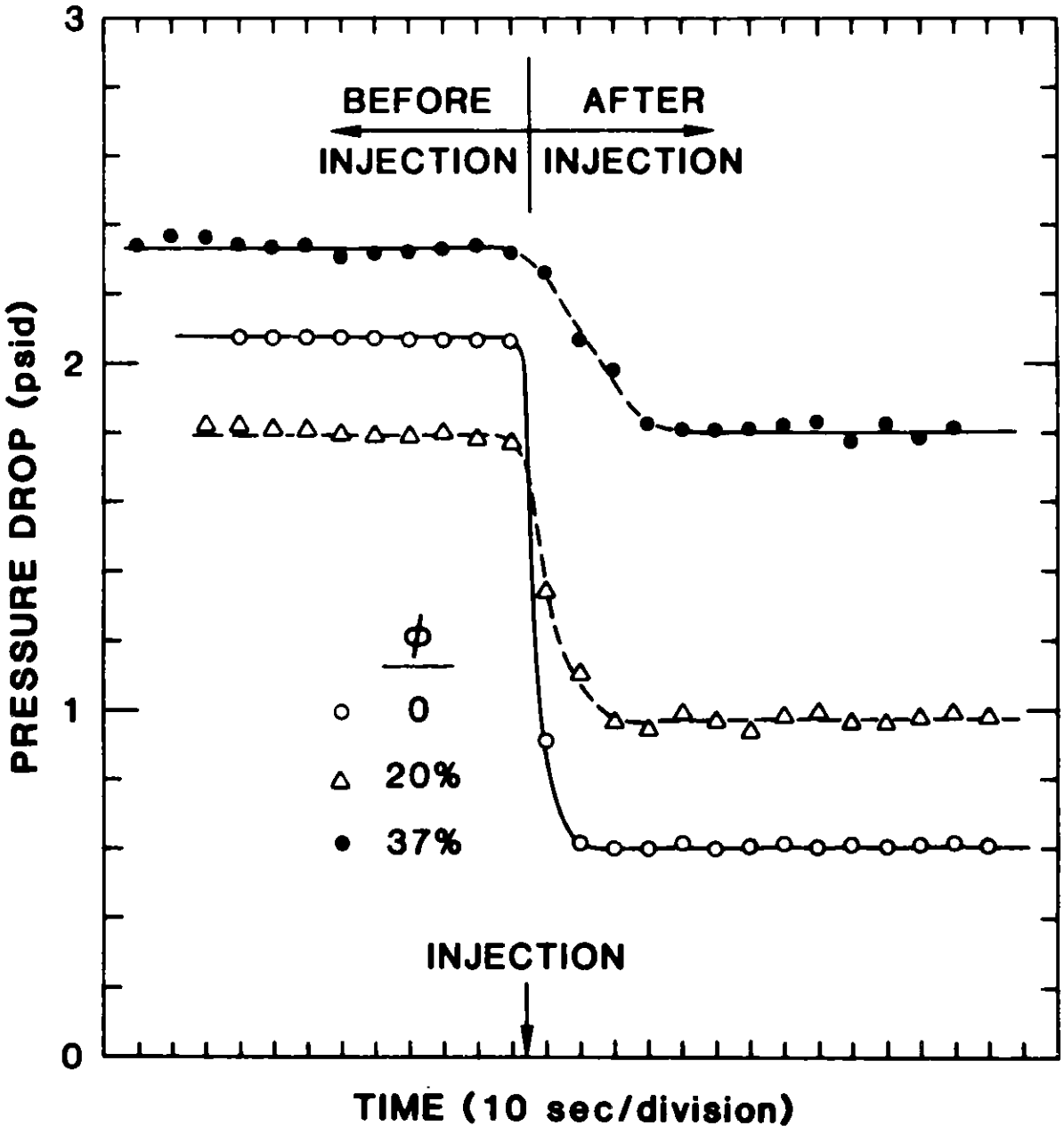

Fig. 25. Effect of Particle Loading (1/20-in.-Diameter Particles) on Response Time and Level of Pressure Drop Reduction for Slurries Injected with the Friction-Reducing Additive Separan to a Concentration of 65 wppm.

Table 4. Pressure Drop Reduction Relative to Water for Separan-containing Slurries at Different Particle Loadings

		Δp_{ave} (psid)		$\left(\frac{\Delta P_{slurry} - \Delta p_{water}}{\Delta p_{water}}\right)$ (%)	
ϕ (%)	$\dot{m}$ (lbm/min)	Without Separan	With Separan	Without Separan	With Separan
0	147	2.06	0.61	0	-70.3
20	140	1.805	0.975	-2.1	-47.5
37	146	2.33	1.81	+16	-10

loading. The curve shown in Fig. 26 also indicates that there may be no pressure drop reduction relative to water when particle loading exceeds 40%. Information of this type has important implications for the future use of combined-concept fluids.

6.2 Radial Fluid Temperature Profiles and Their Changes As a Function of Particle Loading

Not only does the friction-reducing additive affect the pressure drop behavior of the slurry flows, it also alters the temperature profile in the pipe drastically. As shown in Fig. 27, the addition of Separan significantly increases the normalized fluid temperature variation across the pipe radius, as well as the wall temperature, compared to the values for slurry without additive.

The temperature profiles shown in Fig. 27 indicate that the slurry at the center portion of the pipe is not actively participating in the heat transfer process and the high wall temperature represents a reduction in heat transfer coefficient on the pipe surface. However, the change in temperature profile with additive becomes less pronounced for slurry flow at higher particle loading (Fig. 27c) as compared to that measured at lower particle loading (Fig. 27b). The small change in the temperature profile can be attributed to the drastic change of temperature field at high particle

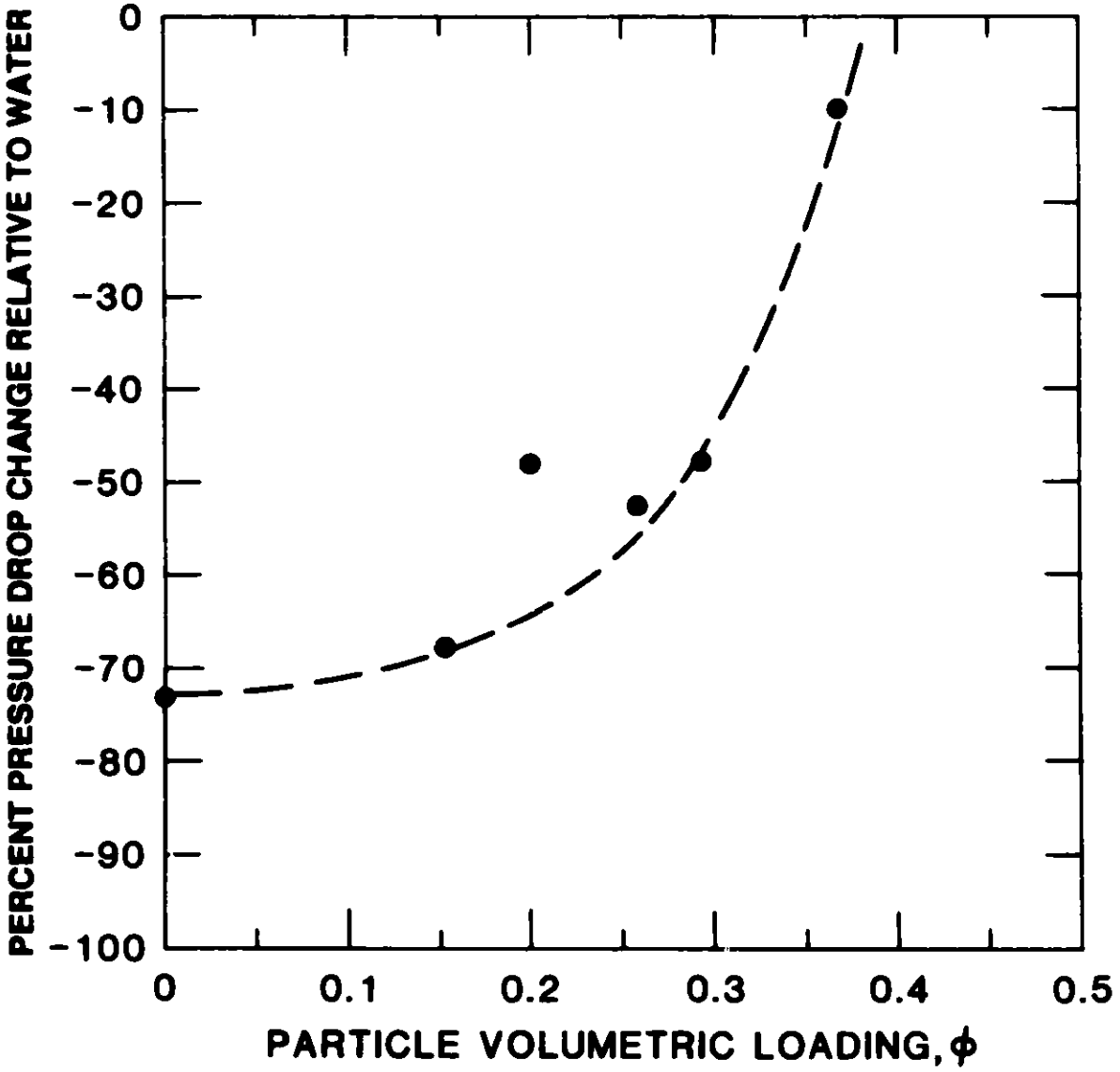

Fig. 26. Effect of Particle Loading (1/20-in.-Diameter Particles) on Percent Pressure Drop Reduction Relative to Water for Slurries with 65 wppm Separan.

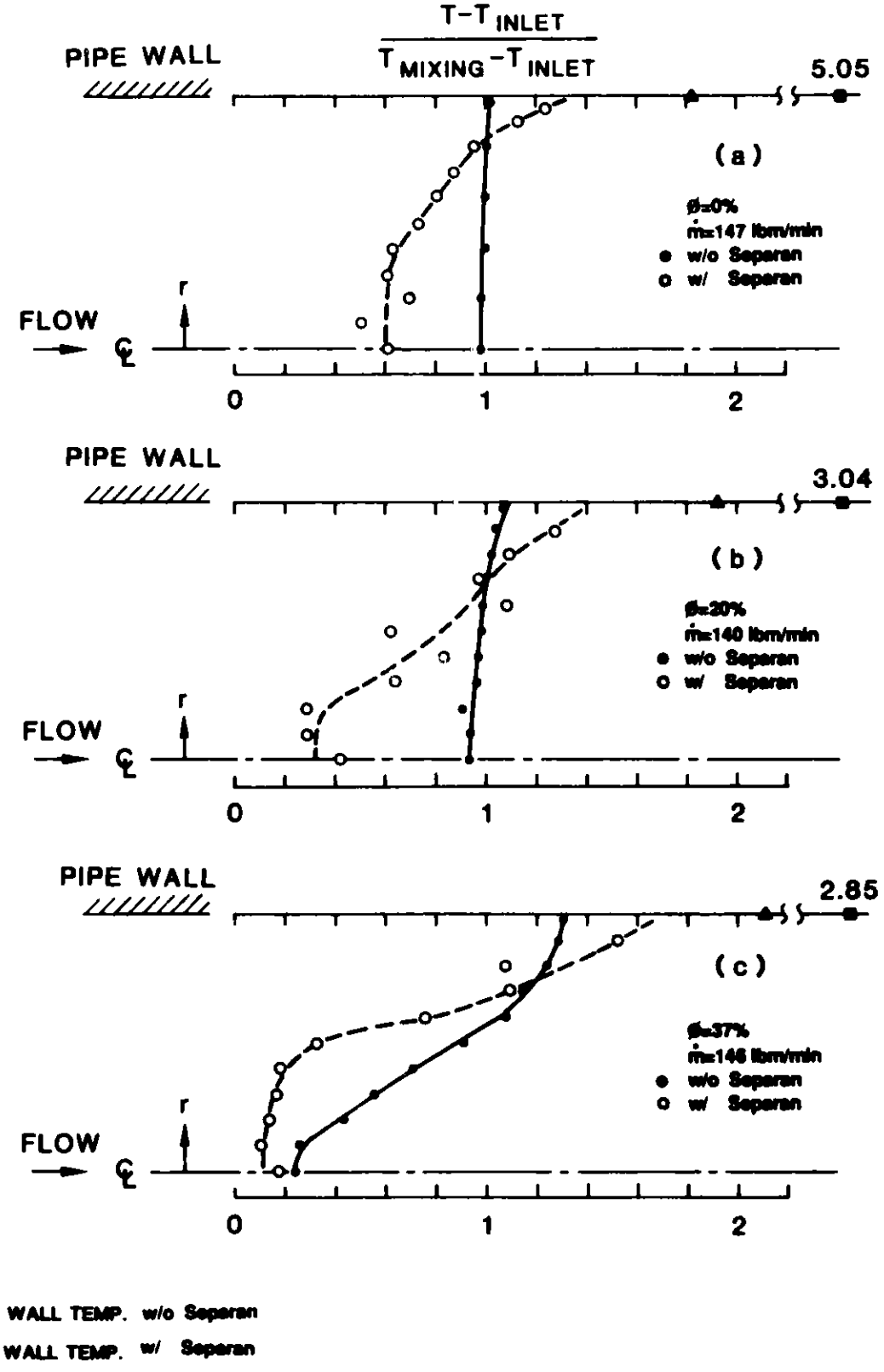

Fig. 27. The Influence of Separan on Radial Fluid Temperature Distribution Measured at the Exit of the Test Section for Pure Water (a) and for Slurry with 1/20-in.-Diameter Particles at Loadings of 20% (b) and 37% (c).

loadings, 35-40%, at which the temperature profile is believed to change from that of a fully developed turbulent flow to a laminar type flow. Under those high-particle-loading conditions, the friction-reducing ability of the additive seems to diminish very quickly.

It is believed that the diminished influence of the friction-reducing additive on slurry temperature profiles at high loadings is related to the fact that a friction-reducing additive exerts its influence by damping turbulent eddies. At high loadings, as pointed out earlier, the slurry flow becomes laminar, and so the additive is less influential. This also explains why the additive is not as effective in reducing slurry pressure drop at high loadings. Hence, several different types of test data support the conclusion that laminarization of slurry flow at high loadings is an important phenomenon which must be understood better before engineering correlations can be developed for pressure drop and heat transfer.

7. CONCLUSIONS AND FUTURE WORK

A slurry heat transfer test facility has been designed and operated. Good progress has been made toward the primary objective of establishing basic understanding, conducting proof-of-concept experiments, and developing engineering design information for improved energy transmission fluids for DHC applications. This report emphasizes the research efforts on pressure drop and heat transfer in non-melting slurries of 1/8 and 1/20-in.-diameter X-HDPE particles and ice slush. A wide range of particle volumetric loadings, from 0 to 45%, were tested. The Reynolds number varied from 6×10^4 to 1.5×10^5. Preliminary heat transfer and pressure drop tests with combined-concept fluids (slurries with polymeric friction-reducing additives) were also performed and significant results were obtained. The following summarizes the important experimental results obtained, which have direct impact on the development and design of advanced energy transmission fluids:

(1) Under some conditions, slurries exhibit significant friction-reducing properties. For example, for a slurry with 1/20-in.-diameter particles, the pressure drop at practical flow rates was less than that of water for particle volumetric loadings up to about 30%. The significance of this result is that the potential benefits

of a phase-change slurry can be realized with little or no pressure drop penalty. This behavior is a strong, but not yet understood, function of particle size.

(2) The pressure drop behavior observed in this study, including reduced pressure drop at moderate loadings and increased pressure drop at higher loadings, appears to represent new phenomena not thoroughly investigated and in some cases not even anticipated in previous work. The results open up exciting possibilities for potential DHC development. However, more comprehensive work is required to accurately assess such possibilities and evaluate the optimal operating conditions.

(3) The heat transfer measurements for a non-melting slurry with 1/8-in.-diameter particles showed a modest enhancement of heat transfer over that of water when presented in the form of Stanton numbers, but the data with 1/20-in.-diameter particles showed a modest degradation. The results indicate that further studies are needed to define the regimes where beneficial effects are present. Testing must also be conducted to assess the effect of phase change, which represents a second heat transfer enhancement mechanism yet to be explored.

(4) The preliminary test results for combined-concept fluids consisting of slurries with friction-reducing additives have demonstrated that the additives can substantially reduce frictional losses for both pure water and slurries with particle loadings ranging up to a moderately high value of around 30%. The friction-reducing additives appear to lose their effectiveness at higher particle loadings of 35-40%. This result indicates that a critical upper-limit particle loading exists for combined-concept fluids. This critical particle loading is sufficiently high to retain the projected benefits associated with phase-change slurries.

(5) The radial fluid temperature distribution in a pipe is altered considerably when a friction-reducing additive is added to a slurry of pure water and X-HDPE particles. A higher wall temperature and lower core temperature have been observed in the heating mode. The

heat transfer coefficient is reduced in the presence of the friction-reducing additive.

(6) A particularly interesting and apparently new phenomenon that came to light in our studies is that of flow re-laminarization. It appears that at flow rates that would normally be considered in the fully turbulent regime, the slurry can revert to laminar behavior if the particle loading is sufficiently high. This critical loading is in the range of 35-40% for 1/20-in.-diameter particles and is a strong function of particle size and flow conditions. The laminarization causes the slurry radial temperature profiles to change from the well-mixed profile characteristic of turbulent flow to a profile with large gradients characteristic of laminar flow. The postulated phenomenon is consistent with the interpretation that loadings above the critical value are accompanied by unexpected large increases in slurry viscosity, to the extent that even with the laminarized flow, the pressure drop is higher than that associated with turbulent conditions at comparable flow rates. The phenomenon is also consistent with the observed decrease of the effectiveness of friction-reducing additives at high slurry particle loadings.

(7) The past work on particle suspension rheology and development of engineering correlations for slurry transport has emphasized the influence of the particle volume fraction. This experimental study has presented evidence to show that the particle size plays an important role in the slurry effective viscosity, pressure drop behavior, and heat transfer. No satisfactory empirical correlations exist to predict these quantities, which are important to design of a DHC system. Further experimental studies of slurry with smaller size particles and with phase change are needed to establish a data base and to develop the needed understanding and correlations.

ACKNOWLEDGMENTS

We gratefully acknowledge the contributions of Professor M. M. Chen, who helped to evaluate the status of the literature for slurry flows and provided many helpful discussions on slurry transport mechanisms. We are also indebted

to Dr. J. Krazinski for his earlier efforts in development of the test plan and his initial experimental work, and to Mr. E. Ohare for his technical assistance. The painstaking care that Ms. C. Bertino exercised in the typing of this manuscript is sincerely appreciated.

This work is performed for the U.S. Department of Energy, Office of Buildings and Community Systems, under Contract No. W-31-109-Eng-38.

REFERENCES

1. Kasza, K. E., and Chen, M. M., "Development of Enhanced Heat Transfer/ Transport/Storage Slurries for Thermal System Improvement," Argonne National Laboratory, ANL-82-50, June 1982.

2. Kasza, K. E., and Chen, M. M., "Improvement of the Performance of Solar Energy or Waste Heat Utilization Systems by Using Phase-Change Slurry as an Enhanced Heat-Transfer Storage Fluid," ASME Trans.; J. Sol. Energy Eng., Vol. 107, pp. 229-236, August 1985.

3. Kasza, K. E., and Chen, M. M., "Assessment of Impact of Advanced Energy Transmission Fluids on District Heating and Cooling Systems (Phase I)," Argonne National Laboratory, ANL-87-21, September 1987.

4. Kasza, K. E., Choi, U. S., and Kaminsky, J., "Optimal Energy Transmission Fluids for District Heating and Cooling Applications," Proceedings of 77th Annual IDHCA Conference, pp. 163-172, Asheville, NC, June 9-11, 1986.

5. Choi, U. S., Cho, Y. I., and Kasza, K. E., "Screening and Degradation Tests of Linear Polymer Additives for District Heating Applications," Argonne National Laboratory, ANL-87-49, December 1987.

6. Toms, B. A., "Some Observations on the Flow of Linear Polymer Solutions Through Straight Tubes at Large Reynolds Numbers," Proc. of the International Congress on Rheology, Vol. 2, pp. 135-141, Scheveningen, North Holland Publ. Co., Amsterdam, 1948.

7. Bobkowicz, A. J., and Gauvin, W. H., "The Effects of Turbulence on the Flow Characteristics of Model Fibre Suspensions," Chem. Eng. Sci., Vol. 22, pp. 229-241, 1967.

8. Boyce, M. P., and Black, E. F., "Fluid Flow Phenomena in Dusty Air," J. Basic Eng., Vol. 92, No. 3, pp. 495-502, 1970.

9. Peters, L. K., and Klinzing, C. E., "Friction In Turbulent Flow of Solid-Gas Systems," Can. J. Chem. Eng., Vol. 50, No. 4, pp. 441-444, 1972.

10. Soo, S. L., "Fluid Dynamics of Multiphase Systems," Blaisdell Pub. Co., Waltham, MA, 1967.

11. Vanoni, V. A., "Transportation of Suspended Sediment by Water," Trans. Am. Soc. Civ. Eng., Publication 2267, Vol. 111, p. 67, 1964.

12. Zandi, I., "Decreased Head Loss in Raw Water Conduits," J. Am. Water Works Assoc., Vol. 59, No. 2, pp. 213-226, 1967.

13. Schlichting, H., "Boundary-Layer Theory," 6th ed., McGraw-Hill Co., New York, 1968.

14. Knudsen, J. G., and Katz, D. L., "Fluid Dynamics and Heat Transfer," McGraw-Hill Co., New York, 1958.

15. Nikuradse, J., "Gesetzmassigkerten der Turbulenten Stromung in glatten Rohren," Forschungschrift No. 356, V.D.I. Verlag, Berlin, 1932.

16. Drew, T. B., Koo, E. C., and McAdams, W. H., "The Friction Factor for Clean Round Pipes," Trans. AIChE, Vol. 28, pp. 56-72, 1932.

17. Knodel, B. D., "R&D Pilot Plant Project for Evaluating A Direct Freeze Ice Slurry Based District Cooling System," Draft Final Report, CBI Research Co., DOE Contract No. DE-FG01-86CE26564, September 1987.

18. Einstein, A., "Investigations on the Theory of the Brownian Movement," Dover, New York, 1956.

19. Zuba, N., "On the Dispersed Two-Phase Flow in the Laminar Flow Regime," Chem. Eng. Sci., Vol. 19, pp. 897-917, 1964.

20. Ackermann, N. L., and Shen, H. T., "Rheological Characteristics of Solid-Liquid Mixtures," AIChE J., Vol. 25, No. 2, pp. 327-332, 1979.

21. Mooney, M., "The Viscosity of a Concentrated Suspension of Spherical Particles," J. Colloid Sci., Vol. 6, pp. 162-170, 1951.

22. Jeffery, D. J., and Acrivos, A., "The Rheological Properties of Suspensions of Rigid Particles," AIChE J., Vol. 22, No. 3, pp. 417-432, 1976.

23. Thomas, D. G., "Transport Characteristics of Suspension: VIII. A Note on the Viscosity of Newtonian Suspensions of Uniform Spherical Particles," J. Colloid Sci., Vol. 20, pp. 267-277, 1965.

24. Vand, V. J., "Viscosity of Solutions and Suspensions I,"J. Phys. Colloid Chem., Vol. 52, pp. 277-299, 1948.

25. Brinkman, H. C., "The Viscosity of Concentrated Suspensions and Solutions," J. Chem. Phys., Vol. 20, pp. 571, 1952.

26. Rutgers, R., "Relative Viscosity of Suspensions of Rigid Spheres In Newtonian Liquids," Rheol. Acta, Vol. 2, pp. 202-210, 1962.

27. Shaheen, E. I., "Rheological Studies of Viscosities and Pipeline Flow of Concentrated Slurries," Powder Technol., Vol. 5, pp. 245-256, 1972.

28. Jinescu, V. V., "The Rheology of Suspensions," Int. Chem. Eng., Vol. 14, No. 3, pp. 397-420, 1974.

29. Turian, R. M., "Slurry and Suspension Transport; An Assessment of Current Research and Long Term Interdisciplinary Needs," Report prepared for National Science Foundation, NTIS No. PB83107839, March 1982.

30. Hanks, R. W., "Hydraulic Design for Flow of Complex Fluids; Course Notes," Richard W. Hanks Assoc., Orem, Utah, 1981.

31. Durand, R., "Transport Hydraulique de Graviers et Galets en Conduite," La Houille Blanche, Vol. 6, pp. 609-619, 1951.

32. Durand, R., and Condolios, E., "Communication de R. Durand et E. Condolios," Compte Rendu des Deuxiemes Journees de L'Hydraulique (Paris, Societe Hydrotechnique de France), pp. 29-55, June 1952.

33. Durand, R., "The Hydraulic Transport of Coal and Solid Materials in Pipes," Proceedings of a Colloquium on the Hydraulic Transport of Coal (Nov. 5-6, 1952), pp. 39-52, National Coal Board, London, England, 1953.

34. Zandi, I., and Govatos, G., "Heterogeneous Flow of Solids in Pipelines," J. Hydr. Div., ASCE, Vol. 93, HY3, pp. 145-159, 1967.

35. Babcock, H. A., "Heterogeneous Flow of Heterogeneous Solids," Advances in Solid-Liquid Flow in Pipes and Its Application, I. Zandi, ed., pp. 125-148, Pergamon Press, New York, 1971.

36. Turian, R. M., and Yuan, T. F., "Flow of Slurries in Pipelines," AIChE J., Vol. 23, pp. 232-243, 1977.

37. Turian, R. M., Hsu, F. L., and Ma, T. W., "Estimation of the Critical Velocity in Pipeline Flow of Slurries," Powder Technol., Vol. 51, pp. 35-47, 1987.

38. Oroskar, A. R., and Turian, R. W., "The Critical Velocity in Pipeline Flow of Slurries," AIChE J., Vol. 26, No. 4, pp. 550-558, 1980.

APPENDIX A. THERMOPHYSICAL PROPERTIES OF WATER AND X-HDPE PARTICLES

A.1 Temperature-Dependent Properties of Water

The viscosity of water varies considerably with temperature. In order to account for the temperature-dependent transport property variations, we used a polynomial least-squares fit technique to compute the properties of water on the basis of data given by Chapman [A1]. The following equations are used for the transport properties:

$$\rho = 4.107 \times 10^{2} - 1.635 \times 10^{1}T + 3.038 \times 10^{-1}T^{2} - 2.796 \times 10^{-3}T^{3} + 1.273 \times 10^{-5}T^{4} - 2.298 \times 10^{-8}T^{5} \quad [\text{lbm/ft}^3], \tag{A.1}$$

$$\mu = 8.548 - 1.934 \times 10^{-1}T + 2.476 \times 10^{-3}T^{2} - 1.860 \times 10^{-5}T^{3} + 7.566 \times 10^{-8}T^{4} - 1.282 \times 10^{-10}T^{5} \quad [\text{lbm/ft-hr}], \tag{A.2}$$

$$k = 3.696 \times 10^{-1} - 2.567 \times 10^{-3}T + 6.331 \times 10^{-5}T^{2} - 6.245 \times 10^{-7}T^{3} + 2.945 \times 10^{-9}T^{4} - 5.448 \times 10^{-12}T^{5} \ [\text{Btu/hr-ft-°F}], \tag{A.3}$$

$$Pr = 2.397 \times 10^{1} - 4.778 \times 10^{-1}T + 4.952 \times 10^{-3}T^{2} - 2.926 \times 10^{-5}T^{3} + 9.382 \times 10^{-8}T^{4} - 1.282 \times 10^{-10}T^{5}. \tag{A.4}$$

The specific heat, Cp, has a constant value of 0.998 Btu/lbm-°F in the temperature range from 70 to 140°F.

A.2 Properties of X-HDPE

The particles used in the slurry heat transfer tests are cross-linked, high-density polyethylene (X-HDPE), developed by Monsanto Research Corporation under DOE contract [A2,A3]. The HDPE has a high latent heat of fusion (72 Btu/lbm) and has been used for thermal energy storage applications. HDPE is a low-cost, widely used commercial plastic produced in the U.S. It is nontoxic, nonvolatile, and insoluble in common heat transfer liquids such as water and ethylene glycol.

Four principal methods are used for cross-linking HDPE: (a) coupling by agents such as vinyl triethoxysilane, (b) electron beam irradiation, (c) gamma irradiation, and (d) chemical cross-linking with peroxides. The X-HDPE used in these experiments is cross-linked by irradiation. The melting temperature and thermal conductivity of HDPE are not changed as a result of the irradiation process. The heat of fusion of the particles is reduced by a few percent with increasing cross-linking. As the X-HDPE particle starts to melt at a temperature of about 270°F (132°C), the X-HDPE changes from a white, opaque crystalline solid to a gel-like, transparent elastic material. A small void inside the 1/8-in.-diameter particle, formed during the production process, becomes visible when the particle starts to melt. However, the particle retains its original shape as it melts. Table A.1 lists the thermophysical properties of X-HDPE, together with those of water.

Table A.1. Thermophysical Properties of X-HDPE

Property	British Units	SI Units	Ratio of X-HDPE Value to Water Value
Density (ρ)	60 lbm/ft^3	960 kg/m^3	0.96
Thermal Conductivity (k)	0.27-0.30 Btu/hr-ft-°F	0.46-0.52 W/m-°C	~0.81
Specific Heat (Cp)	0.55 Btu/lbm-°F	2.31 kJ/kg-°C	~0.55
Latent Heat of Fusion	72 Btu/lbm	168 kJ/kg	~0.5*
Melting Point	270.5°F	132.5°C	---
Linear Thermal Expansion Coefficient**	59×10^{-6} to 110×10^{-6} in./in.-°F	11×10^{-5} to 20×10^{-5} m/m-°C	~0.3-0.55

*The latent heat of fusion for water is measured at 0°C.
**Based on data in CRC Handbook of Chemistry and Physics, 63rd Edition, 1983.

HDPE particles of two different sizes, with nominal diameters of 1/8 and 1/20 in., respectively, were used in the present study. The actual 1/8-in. HDPE particle is somewhat elliptical in shape.

References

A1. Chapman, A. J., "Heat Transfer," 4th Edition, MacMillan Publishing Co., New York, 1984.

A2. Botham, R. A., Ball, G. L., III, Jenkins, G. H., and Salyer, I. O., "Form-Stable Crystalline Polymer Pellets for Thermal Energy Storage -- High Density Polyethylene Intermediate Products," Oak Ridge National Laboratory Report, ORNL/SUB-7394/4, Prepared by Monsanto Research Corporation, Jan. 1978.

A3. Cole, R. L., "Thermal Storage Device Based on High-Density Polyethylene, Interim Progress Report," Argonne National Laboratory, ANL-83-52, June 1983.

APPENDIX B. DATA REDUCTION PROCESS FOR HEAT TRANSFER ANALYSIS

Although the heat transfer associated with the single-phase turbulent flow of liquids in pipes is well understood, experiments with pure water were conducted both to validate the experimental procedures and to provide a comparative basis for evaluating the heat transfer enhancement associated with slurry flows. The data reduction procedures for both pure water and slurry heat transfer analysis are discussed here.

B.1 Parameters Used in Heat Transfer Analysis

Borrowing from single-phase flow theory, the heat transfer associated with pipe flows can be expressed in terms of the Nusselt (Nu) and Stanton (St) nondimensional heat transfer numbers:

$$Nu_i = \frac{h_i x_i}{k} \qquad (B.1)$$

$$St = \frac{h_{av}}{\rho C p U_{av}}$$

where

$$h_i = \frac{q_i}{T_{win,i} - T_{b,i}} \qquad (B.2)$$

is the local heat transfer coefficient and h_{av} is the average heat transfer coefficient. The local heat flux in the i^{th} segment of test section, q_i, is determined from the measured power input, and the thermal conductivity, k, is evaluated at the local mean temperature $(T_{win,i} + T_{b,i})/2$. The local bulk fluid temperature $T_{b,i}$ can be determined from the overall energy balance equation, which will be discussed in Section B.3.

B.2 Tube Inside Wall Temperature

The tube inside wall temperature, T_{win}, used in Eq. (B.2), is calculated on the basis of a steady-state heat conduction equation with a constant heat source and insulated wall boundary condition as derived by Matthys [B1]:

$$T_{win} = T_{wout} - \frac{Q}{2\pi(r_o^2 - r_i^2)L\, k_t}\left[r_o^2 \ln\left(\frac{r_o}{r_i}\right) + \frac{r_i^2 - r_o^2}{2}\right] \qquad (B.3)$$

where k_t, the thermal conductivity of the stainless steel tube, is ~15 W/m-°C; r_o, the outside tube radius, is 0.5 in. (0.0127 m); and r_i, the inside tube radius, is 0.472 in. (0.01199 m). Given the measured power input and outside wall temperature for each segment of the test section, the inside wall temperature can be calculated. Figure B.1 shows the temperature difference across the tube wall and the power input versus the flow rate of pure water. The temperature drop across the tube wall varied from 1.5°F (0.8°C) at 48 lbm/min (22 kg/min) to 7°F (3.9°C) at 308 lbm/min (140 kg/min).

B.3 Bulk Fluid Temperature

The bulk fluid temperature at each segment of the test section, $T_{b,i}$, is simply the sum of the inlet fluid temperature of the segment and the bulk fluid temperature rise within the segment. This bulk fluid temperature rise is determined by the measured power input to the axial segment in question and the product of the mass flow rate and the specific heat of the fluid. The typical power input distributions along the five segments of the test section for different pump settings (i.e., flow rates) are presented in Fig. B.2. The average water flow velocities in the tube corresponding to these pump settings are plotted in Fig. B.3. The bulk fluid temperature rise across each of the segments, $\Delta T_{b,i}$, is then determined by the following equation:

$$\Delta T_{b,i} = \frac{Q_i}{\dot{m}\ Cp} \tag{B.4}$$

where $\dot{m}$ is the mass flow rate and Cp is the effective specific heat of the fluid. The bulk fluid temperature can be calculated in this fashion along the pipe length for each segment from the inlet to the outlet. Figure B.4 shows the variation of wall and bulk fluid temperature along the test section for pure water at pump setting 4. The accuracy of the bulk fluid temperature calculated at the outlet of the test section by using Eq. (B.4) can be checked by comparison with the measured fluid outlet temperature and the overall energy balance of the system.

The discrepancy between the measured overall energy balance and the calculated value $(\dot{m}Cp\Delta T_b - Q)/Q$, which varies from only -1% to -1.8% in tests of pure water, is attributed to the heat loss through the insulation cover of the outer tube wall of the test section.

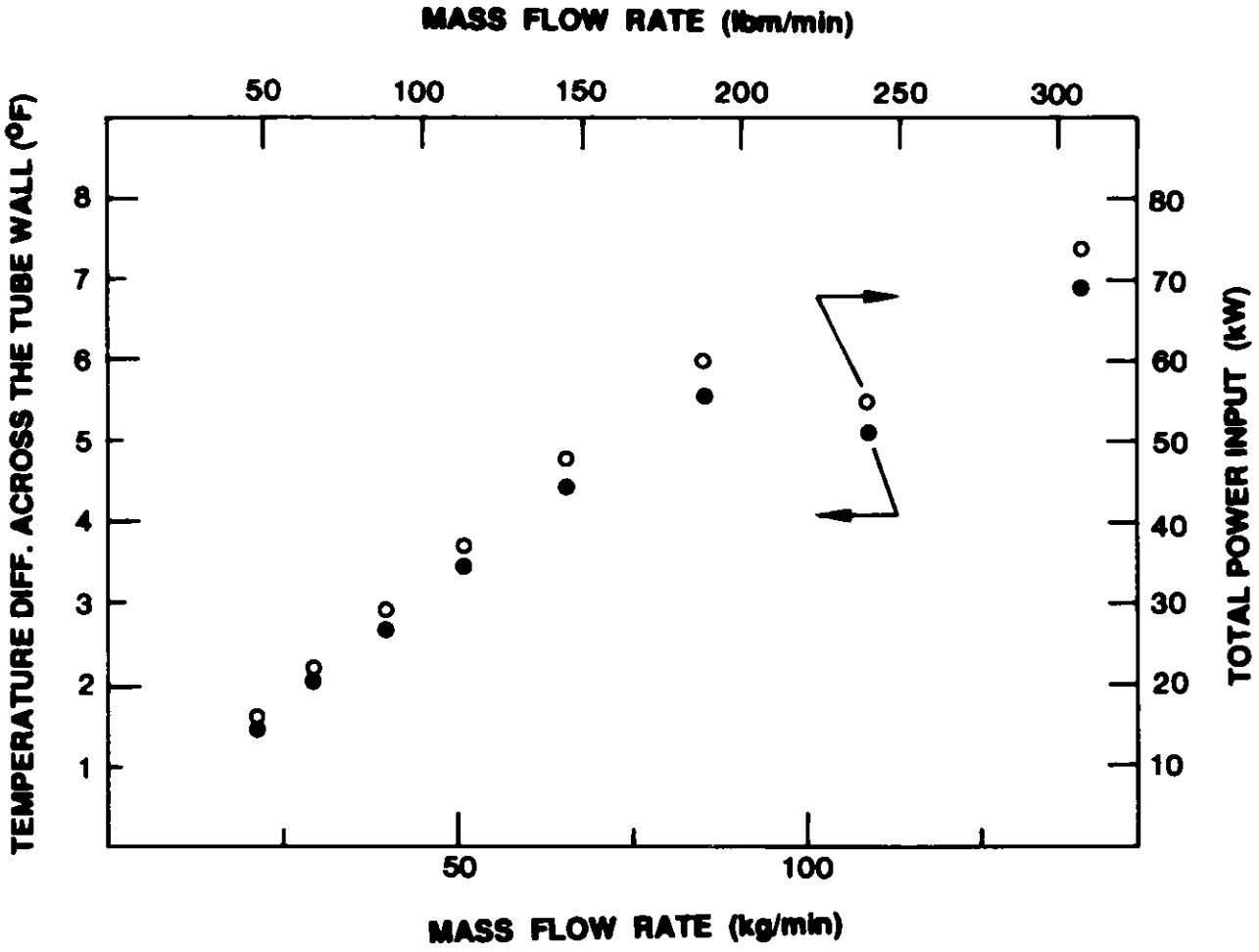

Fig. B.1. Temperature Drop Across the Tube Wall and Power Input at Various Mass Flow Rates of Water.

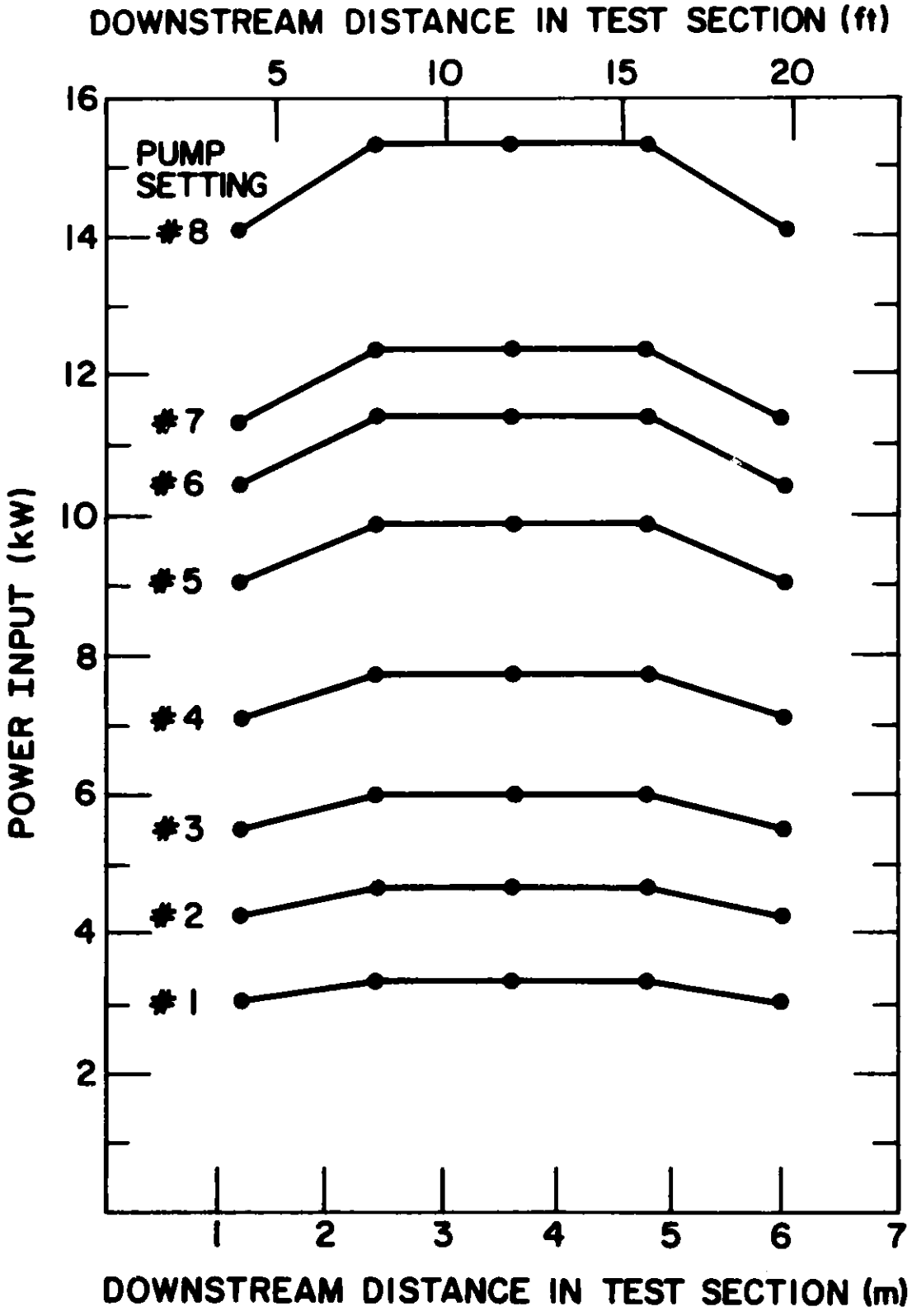

Fig. B.2. Power Input Distribution Along the Test Section.

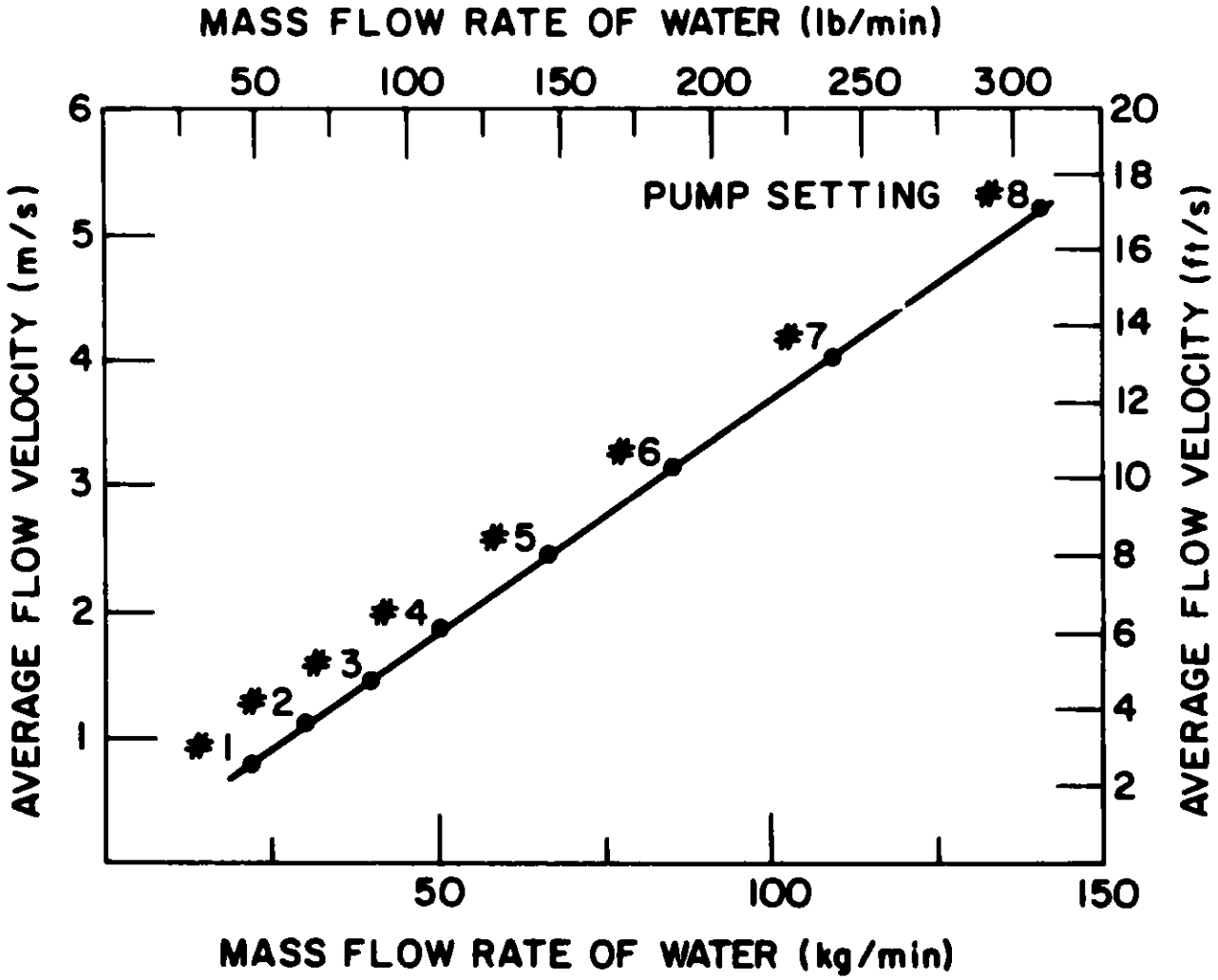

Fig. B.3. Average Pipe Flow Velocity Versus Mass Flow Rate for Different Pump Settings.

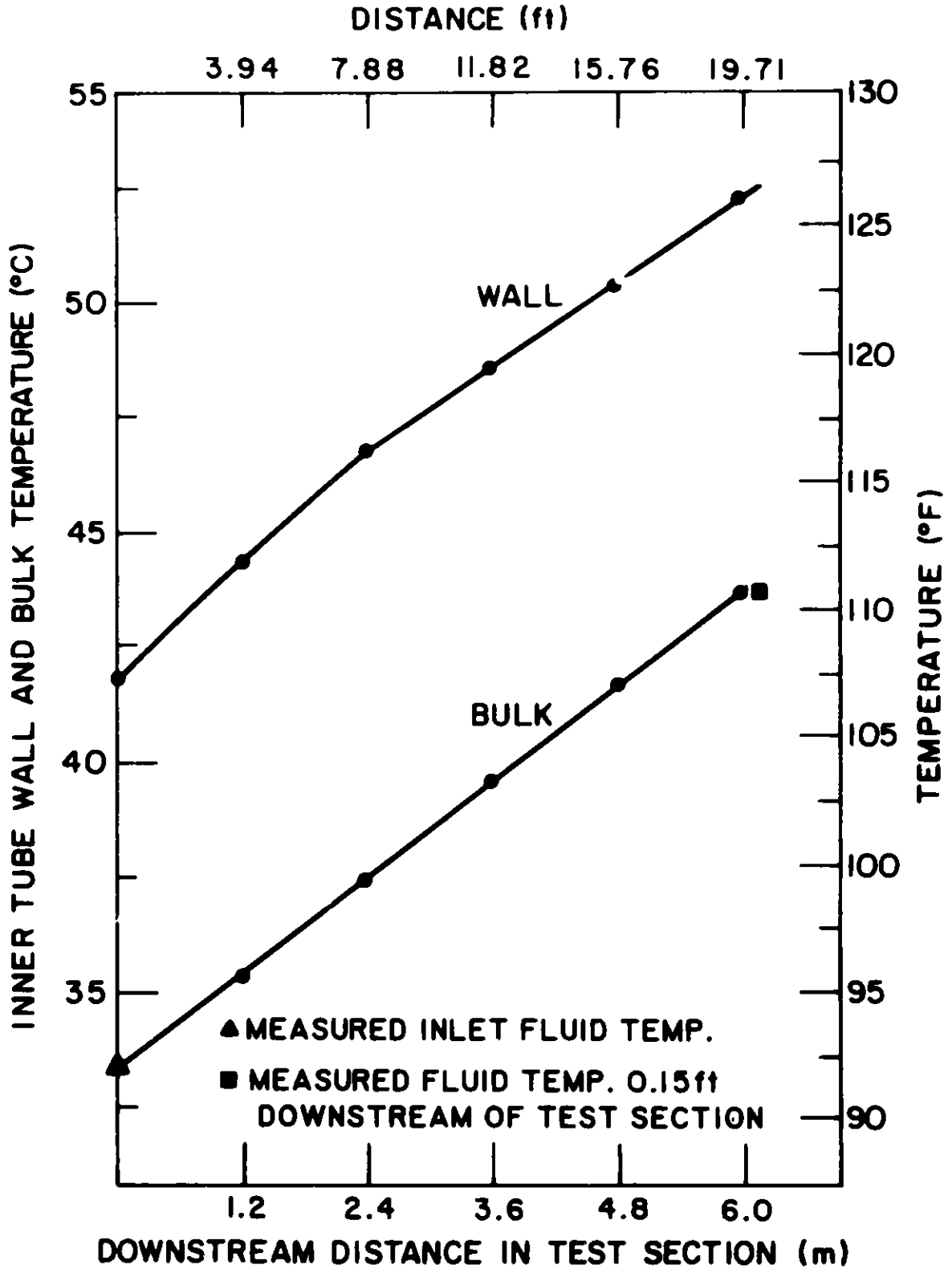

Fig. B.4. Variation of Tube Wall and Bulk Fluid Temperature Along the Test Section for Pump Setting Number 4.

Figure B.5 shows the temperature differences between the inside tube wall and the bulk fluid, calculated from Eqs. (B.3) and (B.4) at each segment of the test section for various flow rates of pure water. Local electrical power input along the tube is not uniform, as shown in Fig. B.2. Because of end effects, i.e., the presence of copper lugs for the electrical connection to the test section, the power inputs to the two end segments are slightly lower than the power inputs to the middle three segments. For the calculation of an averaged heat transfer coefficient, data from the middle three segments of the test section, ~12 ft (3.66 m) in length, were used. As mentioned previously, the power inputs used for the different tests of slurry mass flow rate (pump settings) were selected to maintain a relatively fixed bulk fluid temperature rise, ~20°F (11.1°C), across the test section. Hence, the variation of $(T_{win} - T_b)$ measured at the exit of the test section for different test conditions is small (Fig. B.5). The smaller temperature difference $(T_{win} - T_b)$ at pump settings 7 and 8 (Fig. B.5) was due to smaller power inputs at these two pump settings (Fig. B.1). These reduced power inputs were selected in order to keep the electric power input within the capacity of the DC power supply, ~70 kW.

B.4 Slurry Thermal Non-Equilibrium and Non-Uniform Radial Temperature Distributions

The data reduction process for slurry heat transfer tests is more complicated than for pure water. The first complication arises from property differences between X-HDPE and water and from the fact that the two phases may not be in thermal equilibrium. As shown in Appendix A, the specific heat of X-HDPE is approximately half that of water (0.55 Btu/lbm-°F compared to 1.0 Btu/lbm-°F for water). A simple, one-dimensional thermal conduction calculation revealed that 1.6 seconds are required to heat the center of 1/8-in.-diameter X-HDPE particles to one-half the temperature of the surrounding fluid, and 3.5 seconds are needed for the center temperature to reach 90% of the fluid temperature. Hence, during heating of a slurry with 1/8-in.-diameter particles, the temperature of the particles lags behind that of the fluid. Because of the average tube flow velocity and test section length, slurry tests with pump settings greater than 4 clearly will not attain thermal equilibrium. If a thermal equilibrium condition is assumed, the overall bulk

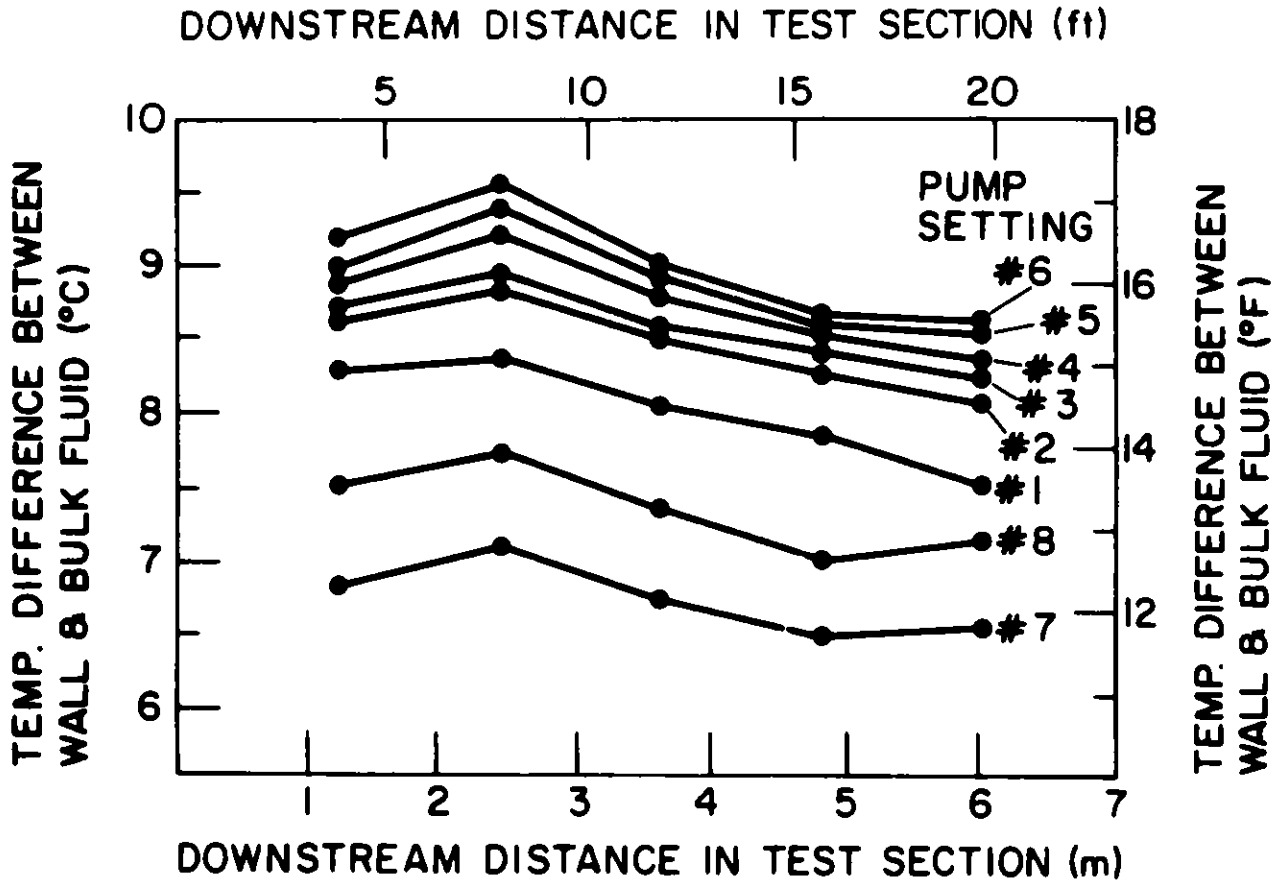

Fig. B.5. Variation of Temperature Difference Between Tube Wall and Bulk Fluid Along the Test Section for Various Flow Rates of Pure Water.

fluid temperature rise for the slurry will be higher than that for pure water at the same flow rates, power inputs, and inlet fluid temperatures because of the smaller effective specific heat for the slurry than for pure water. Even for cases with low flow rates, thermal equilibrium may not be reached because of nonuniform fluid temperature along the axial direction of the test section.

The second complication arises from the potentially nonuniform radial temperature profile in pipe flows under highly loaded conditions. It is recognized that the thermal boundary layer is very thin for a fully developed single-phase turbulent pipe flow. The bulk fluid temperature in the pipe is very close to the fluid temperature measured at the pipe centerline, assuming that good mixing occurs. However, the difference between the bulk fluid temperature and the centerline fluid temperature could be very large in a highly loaded slurry flow owing to a change of turbulent flow regime. The slurry heat transfer analysis thus becomes more complex and difficult.

B.5 Slurry Bulk Temperature and Bulk Temperature Rise

The definition of bulk fluid temperature at a given pipe cross section for a single-phase flow is

$$T_b = \frac{\int \rho u C_p T \, dA}{\int \rho u C_p \, dA} . \tag{B.5}$$

For two-phase slurry flow, the bulk fluid temperature is then expressed as

$$T_b = \frac{\int \sum_{i=1}^{2} (\rho u C_p T)_i \, dA}{\int \sum_{i=1}^{2} (\rho u C_p)_i \, dA} . \tag{B.6}$$

The bulk fluid temperature rise from one cross section to another along the flow direction is due to the electrical power input to that test section; this rise is expressed in a form similar to that of Eq. (B.4),

$$\Delta T_{b,i} = \frac{Q_i}{\dot{m}_{slurry} C_{p_{slurry}}} . \tag{B.7}$$

If the thermal equilibrium condition is assumed, the effective specific heat of the slurry can be estimated by the equation

$$Cp_{slurry} = Cp_{HDPE}\,\varepsilon + Cp_{H2O}\,(1 - \varepsilon) \qquad (B.8)$$

where ε, the particle mass fraction, is the ratio of total dry X-HDPE particle weight to total slurry weight measured during the test.

For a slurry flow with thermal nonequilibrium conditions, the fluid temperature will not be the same as that of the particles. The determination of the bulk fluid temperature rise then ceases to be a straightforward process because the effective specific heat of the slurry is no longer a quantity that can be easily defined.

There are two measurable quantities which may be used to determine whether or not the slurry is in a thermal equilibrium condition. The first one is the total energy input to the test section, which takes into account the heat loss through the outer tube wall. As mentioned previously, a fairly constant heat loss, ~1.5% of total heat input, was found in the pure water test. Since the test conditions for slurry are the same as that for pure water, the heat loss for slurry flows is assumed to be similar to that for pure water. If the particle temperature differs greatly from the fluid temperature, a considerable difference will be observed between the measured heat input and the calculated energy absorption by the slurry, $Q = \dot{m}_{slurry} Cp_{slurry} \Delta T_b$, assuming T_b at the exit of the test section is the same as the measured fluid temperature. The second quantity that can be used to check the thermal non-equilibration is the bulk temperature obtained at the exit of the test section. If the slurry is highly non-equilibrated, a large difference will appear between the calculated bulk temperature, based on total energy balance across the test section, and the measured value, either based on the radial temperature profile at the test section exit or obtained at the end of the flow stream before the slurry enters the weighing tank.

A model has been developed to determine the degree of thermal equilibration based on total energy input and the bulk fluid temperature at the exit of the test section. With the estimated degree of thermal equilibration, the effective specific heat of the slurry can be obtained for heat transfer analysis.

The degree of thermal equilibration, δ, is defined as

$$\delta = \frac{T_{HDPE)exit} - T_{HDPE)in}}{T_{H2O)exit} - T_{H2O)in} \quad (B.9)$$

where δ is 1.0 if the slurry is in a thermal equilibrium condition, i.e., equal temperatures for particle and fluid.

The exit particle temperature $T_{HDPE)exit}$ in Eq. (B.9) is determined from the energy conservation equation

$$Q = \dot{m}_{HDPE} Cp_{HDPE} (T_{exit} - T_{in})_{HDPE} + \dot{m}_{H2O} Cp_{H2O} (T_{exit} - T_{in})_{H2O} \quad (B.10)$$

where the heat input, Q, is a measured value that takes into account heat loss to the ambient.

After the degree of thermal equilibration, δ, is calculated, the effective specific heat of the slurry can be obtained from a modification of Eq. (B.8),

$$Cp_{slurry} = Cp_{HDPE} \varepsilon \delta + Cp_{H2O} (1 - \varepsilon). \quad (B.11)$$

It is evident that the higher the degree of thermal equilibration, δ, the smaller will be the difference between the values of Cp_{slurry} expressed by Eqs. (B.8) and (B.11). This effective slurry specific heat is used again in Eq. (B.7) to compute the local bulk temperature rise.

Figure B.6 shows the axial bulk fluid temperature profiles along the test section obtained from a slurry heat transfer test (1/8-in.-diameter particles with 30% particle volumetric loading) and from a pure-water test. The calculated bulk temperatures at the exit of the test section for both pure water and slurry are very close to the values measured 0.145 ft (0.044 m) downstream of the test section. The degree of thermal equilibration for the slurry test shown in Fig. B.6 was found to be 0.74. The degree of thermal equilibration obtained from other slurry tests with 1/8-in.-diameter particles has shown an average value of about 0.75. For slurry tests with smaller particles (1/20 in. diameter), the degree of thermal equilibration was very close to 1.0.

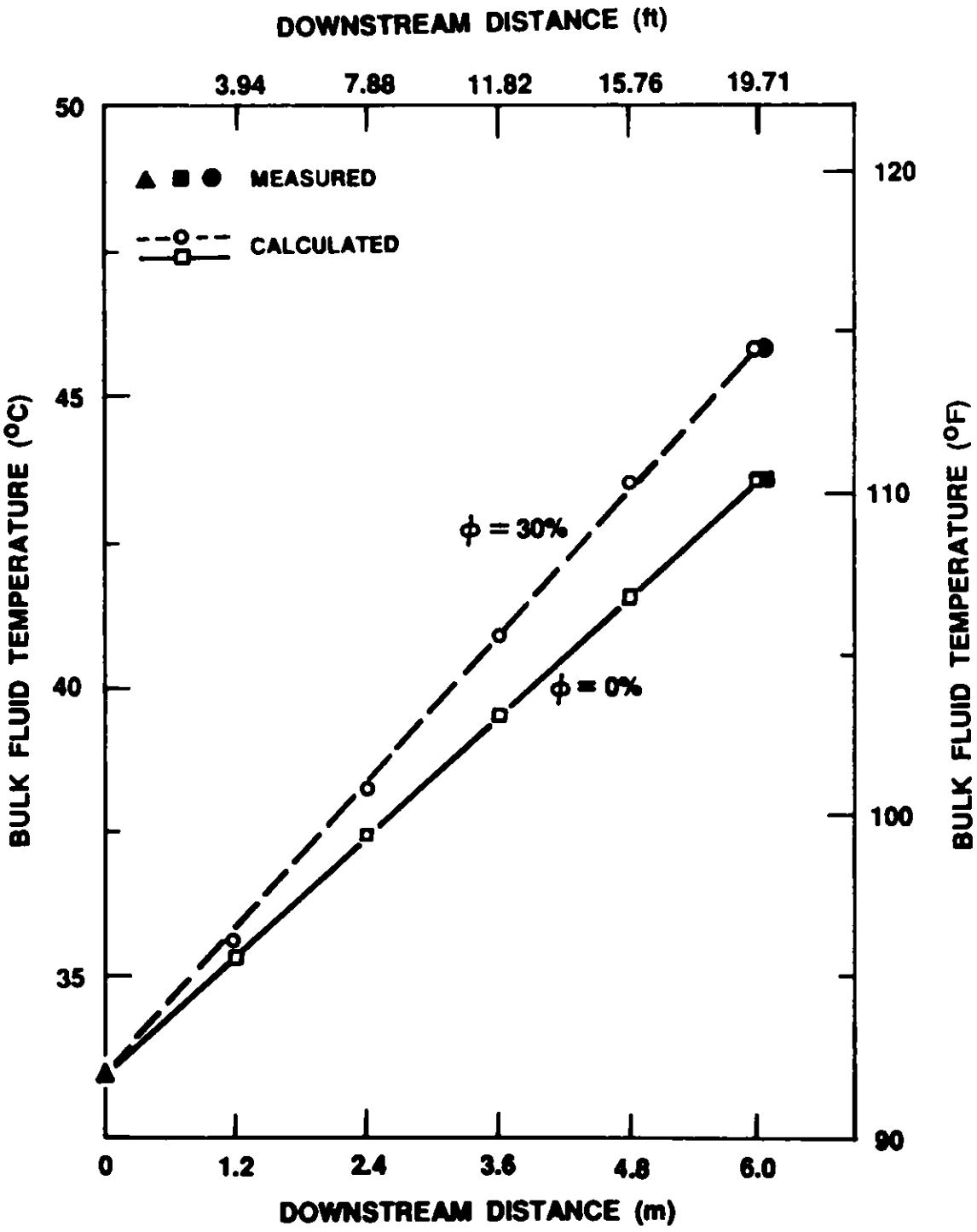

Fig. B.6. Axial Bulk Fluid Temperature Variation Along the Test Section for Pure Water and Slurries with 1/8-in.-Diameter Particles.

B.6 Entrance Effect on Thermal Development

The hydrodynamic entrance effect for laminar flow in a circular pipe is known to be limited within a dimensionless pipe length, $x/D \leq 0.05\ Re$, where D is the pipe diameter [B2]. The entrance length in a turbulent flow becomes independent of Reynolds number and can be approximated as

$$10 \leq \frac{x}{D} \leq 60 \ .$$

The thermal entrance length for laminar flow depends on the Reynolds number and Prandtl number of the fluid and may be expressed as

$$\frac{x}{D} \sim 0.05\ Re\ Pr \ .$$

Heat transfer in the entrance region for turbulent water flow in a circular pipe was studied by Malina and Sparrow [B3] and Allen and Eckert [B4]. They defined the thermal entrance length in terms of the dimensionless downstream distance x/D at which the local heat transfer coefficient h_x approaches to within 5% of the value for fully developed flow. Their results revealed that the entrance length for Pr = 3 was only 1.3 diameters and 3.7 diameters for Reynolds numbers of 1.0×10^5 and 1.5×10^5, respectively.

In our slurry heat transfer investigation, the Prandtl number of water is about 4.5 [at about 100°F (38°C)] and the Reynolds number varies from 3×10^4 to 2×10^5. The thermal entrance length will be far less than 4 ft (1.2 m), which is the length of each segment of the test section, if Malina and Sparrow's theory is applied.

As described in the experimental study of Allen and Eckert [B4], the flow attained the hydrodynamically fully developed condition before entering the test section. The thermal boundary layer developed within the entrance region, which had a uniform wall heat flux boundary condition. The viscosity near the pipe wall was reduced because of a rising water temperature. Hence, the local friction coefficient began to decrease in the direction of flow. In the meantime, the gradually rising fluid bulk temperature caused the value of the local heat transfer coefficient to have a concave profile as a function of x/D, changing from a very high value at the start of heating and approaching a

minimum value, then rising farther downstream and approaching an asympotic value (Fig. B.7).

The thermal development in the entrance region of a pipe, $x/D \leq 10$, can be related to the growth of the thermal boundary layer. The local heat transfer coefficient becomes inversely proportional to the thickness of the thermal boundary layer. However, the measured local heat transfer coefficient for pure water increases linearly from segment 1 to segment 4 (Fig. B.8). These results demonstrate that the thermal entrance effect did not play a role in our heat transfer analysis.

B.7 Heat Transfer Correlations for Single-Phase Turbulent Pipe Flow

Some correlations are available in the literature for predicting heat transfer coefficients for single-phase turbulent flow in smooth circular pipes. The most popular correlations used by heat transfer engineers are the Dittus-Boelter [B5] and Sieder-Tate [B6] correlations, which were derived in the 1930s. However, both correlations underestimate the experimental data by as much as 20-25% and are considered too conservative. Lorenz et al. [B7] conducted experimental investigations and found that the best correlation was the one proposed by Petukhov and Popov [B8,B9], which gave values within ±5% of the experimental data over the Reynolds number range from 3×10^4 to 2×10^5 for water at Pr = 6 (80°F) and Pr = 11.6 (40°F).

Local heat transfer measurements of turbulent flow of water in a uniformly heated circular tube at Pr = 8 with a Reynolds number in the range from 1.5×10^4 to 1.0×10^5 were reported by Allen and Eckert [B4]. Their data are in good agreement with the analytical prediction of Sparrow et al. [B3,B10], which accounted for the fluid bulk temperature rise and local property variations. The four heat transfer correlations mentioned above are listed in Table B.1.

A series of tests was performed with water to compare our heat transfer measurement with existing heat transfer correlations for turbulent pipe flow of water with a bulk fluid temperature rise of 20°F (92°F to 112°F) in the Reynolds number range from 3×10^4 to 2×10^5. We used our measured Nusselt numbers, Nu, to compute the constant C in the Sparrow-Hallman-Siegel correlation at 10 different flow rates:

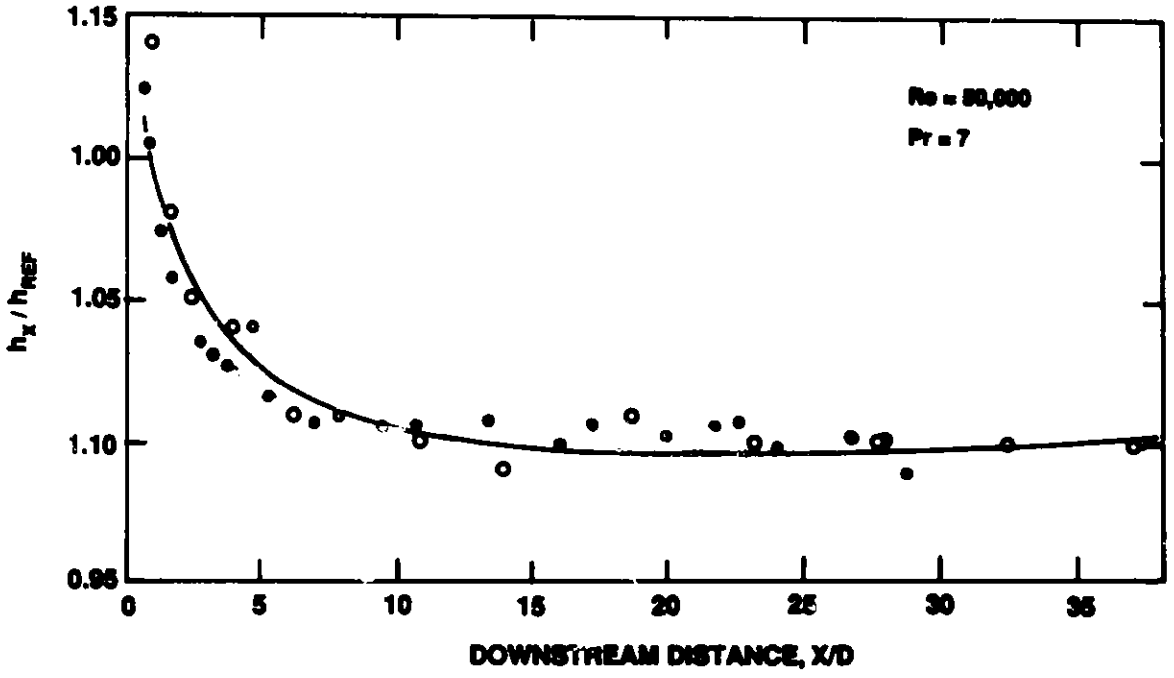

Fig. B.7. Thermal Entrance Effect on Local Heat Transfer Coefficient, Measured and Plotted by Allen and Eckert [B4]. Explanations of the symbols can be found in the original paper.

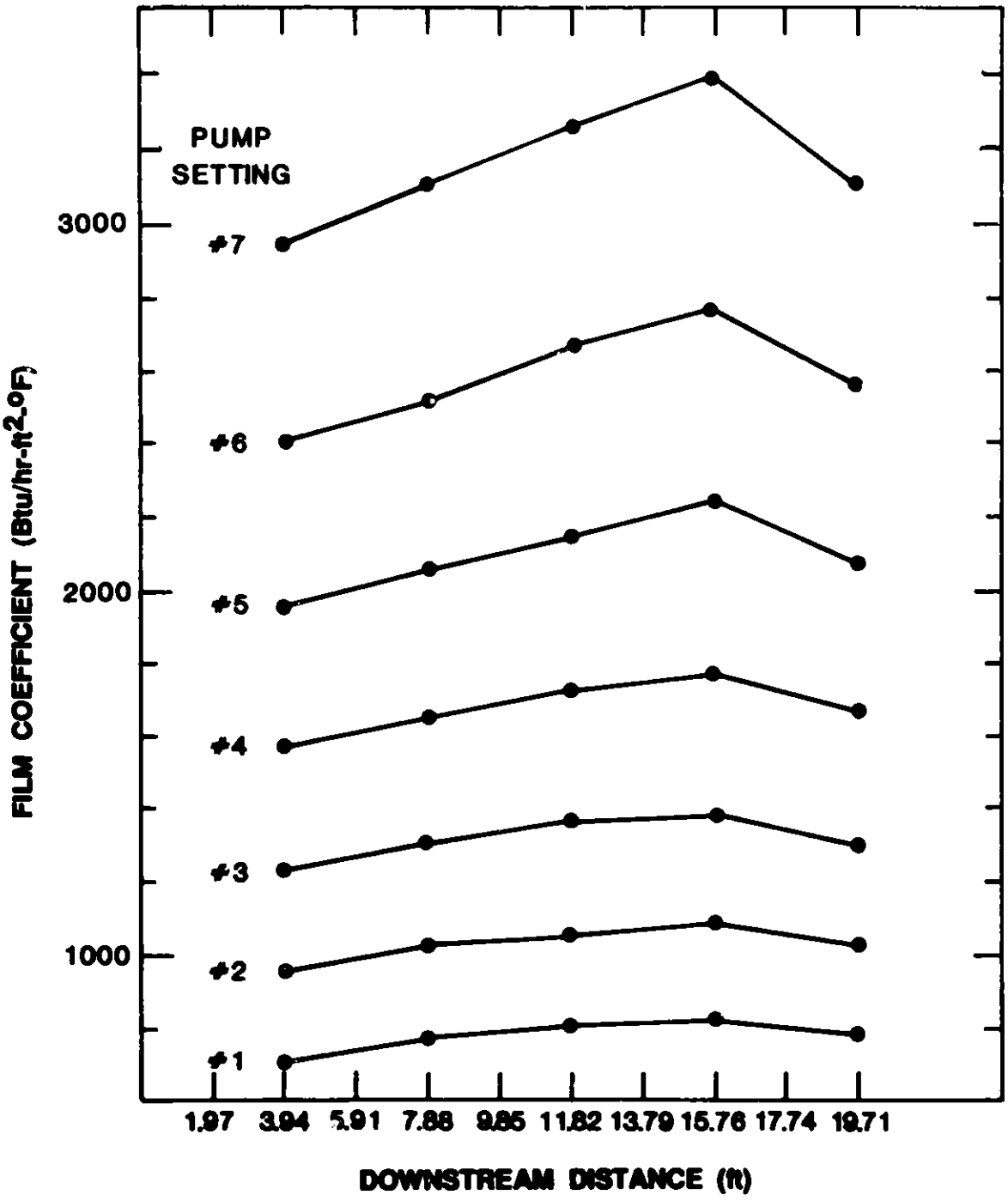

Fig. B.8. Film Coefficients Measured at Five Segments of the Test Section.

Table B.1. Heat Transfer Correlations

Name	Formula	Conditions and Remarks
Dittus-Boelter [B5]	$Nu = 0.023\ Re^{0.8}\ Pr^{0.4}$	$0.5 < Pr < 120$ $2.3 \times 10^2 < Re < 10^7$
Sieder-Tate [B.6]	$Nu = 0.027\ Re^{0.8}\ Pr^{1/3}\ (\frac{\mu}{\mu_c})^{0.14}$	$0.5 < Pr < 120$ $2.3 \times 10^2 < Re < 10^7$ μ: Viscosity at bulk temp. μ_c: Viscosity of continuous phase at wall temp.
Petukhov-Popov [B8,B9]	$Nu = \frac{(\frac{f}{8})\ Re\ Pr}{K_1 + K_2(\frac{f}{8})^{1/2}(Pr^{2/3} - 1)}$ where $K_1 = 1 + 3.4\ f$ $K_2 = 11.7 + 1.8\ Pr^{-1/3}$ $f = (1.82 \log_{10} Re - 1.64)^{-2}$	$0.5 < Pr < 2 \times 10^3$ $10^4 < Re < 5 \times 10^6$
Sparrow et al. [B3, B10]	$Nu = C\ Re^{0.84}\ Pr^{0.42}$	$10^4 < Re < 2 \times 10^5$

$$Nu = C\ Re^{0.84}\ Pr^{0.42}. \qquad (B.12)$$

The results showed that the maximum variation of C was only 3% of the average value of 0.0166.

Figure B.9 presents the ratios of measured Nusselt numbers to predicted Nusselt numbers based on three correlations, D-B (Dittus-Boelter), P-P (Petukhov-Popov), and S-H-S (Sparrow-Hallman-Siegel). The D-B correlation clearly underpredicted the experimental data by 10-25%. The P-P correlation agreed within ±4% of the experimental data. The theoretical analysis of S-H-S was also in close agreement, ±5%, with the experimental data.

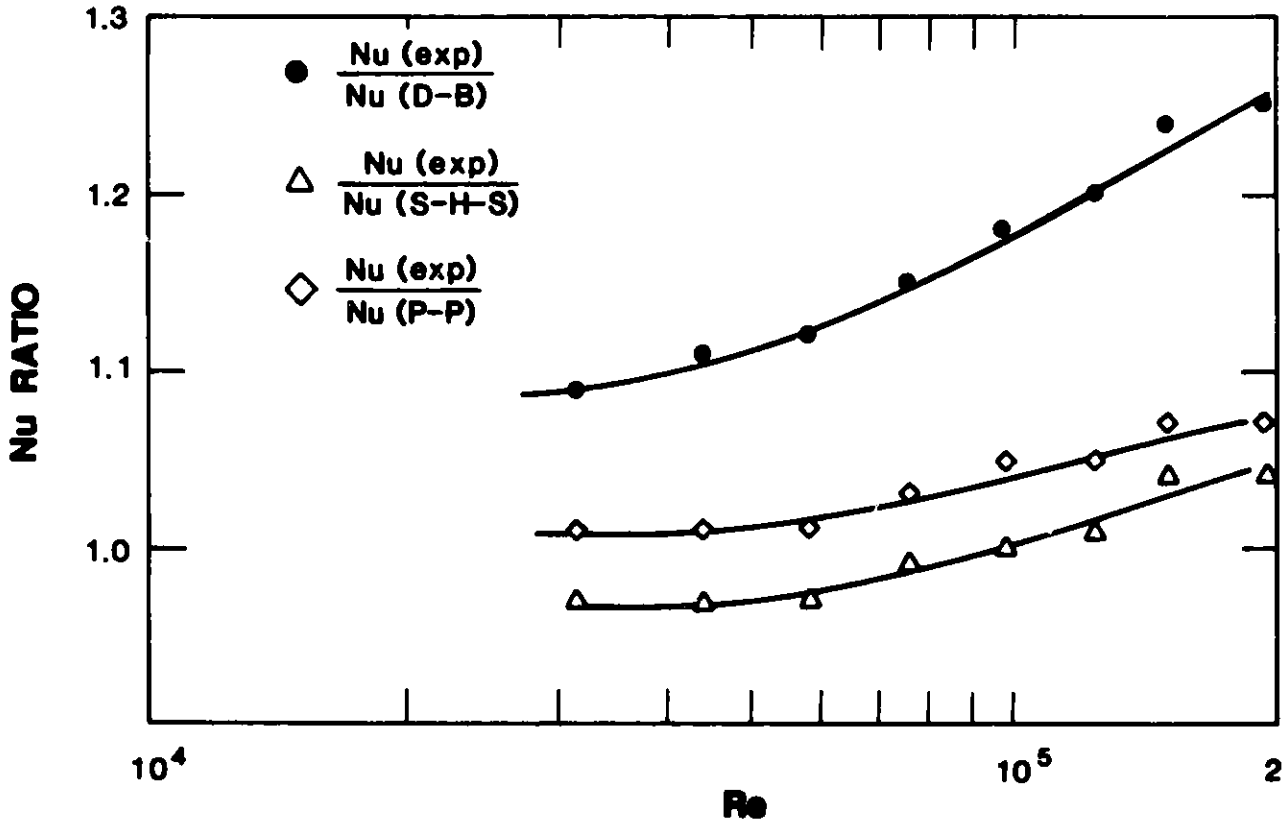

Fig. B.9. Ratios of Nusselt Numbers Measured in the Present Study to Those Calculated from Correlations.

References

B1. Matthys, E. F., "An Experimental Study of Convective Heat Transfer, friction, and Rheology for Non-Newtonian Fluids: Polymer Solutions, Suspensions of Fibers, and Suspensions of Particulates," Ph.D. Thesis, California Institute of Technology, May 1985.

B2. Incropera, F. P., and DeWitt, D. D., "Fundamentals of Heat Transfer," John Wiley & Sons, New York, 1981.

B3. Malina, J. A., and Sparrow, E. M., "Variable-Property, Constant-Property, and Entrance-Region Heat Transfer Results for Turbulent Flow of Water and Oil in a Circular Tube," Chem. Eng. Sci., Vol. 19, pp. 953-962, 1964.

B4. Allen, R. W., and Eckert, E. R. G., "Friction and Heat Transfer Measurements to Turbulent Pipe Flow of Water (Pr = 7 and 8) at Uniform Wall Heat Flux," J. Heat Transfer, pp. 301-310, Aug. 1964.

B5. Dittus, F. W., and Boelter, L. M. K., "Publications in Engineering," University of California, Vol. 2, p. 443, 1930.

B6. Seider, E. N., and Tate, G. E., "Heat Transfer and Pressure Drop of Liquids in Tubes," Ind. Eng. Chem., Vol. 28, pp. 1429-1435, 1936.

B7. Lorenz, J. J., Yung, D. T., Panchal, C. B., and Layton, G. E., "An Assessment of Heat-Transfer Correlations for Turbulent Water Flow Through a Pipe at Prandtl Numbers of 6.0 and 11.6," Argonne National Laboratory, ANL/OTEC-P5-11, Jan. 1982.

B8. Petukhov, B. S., "Heat Transfer and Friction in Turbulent Pipe Flow with Variable Physical Properties," Adv. Heat Transfer, Vol. 6, pp. 503-564, 1970.

B9. Petukhov, B. S., and Popov, V. N., "Theoretical Calculation of Heat Exchange and Friction Resistance in Turbulent Flow in Tubes of Incompressible Fluid with Variable Physical Properties," High Temp. U.S.S.R. (Teplofizika Vysokikh Temperature), No. 1, pp. 69-93, 1963.

B10. Sparrow, E. M., Hallman, T. M., and Seigel, R., "Turbulent Heat Transfer in the Thermal Entrance Region of a Pipe with Uniform Heat Flux," Appl. Sci. Res., Section A, Vol. 7, pp. 37-52, 1955.

Distribution for ANL-88-15

Internal:

H. Drucker
R. Weeks
W. Schertz
K. Kasza (5)
S. Choi
K. Liu (25)
J. Oras
T. Kuzay
C. Till
W. Shack
D. Raske
A. Raptis
D. Kupperman
S. Sheen
Y. Chang
J. Karvelas
A. Thomas
H. Stevens
A. Wolsky
P. Kier
J. Tschanz
E. Stefanski
ANL Patent Dept.
ANL Contract File
ANL Libraries
TIS Files (3)

External:

DOE-TIC, for distribution per UC-95D and UC-231 (222)
J. Millhone, DOE
J. Holmes, DOE
R. Jones, DOE
J. Kaminsky, DOE
F. Collins, DOE
L. Delacroix, DOE
D. Goldman, DOE-CH
F. Herbaty, DOE-CH
Materials and Components Technology Division Review Committee
P. Alexander
C. Li
L. Jardine
R. Scholl
S. Green
P. Shewmon
R. Greenkorn
R. Smith